

UNIVERSITÉ DU QUÉBEC

**MÉMOIRE PRÉSENTÉ À
L'UNIVERSITÉ DU QUÉBEC À CHICOUTIMI
COMME EXIGENCE PARTIELLE
DE LA MAÎTRISE EN INGÉNIERIE**

**PAR
LIN ZHANG**

**A KINETIC STUDY OF HYDROGEN ABSORPTION AND DEGASSING
BEHAVIOUR OF DURALCAN™ COMPOSITES**

NOVEMBRE 1996



Mise en garde/Advice

Afin de rendre accessible au plus grand nombre le résultat des travaux de recherche menés par ses étudiants gradués et dans l'esprit des règles qui régissent le dépôt et la diffusion des mémoires et thèses produits dans cette Institution, **l'Université du Québec à Chicoutimi (UQAC)** est fière de rendre accessible une version complète et gratuite de cette œuvre.

Motivated by a desire to make the results of its graduate students' research accessible to all, and in accordance with the rules governing the acceptance and diffusion of dissertations and theses in this Institution, the **Université du Québec à Chicoutimi (UQAC)** is proud to make a complete version of this work available at no cost to the reader.

L'auteur conserve néanmoins la propriété du droit d'auteur qui protège ce mémoire ou cette thèse. Ni le mémoire ou la thèse ni des extraits substantiels de ceux-ci ne peuvent être imprimés ou autrement reproduits sans son autorisation.

The author retains ownership of the copyright of this dissertation or thesis. Neither the dissertation or thesis, nor substantial extracts from it, may be printed or otherwise reproduced without the author's permission.

RÉSUMÉ

Ce travail s'inscrit dans le cadre d'un programme de recherche visant à étudier l'impact de l'hydrogène dans les alliages d'aluminium et à mesurer par différentes méthodes la solubilité de ce gaz dans le métal liquide. L'objet de ce mémoire de maîtrise porte particulièrement sur la cinétique de dégazage et d'absorption de l'hydrogène dans deux composites de type DURALCAN^{MD}, produits par une usine pilote de la compagnie ALCAN: l'un pouvant être mis en forme par filage [W6D.22A ou 6061/Al₂O_{3(p)}] et l'autre développé spécialement pour les applications en fonderie [F3S.20S ou Al-Si-Mg/SiC_(p)]. L'objectif principal est d'étudier l'effet des particules de renfort (Al₂O₃, SiC) sur la cinétique et le mécanisme d'absorption de l'hydrogène dans ces matériaux hétérogènes. Il s'agit d'un travail original et d'intérêt tant sur le plan scientifique qu'industriel.

Les variations des teneurs en hydrogène en fonction du temps dans les composites susmentionnés sont évaluées dans différentes conditions expérimentales favorisant soit l'absorption ou le dégazage de ce gaz. Un appareil de type "Alscan" est utilisé pour évaluer le dosage d'hydrogène. Pour fins de comparaison, les mêmes expériences sont réalisées parallèlement avec les alliages constituant les matrices de ces deux composites.

Les résultats expérimentaux sont présentés sous forme de courbes montrant l'évolution de la teneur en hydrogène en fonction du temps. L'analyse de ces données à l'aide d'un modèle mathématique simplifié permet de mettre en évidence et d'évaluer les paramètres cinétiques des processus d'absorption et de dégazage des deux composites et de leur matrices. Les paramètres ainsi déterminés sont nettement différents d'un composite à l'autre; ils montrent notamment que la vitesse d'absorption d'hydrogène dans le composite contenant des particules d'alumine est plus grande que dans le cas où le carbure de silicium constitue les éléments de renfort. Ces résultats discutés en considérant le rôle de la couche d'oxyde qui flotte sur le métal liquide et la composition des alliages constituant les matrices des deux composites.

L'effet des conditions environnementales sur la cinétique d'absorption d'hydrogène est étudié. On observe que la teneur d'hydrogène dissous dans le liquide atteint une valeur d'équilibre qui est fonction de la pression partielle de la vapeur d'eau dans l'atmosphère; la relation $[H]_e - p_{H_2O}$ obéit à la loi de Sieverts. La vitesse d'absorption d'hydrogène est évidemment fonction du taux d'humidité dans l'air, principale variable et force motrice du processus; cependant, les coefficients de transfert de masse développés dans le modèle mathématique demeurent les mêmes pour un composite ou un alliage donné, peu importe les conditions environnementales.

Le temps nécessaire pour absorber l'hydrogène jusqu'à la moitié de la valeur d'équilibre est évalué dans différentes conditions expérimentales. Ces calculs montrent que ce temps est de l'ordre d'une demi-heure et qu'il est plus court pour les composites que leur matrices correspondantes en alliage d'aluminium. L'effet du rapport surface libre (A) de métal fondu sur son volume (V) fait également l'objet d'expériences. Les résultats montrent que le taux d'absorption de l'hydrogène est directement proportionnel au rapport (A/V); on doit donc en conclure que le processus est contrôlé par les réactions et la diffusion aux interfaces avec la couche d'oxyde qui se forme au-dessus du matériau liquide.

ABSTRACT

The kinetic behaviour of hydrogen absorption and degassing has been experimentally investigated by acquiring hydrogen concentration-time profiles with Alscan apparatus in molten DURALCAN™ composites, W6D.22A (6061/Al₂O_{3(p)}) from wrought alloy family and F3S.20S (Al-Si-Mg/SiC_(p)) from foundry alloy family, and their matrix alloys under certain experimental conditions. This work is a part of the project on hydrogen absorption and solubility in molten aluminum alloys and aluminum matrix composites. The main objective of the present work is to study the effect of the reinforcing particles on hydrogen absorption behaviour in these materials.

The kinetic parameters of the processes of hydrogen absorption and degassing for the composites and their matrices have been evaluated with the experimental data according to the mathematical models developed on the basis of the mathematical analysis of these processes. The effect of the reinforcing ceramic particles in the composites on the kinetics of hydrogen absorption and degassing has been studied by comparing the kinetic parameters of the composites to those of their matrices. It has been found that the ceramic particles can increase the rate of hydrogen absorption and the effect of Al₂O₃ particles is stronger than that of SiC particles. The mechanism of the effect of these ceramic particles has been discussed.

The effect of the environmental conditions on the rate of hydrogen absorption and degassing has been studied. It was found that the equilibrium value of hydrogen concentration in the process of hydrogen absorption increases with increasing water partial pressure in the atmosphere and their relationship obeys Sieverts' law. The environmental condition can influence the rate of hydrogen absorption by changing the value of the driving force of the process, while the rate constant, or the mass transfer coefficient, for hydrogen absorption was found to be independent of the atmospheric conditions. The rate constant for degassing is also independent of the atmospheric conditions above the melt during degassing.

A half-recover time of hydrogen absorption has been evaluated for the composites and their matrices. The results show that the rate of hydrogen absorption is higher for the composites than that of their matrices and the time needed to absorb hydrogen to a half of the equilibrium level is shorter for the composites than the matrices.

Finally, the effect of the ratio of melt surface area, **A**, to its volume, **V**, has been evaluated by the experiments with various values of **A/V** ratio. The results indicate that the rate of hydrogen absorption will be higher if the area of the melt surface is increased with respect to a same volume of metal.

ACKNOWLEDGEMENT

First of all I would like to thank my director Dr. Michel Bouchard and co-director Dr. Hua Liu, professors with Université du Québec à Chicoutimi, for their supervision for the entire work of this project.

I would like to acknowledge Dr. Mihriban O. Pekguleryuz, director of Alcan-UQAC Chair in Solidification and Metallurgy of Aluminum, for her continuous support on this project. I also thank Mr. Celil Aliravci and Dr. Dariyoush Emadi for their helpful advice and discussions.

I would like to thank Mr. Gilles Lemire and also Mr. Régis Boucher for their help in the laboratory to prepare the necessary setups for the experiments.

The Arvida Research and Development Center of Alcan International Ltd. should be gratefully acknowledged for their critical evaluation of this work and useful advice. The Dubuc Plant of Alcan Ltd. and Bomem Inc. should also be acknowledged for supplying the materials.

Finally, I would like to thank all the persons who have made their contributions, in one way or another, to this work as well as my family and my friends.

TABLE OF CONTENTS

CHAPTER 1	
INTRODUCTION	1
1.1 A DESCRIPTION OF THE PROBLEM	2
1.2 OBJECTIVE	5
1.3 METHODOLOGY	5
CHAPTER 2	
LITERATURE REVIEW	7
2.1 HYDROGEN IN ALUMINUM	8
2.1.1 Solubility	8
2.1.2 The Sources of Hydrogen during Melting and Casting	16
2.1.3 Hydrogen-Generated Defects	18
2.1.3.1 Porosity in Aluminum Castings	18
2.1.3.2 Effects on Mechanical Properties	20
2.2 DEGASSING ALUMINUM MELTS	23
2.2.1 Introduction	23
2.2.2 Mechanisms of Hydrogen Elimination	23
2.2.3 An Overview of the Methods of Degassing	25
2.2.4 Degassing Efficiency and Determining Factors	32
2.3 HYDROGEN ABSORPTION IN ALUMINUM MELTS	38
2.3.1 Introduction	38
2.3.2 Adsorption of Hydrogen on Melt Surfaces	38
2.3.3 Diffusion of Hydrogen in Liquid Metals	40
2.3.4 Mechanism of Hydrogen Absorption	41
2.3.5 Method of Avoiding Hydrogen Absorption	43
CHAPTER 3	
EXPERIMENTAL PROCEDURE	45
3.1 MATERIALS	46
3.1.1 The Selection of Materials	46
3.1.2 Description of Materials	46
3.2. DESCRIPTION OF EXPERIMENTAL SETUP	49
3.2.1 The Furnace and the Crucible	49
3.2.2 The Stirrer and the Protection Gas	50
3.3 DEGASSING AND RE-ABSORPTION	52
3.3.1 Melting of the Sample	52
3.3.2 Degassing Aluminum Melt	53

3.3.3 Hydrogen Re-absorption of the Melt	55
3.3.4 Measurement of Humidity Level	58
3.4 EFFECT OF SURFACE-TO-VOLUME RATIO ON HYDROGEN ABSORPTION	58
3.5 MEASUREMENT OF HYDROGEN CONTENT	60
3.5.1 Introduction	60
3.5.2 Theory of Operation	61
3.5.3 A Description of Alscan Analyzer	62
3.5.3.1 The Probe	62
3.5.3.2 The Recirculation Loop	63
3.5.4 Measurement Procedure	65
CHAPTER 4	
APPROACH TO MATHEMATICAL ANALYSIS OF DEGASSING AND ABSORPTION	70
4.1 INTRODUCTION	71
4.2 INTERPHASE MASS TRANSFER	72
4.2.1 Mixing	72
4.2.2 The Mass Transfer Coefficient	74
4.2.3 Mass Transfer in a Two-phase System	75
4.2.4 Effect of the Ratio of Surface Area to Melt Volume	79
4.3 MATHEMATICAL MODELS FOR HYDROGEN ABSORPTION AND DEGASSING	80
4.3.1 Melt-Side and Gas-Side Mass Transfer Resistances	80
4.3.2 Pick-up of Hydrogen from Water Vapour	83
4.3.3 Mathematical Models for Hydrogen Absorption and Degassing	87
4.4 DATA PROCESSING	89
4.4.1 Curve Fitting with the Least-Square Method	89
4.4.2 A Description of the Program	91
CHAPTER 5	
RESULTS AND DISCUSSIONS	93
5.1 EXPERIMENTAL RESULTS	94
5.1.1 Characteristics of the Variation of Hydrogen Concentration	94
5.1.2 The Kinetic Parameters	102
5.2 ANALYSES AND DISCUSSIONS	115
5.2.1 Rates of Degassing and Hydrogen Absorption	115
5.2.2 Effects of the Reinforcing Particles	122
5.2.3 Effects of the Atmospheric Conditions	127
5.2.4 The Half-Recover Period of Hydrogen Absorption	133
5.2.5 Effect of the Ratio of Melt Surface Area to its Volume	135
5.3 SOURCES OF ERROR	139
CONCLUSIONS	144

REFERENCES 149

APPENDIX
A LIST OF THE PROGRAM USED FOR DATA ANALYSIS 155

LIST OF FIGURES

Figure 1-1.	Solubility of hydrogen at atmospheric pressure in aluminum.	3
Figure 1-2.	Porosity as a function of hydrogen content in sand cast aluminum and aluminum alloy bars.	3
Figure 2-1.	Hydrogen solubility in liquid pure aluminum at 700 °C at various pressures.	9
Figure 2-2.	Interdendritic porosity in an ingot of 99.2 % Al	19
Figure 2-3.	Ultimate tensile strength versus hydrogen porosity for sand cast bars of three aluminum alloys.	21
Figure 2-4.	Effect of ingot porosity on short-transverse tensile properties of 3-inch thick D.T.D. 5020A plate hot rolled from 11 in. × 44 in. D.C. ingot.	22
Figure 2-5.	Gas purging control volume.	34
Figure 2-6.	Degassing efficiency (Z^0) ² vs the dimensionless bubble contact area $\Psi/[\%H]$	36
Figure 2-7.	Degassing efficiency as a function of purge gas bubble size for two melt hydrogen concentrations.	37
Figure 2-8.	Degassing performance of a lance, porous plug, and an impeller.	37
Figure 3-1.	Photomicrographs of two DURALCAN™ composites, F3S.20S (above), and W6D.22A (below).	48
Figure 3-2.	The ingots of DURALCAN™ composites and their matrices, a) composites, and b) matrices.	49
Figure 3-3.	A schematic showing the furnace and crucible used in the experiments.	51
Figure 3-4.	The use of stirrer and nitrogen in the experiment.	52

Figure 3-5.	A schematic illustration of degassing and hydrogen re-absorption, (a) degassing, (b) re-absorption.	56
Figure 3-6.	A sketch of an Alscan probe.	64
Figure 3-7.	The recirculation loop of an Alscan analyzer.	65
Figure 3-8.	A schematic illustration of the function of Alscan analyzer.	66
Figure 3-9.	Alscan dynamic curves for W6D.22A composite and its matrix alloy.	68
Figure 4-1.	Velocities are low along the interface so that the transfer of H atoms depends on the slow mechanism of diffusion.	73
Figure 4-2.	A melt-gas system shows the concentrations c_j and c_{ji} in the melt and pressures p_{ji} and p_{bj} in the gas phase.	76
Figure 4-3.	Some of the steps involved in the transfer of H across the aluminum melt-gas interface	84
Figure 4-4.	Flow chart of the program.	92
Figure 5-1.	Alscan readings of hydrogen concentration of W6D.22A composite during degassing and hydrogen re-absorption (Experiment No. WC1).	96
Figure 5-2.	Alscan readings of hydrogen concentration of the matrix alloy of W6D.22A (Experiment No. WM3).	97
Figure 5-3.	Alscan readings of hydrogen concentration of F3S.20S composite during degassing and hydrogen re-absorption (Experiment No. FC3).	98
Figure 5-4.	Alscan readings of hydrogen concentration of the matrix alloy of F3S.20S composite (Experiment No. FM2).	99
Figure 5-5.	The end cycle Alscan readings of hydrogen concentration of W6D.22A composite (Experiment No. WC1).	100
Figure 5-6.	The end cycle Alscan readings of hydrogen concentration of the matrix alloy of W6D.22A composite (Experiment No. WM3).	100
Figure 5-7.	The end cycle Alscan readings of hydrogen concentration of F3S.20S composite (Experiment No. FC3).	101

Figure 5-8.	The end cycle Alscan readings of hydrogen concentration of the matrix alloy of F3S.20S composite (Experiment No. FM2).	101
Figure 5-9.	The fitted curves for hydrogen absorption in W6D.22A composite under different environmental conditions.	103
Figure 5-10.	The fitted curves for hydrogen absorption of the matrix alloy of W6D.22A under different environmental conditions.	104
Figure 5-11.	The fitted curves for hydrogen absorption of F3S.20S composite under different environmental conditions.	105
Figure 5-12.	The fitted curves for hydrogen absorption of the matrix alloy of F3S.20S under different environmental conditions.	106
Figure 5-13.	The fitted curves for degassing of W6D.22A composite under different environmental conditions.	108
Figure 5-14.	The fitted curves for degassing of the matrix alloy of W6D.22A under different environmental conditions.	109
Figure 5-15.	The fitted curves for degassing of F3S.20S composite under different environmental conditions.	110
Figure 5-16.	The fitted curves for degassing of the matrix alloy of F3S.20S under different environmental conditions.	111
Figure 5-17.	The hydrogen absorption rate of W6D.22A and its matrix alloy at different times during the process of absorption.	117
Figure 5-18.	The hydrogen absorption rate of F3S.20S composite and its matrix alloy at different times during the process of absorption.	118
Figure 5-19.	The rate of degassing for some of the experiments at different times during the degassing process.	120
Figure 5-20.	A comparison of the rate constant of hydrogen absorption, k_a , for different materials (markers represent the mean values).	123
Figure 5-21.	A comparison of the degassing rate constant, k_d , for different materials (markers represent the mean values).	124
Figure 5-22.	A diagram showing that k_a is constant with the water partial pressure in the atmosphere.	127

Figure 5-23.	A diagram showing that the k_d values were constant with the flow rate of N_2	129
Figure 5-24.	Relationship of the equilibrium hydrogen content of absorption and the water partial pressure in the atmosphere.	130
Figure 5-25.	Relationship between the equilibrium values of hydrogen content and water partial pressure for degassing.	131
Figure 5-26.	A graphical illustration of the half-recover period for hydrogen absorption of molten W6D.22A composite and its matrix alloy.	134
Figure 5-27.	A graphical comparison of the half-recover period, $t_{1/2}$, for hydrogen absorption of the composites and their matrices.	134
Figure 5-28.	A diagram showing the effect of A/V on the rate of hydrogen absorption.	138
Figure 5-29.	Failure Alscan readings during hydrogen absorption of molten W6D.22A composite.	140
Figure 5-30.	A comparison of the calculated values of hydrogen content to the expected values at the beginning of degassing.	141

LIST OF TABLES

Table 2-1	Temperature Dependence of Hydrogen Solubility in Liquid Pure Aluminum	13
Table 2-2	Temperature Dependence of Hydrogen Solubility in Some Liquid Aluminum Alloys	13
Table 2-3	Interaction Coefficients in Liquid Al-H-i Alloys	16
Table 3-1	Chemical Compositions of the Matrices of W6D.22A and F3S.20S	47
Table 3-2	A Summary of the Experimental Conditions	59
Table 3-3	Values of the Ratio of Melt Surface Area to its Volume	60
Table 5-1	Evaluated Hydrogen Absorption Parameters	113
Table 5-2	Evaluated Degassing Parameters	114
Table 5-3	The Half-recover Period for the Composites and their Matrices	135
Table 5-4	Results of k_a from Experiments with various A/V values	137

LIST OF SYMBOLS

A	area
	constant defined in Eqn. (2.7)
a_i	activity of i in solution
B	constant defined in Eqn. (2.7)
C	total molar concentration
C_i, c_i	molar concentration of i
CF(A)	alloy correction factor
CF(T)	temperature correction factor
D	diffusion coefficient
d	diameter
f_H	activity coefficient of hydrogen
\dot{G}	flow rate of inert gas
ΔG^0	change of free energy
[H]	hydrogen content
$\Delta[H]$	driving force for hydrogen absorption or for degassing
$[H]_0$	initial hydrogen content
$[H]_e$	equilibrium hydrogen content
ΔH^0	change in enthalpy
j	molar flux
K	equilibrium constant
k, k_M	mass transfer coefficient
k_a	hydrogen absorption rate constant
k_d	degassing rate constant
k_t	total mass transfer coefficient
L	characteristic vessel dimension
M_i	molecular weight of i
N_A^0	total molar flux of A
N_{Ax}	molar flux of A in x-direction
\dot{n}	molar flux
P	pressure
P_{atm}	atmospheric pressure

P_E	total external pressure
P_{gas}	equilibrium hydrogen pressure inside a pore
P_{met}	pressure of metal head
P_{shrink}	pressure due to the contraction of the metal during solidification
P_{surface}	pressure associated to surface tension
p_i	partial pressure of i
	internal pressure
P_{inert}	inert gas partial pressure
R	gas constant
r	rate
r^2	coefficient of regression
S	hydrogen solubility in liquid aluminum
s_i	standard deviation of the value of i
T	temperature in Kelvin
t	time
$t_{1/2}$	half-recover period
V	volume
v_{Ax}	velocity of A in x-direction
v_{max}	maximum velocity
v_x^*	local molar average velocity in x-direction
X_i	mole fraction of i in solution
$(Z^0)^2$	degassing efficiency
γ_i	activity coefficient of i
δ_2	thickness of the melt boundary layer
κ_B	Boltzmann constant
λ	ratio between the resistances to diffusion in the gas phase and in the melt phase
μ	viscosity
ρ	second order interaction coefficient
	density
τ_m	mixing time
$\psi/[\%H]$	dimensionless contact area
ϵ	first order interaction coefficient
$\dot{\epsilon}$	energy

CHAPTER 1
INTRODUCTION

CHAPTER 1

INTRODUCTION

1.1 A DESCRIPTION OF THE PROBLEM

Hydrogen is appreciably soluble in both solid and molten aluminum [1]. Molten aluminum reacts with water vapour in the atmosphere, adsorbed water, water present as hydrated oxide films on scrap, water adsorbed on or combined in furnace refractory and even the surface contamination of the initial charge. Solid aluminum also reacts with moisture in a furnace atmosphere to form hydrogen. These reactions are the sources of hydrogen both in solid and liquid aluminum caused by diffusion from the surface. The amount of hydrogen present in solid aluminum can be significantly greater than the equilibrium solubility value either because of the presence during solidification of such excess amount, or because of reactions of furnace moisture on the surface of the metal and subsequent diffusion of hydrogen into the body of the solid. The former probably is the dominant factor which leads to an excessive amount of hydrogen remained in solid aluminum alloys during casting due to the big difference of hydrogen solubility in liquid and solid aluminum, although alloy composition, inclusion content and casting technique are also important factors. The solubility of hydrogen at atmospheric pressure in pure aluminum is illustrated in Fig. 1-1. Hydrogen in excess of the solid solubility in aluminum and aluminum

alloys is generally considered deleterious, and its effects have long been recognized and well documented [1-6]. These may be directly attributed to the formation of porosity in castings, ingots, and wrought products, although other hydrogen induced defects, such as bright flakes in forging, blisters on aluminum sheet, and high-temperature deterioration during heat treating as well as hydrogen embrittlement are also found and reported.

A large amount of research has been made with respect to the influence of gas content in molten aluminum on the formation of porosity. For molten aluminum and its alloys, threshold

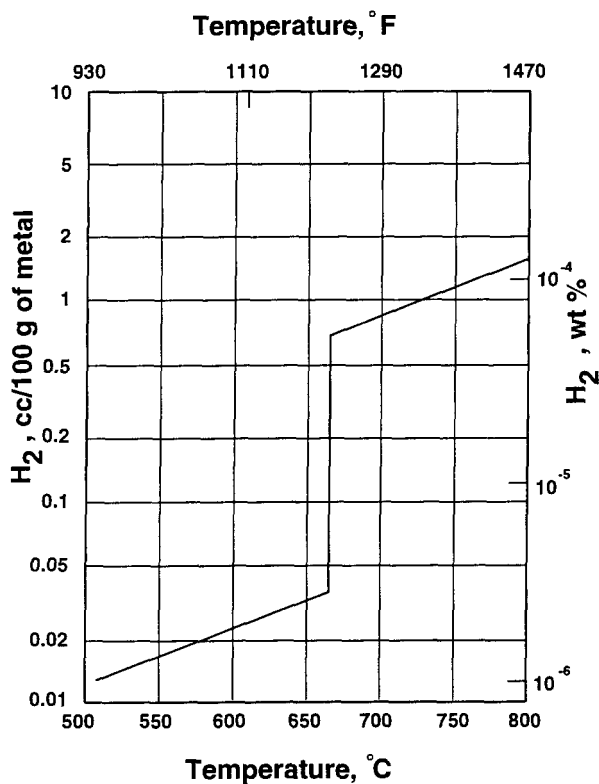


Figure 1-1. Solubility of hydrogen at atmospheric pressure in aluminum [1].

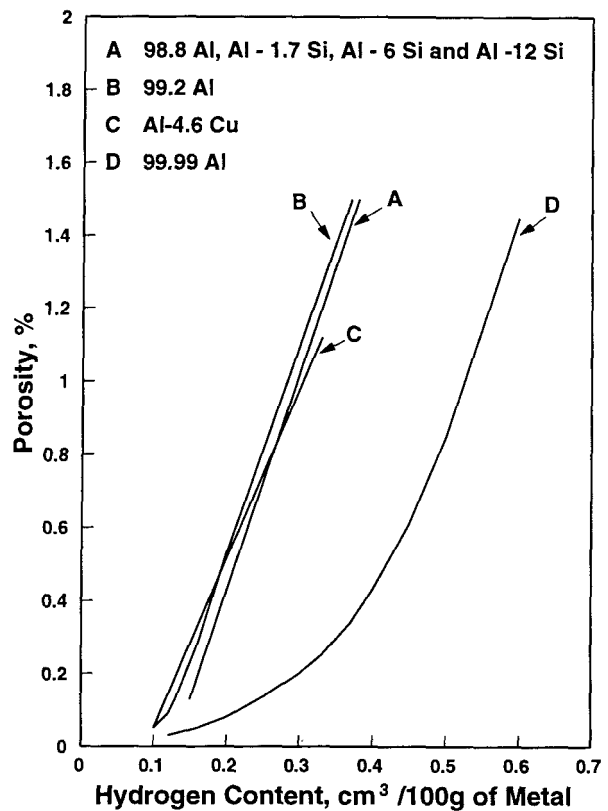


Figure 1-2. Porosity as a function of hydrogen content in sand cast aluminum and aluminum alloy bars [3].

hydrogen values were reported under which the ingots or castings will be free of porosity [4,6-8]. A relationship of hydrogen content and porosity in aluminum and its alloys is shown in Fig. 1-2.

It can be seen from the previous work that to prevent the formation of porosity in castings and the existence of other hydrogen induced defects, the hydrogen content in aluminum melts should be reduced to a very low level (<0.05 ml/100 g) before casting. Since industrial casting process is conducted in an environment containing sources of hydrogen, as those mentioned above, hydrogen can easily be picked up and absorbed by molten aluminum. A process is needed in industrial casting operations to remove hydrogen from aluminum melt and to control the hydrogen content in molten aluminum alloy before casting. This process is usually referred to as degassing in foundry practice and becomes imperative to a successful casting operation. Degassing and hydrogen absorption are dynamic processes which involve several chemical and kinetic relations. In order to well understand these important processes in industry, it is necessary to study them from both a chemical and a kinetic perspective.

The chemical and kinetic study on the processes of degassing and hydrogen absorption in molten pure aluminum and in some aluminum alloys have been performed by several investigators [9-16]. However, information concerning degassing and hydrogen absorption behaviour in molten DURALCANTM composites is very limited in published literature. This hydrogen behaviour in molten DURALCANTM composites has been believed to be different from that in pure aluminum and aluminum alloys due to the presence of a large concentration of reinforcing SiC and Al₂O₃ particles (10% vol. to 20% vol. for commercial DURALCANTM

composites).

1.2 OBJECTIVE

The objective of this work is to study the kinetics of degassing and hydrogen absorption of molten DURALCANTM composites and their matrix alloys. This will help to create a better understanding of the effect of reinforcing SiC and Al₂O₃ particles on hydrogen absorption behaviour in these materials. In particular, the results of the present work will contribute to the management of industrial process and facilitate the quality control of castings of DURALCANTM composites.

1.3 METHODOLOGY

The following steps are performed in this present investigation:

1. Select typical wrought and foundry DURALCANTM composites and their matrices for the investigation of degassing and hydrogen absorption.
2. Establish an experimental setup for the acquisition of degassing and hydrogen absorption data under various atmospheric conditions.
3. Study the environmental and process parameters that influence degassing and hydrogen absorption in the experiments. Determine relevant experimental procedures.
4. Derive mathematical models for hydrogen absorption and degassing of aluminum melts according to the relevant chemical reactions and physical processes. Determine kinetic

parameters for degassing and hydrogen absorption of aluminum melts.

5. Carry out experiments of degassing and hydrogen absorption on both DURALCAN™ composites and their matrices with fixed process parameters and under various environmental conditions. Monitor and record hydrogen content-time profiles of the melts for the processes of degassing and absorption.
6. Calculate the kinetic parameters of hydrogen absorption and degassing for DURALCAN™ composites and their matrices with the observed values of hydrogen content at different times of degassing and absorption, by means of mathematical regression according to the derived mathematical models for degassing and hydrogen absorption.
7. Study the degassing and hydrogen absorption characteristics, with given process conditions, of both wrought and foundry DURALCAN™ composites as well as their matrices by evaluating the corresponding kinetic parameters. Evaluate the effects of reinforcing SiC and Al₂O₃ particles on degassing and hydrogen absorption behaviour in these materials.
8. Investigate the effects of particular process parameter on the kinetic behaviour of degassing and hydrogen absorption of aluminum melts.

CHAPTER 2
LITERATURE REVIEW

CHAPTER 2

LITERATURE REVIEW

2.1 HYDROGEN IN ALUMINUM

2.1.1 Solubility

Hydrogen is the only gas with measurable solubility in pure aluminum. Values of hydrogen concentration in equilibrium with the gas at atmospheric pressure (101325 Pa) are shown in Fig. 1-1. The solubility is much higher in liquid than in solid metal. At the melting point, 660 °C, the concentrations of hydrogen in equilibrium are 0.7 and 0.04 cm³ per 100 grams of metal for the liquid and solid aluminum, respectively.

It is well known that hydrogen solubility is proportional to the square root of hydrogen partial pressure, P_{H_2} . This proportionality, also true for the solution of other diatomic gases like N₂ and O₂ in liquid metals provided the solution is dilute, has been found for a long time in such sufficient number of experiments that it has been called a law of Sieverts. Some of the results on hydrogen solubility in liquid pure aluminum from three different research groups are shown

in Fig. 2-1. It can be seen that Sieverts' law is completely followed. According to the work of Opie and Grant [16], Sieverts' law is also obeyed by molten aluminum-copper alloys from 0 to 50.5 percent copper, and by molten aluminum-silicon alloys from 0 to 18 percent silicon with melt temperature ranging from 700 °C to 1000 °C. The most recent experimental values of hydrogen solubility in liquid aluminum-copper binary alloys from 0 to 10 percent copper have been obtained by Liu et al [22], which are in good agreement with that of Opie and Grant. Similar research work was conducted by Anyalebechi et al [18] in liquid aluminum-lithium binary alloys containing 1, 2 and 3 percent lithium, and the results show that Sieverts' law is obeyed by these alloys with

melt temperature ranging from 640 °C to 800 °C and pressure from 5.3×10^4 to 10.7×10^4 P_a. This relationship between hydrogen solubility in aluminum and its partial pressure directly leads to a conclusion that hydrogen exits in its atomic form in

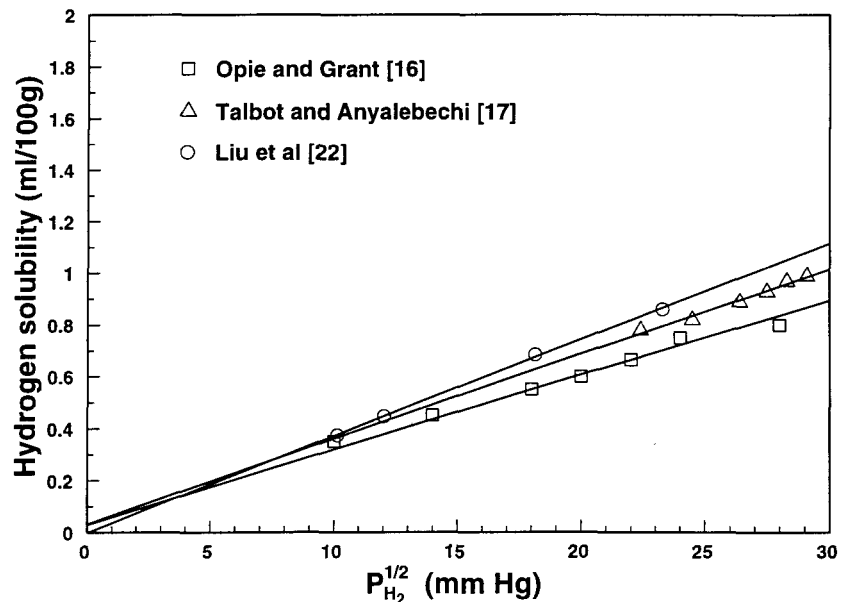


Figure 2-1. Hydrogen solubility in liquid pure aluminum at 700 °C under various pressures.

aluminum solution, i.e., its absorption process could be expressed by the following equation:



In other words, the dissociation of diatomic hydrogen in liquid aluminum is the fundamental feature of the whole dissolution process in liquid aluminum. No analysis and explanation to this phenomena have been given except in the paper of Talbot and Anyalebechi [17] that the dissociation of hydrogen is attributed to interaction of hydrogen atoms with the interatomic electronic environment in metals. It should be noted that Eqn. (2.1) describes the dissociation of diatomic hydrogen in contact with liquid aluminum. Such a reaction ($H_2(g) \rightarrow 2H(g)$) could hardly occur without aluminum, since its equilibrium constant at 700 °C is in the order of 10^{-18} .

Like the dependence of hydrogen solubility on pressure, its dependence on temperature is also of great importance. Consider the absorption equation {Eqn. (2.1)}, the equilibrium constant **K** can be expressed as [20]:

$$K = \frac{a_H}{\sqrt{p_{H_2}}} = \frac{\gamma_H X_H}{\sqrt{p_{H_2}}} \quad (2.2)$$

where a_H is hydrogen activity,

γ_H is activity coefficient,

X_H is hydrogen mole fraction in liquid aluminum, and

p_{H_2} is hydrogen partial pressure, in atm.

For a dilute solution like the one of hydrogen in liquid aluminum, the γ_H in Eqn. (2.2) could be

regarded as constant because Henry's law is valid. Since hydrogen solution in aluminum is sufficiently dilute and hydrogen gas in atmosphere can be regarded as ideal, we can make use of Eqn. (2.3) which is an alternative form of Van't Hoff equation [19,20]:

$$\ln K = -\frac{\Delta H^0}{RT} + \text{constant} \quad (2.3)$$

or

$$\ln \left(\frac{\gamma_H X_H}{\sqrt{P_{H_2}}} \right) = -\frac{\Delta H^0}{RT} + \text{constant} \quad (2.4)$$

In Eqns. (2.3) and (2.4), ΔH^0 is the change in enthalpy occurs when 0.5 mole of H_2 dissolves, according to Eqn. (2.1), in aluminum to form a dilute solution with hydrogen content of 1 cm^3 in standard state (273 K and 1 atm.) per 100 grams of metal which in engineering practice is usually chosen as the reference state for hydrogen solution in aluminum. Since γ_H is constant, Eqn. (2.4) could be rewritten as:

$$\ln \left(\frac{X_H}{\sqrt{P_{H_2}}} \right) = -\frac{\Delta H^0}{RT} + \text{constant} \quad (2.5)$$

The hydrogen mole fraction, X_H , in Eqn. (2.5) can be replaced by its equilibrium content represented by a symbol S which is hydrogen solubility. Eqn. (2.5) then becomes:

$$\ln \left(\frac{S}{\sqrt{P_{H_2}}} \right) = -\frac{\Delta H^0}{RT} + \text{constant} \quad (2.6)$$

or

$$\ln\left(\frac{S}{\sqrt{P_{H_2}}}\right) = -\frac{A}{T} + B \quad (2.7)$$

where **S** is hydrogen solubility in cm³ (STP)/100g, and **A** ($=\Delta H^0/R$) and **B** are constants. Eqn. (2.7) is based on the assumption that ΔH^0 is temperature independent within a certain range of melt temperature, which is usually safe for the practical operation of liquid aluminum. Eqn. (2.7) gives not only the dependence of solubility on temperature but also its dependence on pressure. A conclusion can be reached that hydrogen solubility in aluminum increases with increasing melt temperature and its logarithmic value has a linear relationship to the reciprocal of temperature for a constant value of hydrogen partial pressure, P_{H_2} . For hydrogen solubility in liquid aluminum and its alloys under 1 atm hydrogen partial pressure, Eqn. (2.7) can be simplified as:

$$\log S = \frac{A}{T} + B \quad (2.8)$$

This linear relationship has been found experimentally by several investigators [4,16,17,22] for molten pure aluminum and some aluminum alloys, and the corresponding values of **A** and **B** in Eqn. (2.8) were evaluated. A comparison is given in Table 2-1 of the equation evaluated by different research groups for liquid pure aluminum under 1 atm hydrogen partial pressure. The solubility equations for some liquid aluminum alloys are given in Table 2-2.

Table 2-1 Temperature Dependence of Hydrogen Solubility in Liquid Pure Aluminum
($p_{H_2} = 1 \text{ atm}$)

Researcher	Equation
Ransley and Neufeld [4]	$\log_{10}S = - 2760/T + 1.356$
Opie and Grant [16]	$\log_{10}S = - 2550/T + 2.62$
Talbot and Anyalebechi [17]	$\log_{10}S = - 2700/T + 2.72$
Liu et al [22]	$\log_{10}S = - 2980/T + 3.09$

Table 2-2 Temperature Dependence of Hydrogen Solubility in Some Liquid Aluminum
Alloys ($p_{H_2} = 1 \text{ atm}$)

Alloy	Opie and Grant [16]	Liu et al [22]
2 % Cu	$\log_{10}S=-2950/T+2.90$	$\log_{10}S=-2804/T+2.89$
4 % Cu	$\log_{10}S=-3050/T+2.94$	$\log_{10}S=-2840/T+2.91$
6 % Cu	-	$\log_{10}S=-2660/T+2.70$
8 % Cu	$\log_{10}S=-3150/T+2.94$	$\log_{10}S=-2699/T+2.73$
10 % Cu	-	$\log_{10}S=-2574/T+2.59$
16 % Cu	$\log_{10}S=-3150/T+2.83$	-
32 % Cu	$\log_{10}S=-2950/T+2.57$	-
2 % Si	$\log_{10}S=-2800/T+2.79$	-
4 % Si	$\log_{10}S=-2950/T+2.91$	-
8 % Si	$\log_{10}S=-3050/T+2.95$	-
16 % Si	$\log_{10}S=-3150/T+3.00$	-
1 % Li	$\log_{10}S=-2113/T+2.568^*$	-
2 % Li	$\log_{10}S=-2797/T+3.329^*$	-
3 % Li	$\log_{10}S=-2889/T+3.508^*$	-

* from the results of Anyalebechi et al [18]

For hydrogen solubility in pure aluminum there have been a number of investigations and their results generally agree with one another. However, for aluminum alloys, relatively fewer data have been experimentally obtained.

Opie and Grant [16] have determined by using Sieverts' method the solubility of hydrogen in molten aluminum-copper and aluminum-silicon alloys. They found that both copper and silicon additions decrease hydrogen solubility, and that copper is more effective than silicon. Similar work has been done by Liu et al [22] on the determination of solubility in molten aluminum-copper alloys with copper concentration ranging from 2 to 10 wt%. Their results are in good agreement with that of Opie and Grant. The hydrogen solubility in liquid aluminum-lithium alloys containing 1, 2 and 3 wt% of lithium has been studied by Anyalebechi et al [18]. According to their work, hydrogen solubility is increased by lithium additions. They have reached a conclusion that lithium raises hydrogen solubility by increasing the entropy of the mixing and that favourable sites for the occlusion of hydrogen atoms exist in lithium-rich clusters. The latter comes from the following argument. Solutions of small atoms in metals can be described in terms of the interaction of solute atoms with the interatomic electronic environment in the solvent, and for hydrogen atoms which can form stable anions, there exist optimum electron densities for which the interaction is energetically most favourable. Consequently, hydrogen atoms tend to occupy sites in structure where the electron density is closest to the optimum.

In the study of hydrogen solubility in liquid aluminum alloys, a concept of interaction coefficient is important to describe the effect of alloying additions. This concept can be defined

as below. In a case of a dilute multi-component solution 1,2,...,m, where 1 is the solvent and 2,3,...,m are solutes, the behaviour of any solute i is dependent on the concentration of all the solutes in the solution. This dependence can be studied through the concepts of interaction coefficients, which can be expressed as [20],

$$\begin{aligned}
 \ln \gamma_i = & \ln \gamma_i^\infty + \sum_{j=2}^m \left(\frac{\partial \ln \gamma_i}{\partial X_j} \right)_{X_1-1} X_j \\
 & + \sum_{j=2}^m \frac{1}{2!} \left(\frac{\partial^2 \ln \gamma_i}{\partial X_j^2} \right)_{X_1-1} X_j^2 + \sum_{j=2}^{m-1} \sum_{k>j}^m \frac{1}{2!} \left(\frac{\partial^2 \ln \gamma_i}{\partial X_j \partial X_k} \right)_{X_1-1} X_j X_k + \dots \\
 & + \sum_{j=2}^m \frac{1}{3!} \left(\frac{\partial^3 \ln \gamma_i}{\partial X_j^3} \right)_{X_1-1} X_j^3 + \sum_{j=2}^{m-2} \sum_{k>j}^{m-1} \sum_{l>k}^m \frac{1}{3!} \left(\frac{\partial^3 \ln \gamma_i}{\partial X_j \partial X_k \partial X_l} \right)_{X_1-1} X_j X_k X_l + \dots \\
 & + \dots
 \end{aligned} \tag{2.9}$$

If the solution is sufficiently dilute, like the one of hydrogen in molten aluminum alloys, all the terms of third order and higher may be neglected. Then Eqn. (2.9) becomes:

$$\ln \gamma_i = \ln \gamma_i^\infty + \sum_{j=2}^m \epsilon_i^{(j)} X_j + \sum_{j=2}^m \rho_i^{(j)} X_j^2 + \sum_{j=2}^{m-1} \sum_{k>j}^m \rho_i^{(j,k)} X_j X_k + \dots \tag{2.10}$$

where ϵ_s and ρ_s are the first and second order interaction coefficients, respectively. Such a concept has been employed by Liu et al [22] in their study of the copper additions on hydrogen solubility in molten binary aluminum-copper alloys, and the corresponding values of first and second order interaction coefficients in Eqn. (2.10) have been evaluated. Sigworth and Engh [11] have presented in their study of hydrogen in aluminum a series of interaction coefficients. Some of them are tabulated in Table 2-3 where the cross products such as $\rho_i^{(j,k)}$ in Eqn. (2.10) and

higher order coefficients have been neglected by the authors.

Table 2-3 Interaction Coefficients in Liquid Al-H-i Alloys

element i	ϵ_H^i	ρ_H^i	T (°C)
Cu	0.030	-0.0004	700-800
Cr	0	-	800-900
Fe	0	-	800-900
Mg	-0.01	-	700-800
Mn	0.06	-	800
Ti	-0.1	-	800-900
Si	0.03	-0.0008	700-800
Sn	0.004	-	800-900

2.1.2 The Sources of Hydrogen during Melting and Casting

A major source of hydrogen in molten aluminum during melting and casting is the moisture in atmosphere. Hydrogen is easily absorbed by molten aluminum and its alloys through a reaction with water vapour,



The standard free energy change for this reaction is highly negative [14,21],

$$\Delta G^0 = -234010 - 17.19T \log T + 98.85T \quad \text{cal/mol} \quad (2.12)$$

Substituting the value of Eqn. (2.12) into the following relationship for this reaction,

$$\Delta G^0 = -RT \ln K \quad (2.13)$$

yields the equilibrium constant for reaction (2.11) being $K=(p_{H_2}/p_{H_2O})^3=10^{42}$ at 700 °C. This value is so high that for practical purposes it implies the complete conversion to hydrogen of all traces of water vapour in contact with the melt [3]. Theoretically, the reaction (2.11) could generate an extremely high hydrogen concentration in equilibrium with water vapour pressure in the atmosphere. However, from the previous discussions, hydrogen concentration in molten aluminum and its alloys is not as high as theoretically expected. This could be explained with the effect of oxide layer on top of melt surface which gives kinetic control to the process of hydrogen absorption [3,14], and also the effects of two major steps involved in the hydrogen pick-up by aluminum melt [23]. These two steps are: (i) water vapour diffusing through the boundary layer to the metal surface where reaction (2.11) takes place; and (ii) hydrogen molecules diffusing back out of the boundary layer, which will be discussed later in the following sections.

Other important sources of hydrogen in aluminum melts are [38]: (a) products of combustion; (b) hydrogen in the metal, which is restrained in pores in molecular state; (c) surface gas on ingot and scrap; and (d) surface gases on melting tools.

2.1.3 Hydrogen-Generated Defects

2.1.3.1 Porosity in Aluminum Castings

Porosity is one of the most important defects related to hydrogen in aluminum castings. The formation of micro-porosity in metal castings is attributed to a combination of two factors [24-26]: gas evolution and the contraction of metal during solidification. In the case of aluminum and its alloys, hydrogen is the only gas which is appreciably soluble in the metal [1,4]. The hydrogen dissolved in liquid aluminum is, therefore, the major contributor to the porosity formed in the castings thereafter, although it is not the only factor that influences the formation of porosity. As a casting solidifies, hydrogen is rejected by the solidifying aluminum phase to the adjacent liquid as a result of the big difference in solubility at the freezing point [1,4,8,27,28] as shown in Fig. 1-1. The hydrogen concentration in the liquid rises until it exceeds a value that is sufficient to nucleate gas bubbles. This is a value for which the equilibrium hydrogen pressure exceeds the sum of the external pressure acting on the liquid, as given by Tynelius [29],

$$P_{gas} \geq P_{atm} + P_{met} + P_{shrink} + P_{surface} = P_{liq} + P_{surface} \quad (2.14)$$

where P_{gas} is the equilibrium hydrogen pressure inside a pore, P_{atm} is the atmospheric pressure, P_{met} is the pressure due to the head of molten metal, P_{shrink} is the pressure due the contraction of the metal during solidification, and $P_{surface}$ is the pressure associated to surface tension. In aluminum alloys solidifying dendritically, the porosity so formed is restricted within the area between the growing dendrites, and it was given the name of interdendritic porosity and has the characteristic shape illustrated in Fig. 2-2 [3].

Ransley and Neufeld [4] have given the expression to calculate the percentage porosity in aluminum castings as follow,

$$\text{Percentage Porosity} = \frac{\rho_{\text{theoretical}} - \rho_{\text{actual}}}{\rho_{\text{theoretical}}} \times 100 \quad (2.15)$$

where $\rho_{\text{theoretical}}$ and ρ_{actual} are the theoretical and actual density of the sample, respectively. In their work, commercial pure aluminum with a purity of 99.2% was casted in a sand mold with adequate feeding, the shape of the castings was a horizontal bar. They found that no porosity occurred until the hydrogen content in the castings was greater than 0.12 ml/100g. This value of 0.12 ml/100g is three times larger than the equilibrium solid solubility of hydrogen in pure aluminum. Ransley and Neufeld ascribed this discrepancy to a supersaturation effect. This critical value of hydrogen content was later termed "the threshold hydrogen content" [7, 27].

Deoras and Kondic have studied the relationship between hydrogen content and percentage porosity in the castings of commercial pure aluminum and some aluminum alloys [8]. The value of percentage porosity was calculated for each of their samples using Eqn. (2.15). They obtained a linear relationship between

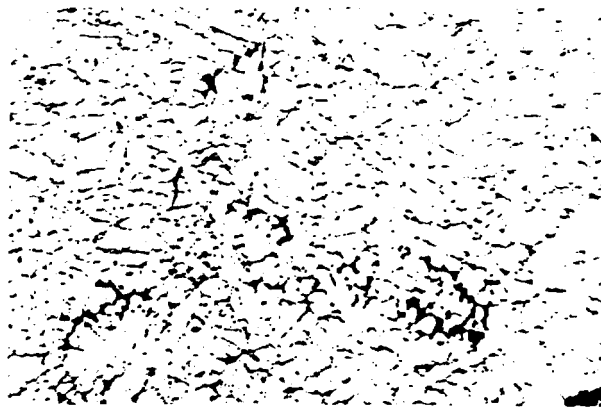


Figure 2-2. Interdendritic porosity in an ingot of 99.2 % Al [3]. 12.5x

hydrogen content and percentage porosity, and the intercept of the line was found to be 0.13 ml/100g, which is almost the same with the threshold hydrogen value reported by Ransley and Neufeld.

Similar results were obtained by Jordan et al [27]. Their investigation of ingots with two sizes has shown that hydrogen and porosity has a linear relationship in semi-continuously cast aluminum-copper-magnesium alloys, and there is a threshold hydrogen content, between 0.12 and 0.14 ml/100 g, below which there is no porosity. The influence of conditions during solidification has also been discussed, and they suggested that the threshold hydrogen content increased with increasing freezing rate. This was later proved by Thomas and Gruzleski [7] who utilized a cylindrical mold with the lower one third of which was surrounded by a water cooled jacket to cast Al-8%Si alloy. They found the threshold hydrogen content was three times higher at the water chilled part of the casting, 0.15 ml/100 g compared to 0.05 ml/100 g in the slowly cooled region.

2.1.3.2 Effects on Mechanical Properties

The deleterious effect of hydrogen on mechanical properties of aluminum and its alloys has long been recognized. It generally falls into two categories: unsoundness in foundry products, and defects in wrought products. Jay and Cibula [30] have studied the effects of porosity on tensile properties of Al-Mg alloys with various Mg contents. Test bars with diameters of 1, 1.5, and 4 inches were cast, and the castings were either well fed or incompletely fed to see the

effects of both gas porosity and shrinkage porosity. According to their results, the tensile properties of both Al-Mg and Al-Cu alloys were reduced by the presence of porosity in the casting, and Al-Mg alloys were more sensitive to the increase of the content of porosity because Al-Mg alloys have a strong tendency to form layer-porosity. They also found that both gas porosity and shrinkage porosity have a similar effect. Opie and Grant [31] have found the similar effect of gas porosity on mechanical properties of Al-5%Si alloy, and the results were illustrated together with those of Jay and Cibula in Fig. 2-3. Gas

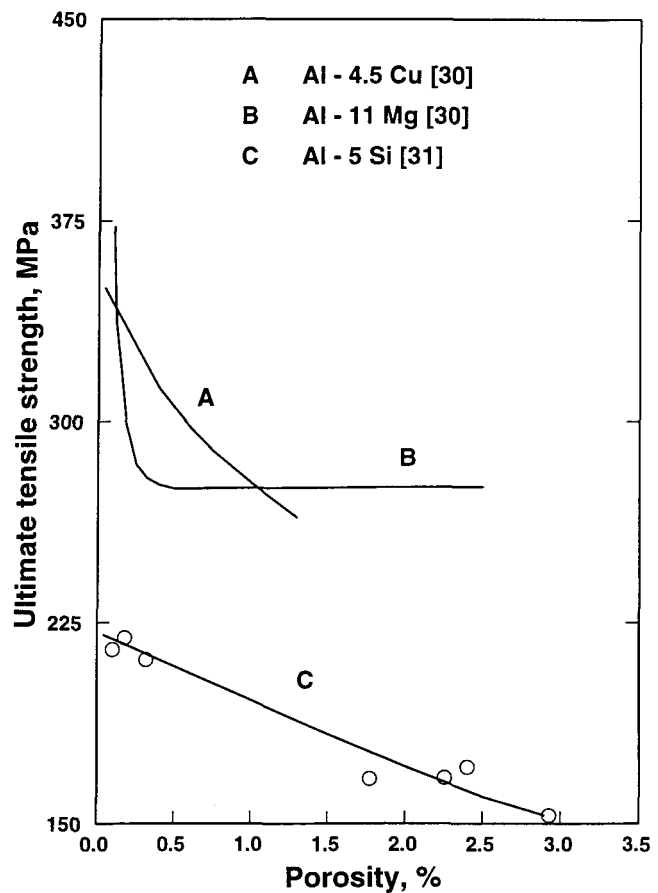


Figure 2-3. Ultimate tensile strength versus hydrogen porosity for sand cast bars of three aluminum alloys.

porosity could also cause potential problems in castings other than the decrease in mechanical properties. One problem is that in some castings which are produced to contain fluids under pressure, inter-dendritic gas porosity could allow leaking [32]; another one is that in sand castings the porosity forms close to the surface of castings as a result of hydrogen absorption by the metal in the mold resulting in poor surface finish [33-36].

The influence of gas porosity on the mechanical properties of wrought products is also

observed. Inter-dendritic gas porosity in ingots cast for subsequent fabrication may not be sealed up completely in later working operations but is flattened into planar discontinuities [3]. These discrete defects reduce the mechanical properties in short-transverse direction of thick plates and forgings by internal notch effect and by the area loss of load-bearing section. Turner and Bryant [37] measured the tensile strength, elongation, and impact values in short-transverse direction in 3-inch and 2-inch thick plates of high-strength Al-Cu-Mg-Si alloy with various values of hydrogen content in cast ingots. They found

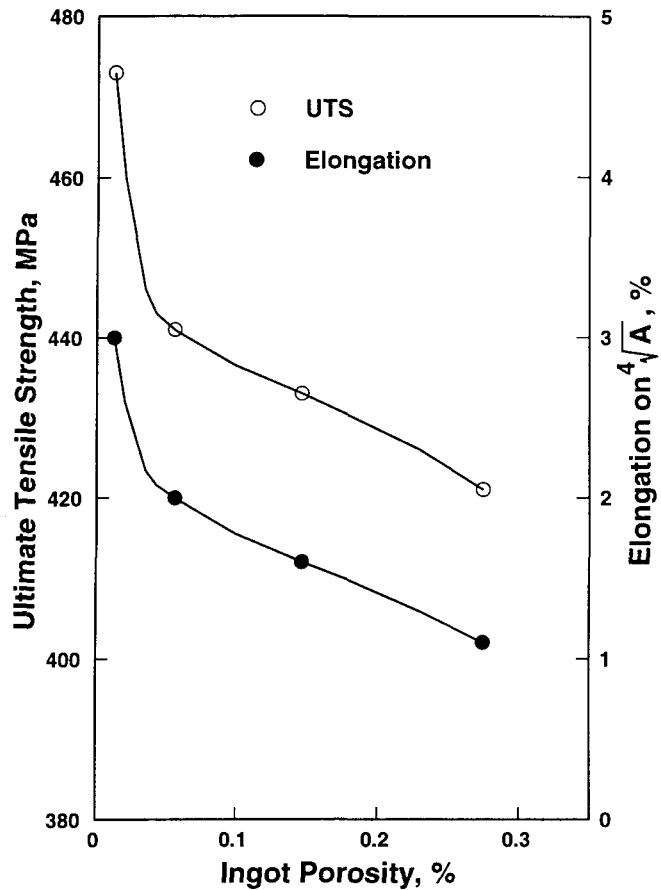


Figure 2-4. Effect of ingot porosity on short-transverse tensile properties of 3-inch thick D.T.D. 5020A plate hot rolled from 11 in. \times 44 in. D.C. ingot [37].

that the mechanical properties of the rolled plates were well correlated with the content of porosity in the cast ingots. Some of their results are given in Fig. 2-4. A modification in hot-working sequences was made to promote a complete welding of gas porosity. A combination of forging and rolling followed by an appropriate heat-treatment was compared with direct rolling, and it has been found to maintain satisfactory short-transverse properties at somewhat higher levels of hydrogen. A fine structure of ingot was also found to have a positive effect on resisting the notch effect of gas porosity. It improved the short-transverse properties at a given hydrogen

level [37].

2.2 DEGASSING ALUMINUM MELTS

2.2.1 Introduction

With the discussions of the deleterious effects of hydrogen on the properties of aluminum and its alloys in the previous section, it is not difficult to understand the necessity of degassing for the purpose of lowering the hydrogen content in the final castings. Fortunately there exist a critical value of hydrogen content as described in the previous section and shown in Fig. 1-2, below which inter-dendritic porosity does not form. This sets finite attainable objectives for the removal of hydrogen from industrial melts before casting.

2.2.2 Mechanisms of Hydrogen Elimination

Two mechanisms of hydrogen elimination from aluminum melts has been described by certain authors [25,38,42]. The first one is precipitation by which hydrogen can escape in the form of small bubbles which rise to the surface. Precipitation will occur only when supersaturation develops enough internal gas pressure, p_i , to overcome the external pressure, P_E .

This internal pressure of the melt is regarded as to be in equilibrium with $P_{H_2} = (\gamma_H X_H / K)^2$,

given in Eqn. (2.14). If a hydrogen bubble forms in the aluminum melt, the total external

pressure, P_E , from Eqn. (2.14), is [38,42],

$$P_E = P + \frac{2T}{r} \quad (2.16)$$

where P is the pressure on the melt being equivalent to P_{liq} of Eqn. (2.14), T is the surface tension of the melt, and r is the radius of the bubble. The second term in the right hand side of Eqn. (2.16) is the $P_{surface}$ of Eqn. (2.14). Similar expression was given by Flemings [25]. We can see from Eqn. (2.16) that at the beginning of bubble formation when r is extremely small, P_E is very large. Consequently, the internal pressure, p_i corresponding to $(\gamma_H X_H / K)^2$, must be very great to overcome P_E to cause precipitation. This condition indicates the reason for the occurrence of supersaturation of gas. This will occur when a gassed melt at high temperature is cooled down to a low temperature near the solidification point, or when the melt is evacuated.

The second mechanism of gas elimination, which is the principle means of gas escape from aluminum melts, is a diffusion-adsorption model. The hydrogen atoms diffuse in the melt or are carried by convection current or by agitation of the melt to a gas-liquid interface. If the hydrogen atoms adsorbed on this interface are not sufficient to be in equilibrium with those in the melt, the hydrogen atoms in the melt will be adsorbed on the interface at a faster rate than they diffuse into the melt. Similarly, if the atmosphere next to the gas-liquid interface contains less moisture than required to maintain the equilibrium hydrogen level on the interface, the hydrogen atoms on the interface will desorb or escape from the melt surface to the atmosphere more rapidly than they are adsorbed from the atmosphere. Therefore, the hydrogen atoms in the melt escape more rapidly than they are absorbed, and the melt is gradually degassed. It is

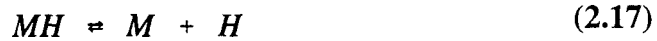
conceivable that a use of an atmosphere low in moisture on top of melt surface will reduce the supply of atomic hydrogen and facilitate degassing. Mechanical stirring can help the hydrogen atoms diffuse faster to the melt surface where they will be adsorbed and escape to the atmosphere. Bubbling the melt with an inert gas has the same effect, and most foundry degassing processes work on this principle [3,25,38,42].

2.2.3 An Overview of the Methods of Degassing

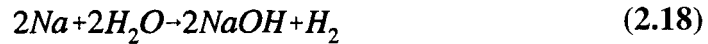
Hydrogen escapes from molten aluminum by evaporation from the melt surface [38-41], but the process is very slow. Cibula [40] indicated that gas-forming elements are accessible to the melt during virtually the whole of the melting-casting cycle, so that the final hydrogen concentration results from a balance between the rates of simultaneous pick-up and loss of the gas. The control of gas, therefore, depends on accelerating hydrogen removal, for which several techniques have been developed as summarized by Eastwood [38]. These techniques include: (i) the use of a hydride former to precipitate hydrogen from the melt as an inclusion, (ii) degassing by mechanical or sonic vibration, (iii) degassing by using a dry atmosphere, and (iv) degassing by solidification and remelting. The most commonly used methods in aluminum industry, however, are bubbling an insoluble gas through the melt to act as a purge and vacuum degassing [3,25,42], which use the mechanisms described previously. The following is a brief description for each of these degassing techniques.

- 1. Degassing by the use of a hydride former.** This is a familiar method of

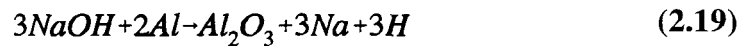
removing gas dissolved in liquid metal. It could be described by the following equation,



Where **M** is the element forming hydride. There are a number of elements, given by Eastwood [38], that form exothermic salt-like hydrides which are stable at room temperature: Li, Na, K, Rb, Cs, Ca, Sr, and Ba. And there are also various elements that form exothermic hydrides which are volatile at room temperature: B, Si, Ge, P, As, Sb, Bi, Se, and Te. The state in molten aluminum of the hydrides formed from above listed elements could be either (a) as an insoluble solid, liquid, or vapour; or (b) as a soluble hydride in the liquid metal. To remove hydrogen from aluminum melts, the first condition is needed. It is obvious from Eqn. (2.17) that if the hydride, **MH**, is insoluble in liquid metal and if it could precipitate out, the reaction would proceed from right to left, and the melt would be degassed. The application of this method was hardly found in the literature review, but there was indeed some discussions on the effects of sodium which is one of the elements that form salt-like hydrides. Sodium affects the hydrogen content in liquid aluminum in two different ways depending on its state when it is added to the melt. Degassing effect was observed if it was used in the form of sodium salt [38]. This may be because sodium or its hydride, NaH, being volatile, may escape and take away some of the hydrogen with it, and degas the metal. The addition of metallic sodium, in the contrary, gases the melt because of the presence of **NaOH** on the melt surface, which is formed as follows:



The aluminum will absorb the hydrogen atoms in the **NaOH** by the following reaction,



This effect of sodium reaction with moisture on top of aluminum melts on the increase of hydrogen content has also been reported by Gruzleski [42] in his book on the process of liquid aluminum.

2. Degassing by vibration. Relatively more discussions were found concerning this method [38,40,42]. The principle is that if the liquid aluminum is supersaturated with hydrogen with respect to a dry atmosphere, it will lose hydrogen by precipitation to the atmosphere, which is the first mechanism of gas elimination described previously in section 2.2.2. In this mechanism, an external energy in the form of various vibrations will facilitate this process by providing necessary nuclei on which hydrogen precipitates. The limitation of this method, according to Gruzleski [42], is two-fold. Firstly it is very slow, and hence, a long time is needed to degas the aluminum melt to a reasonable low hydrogen level. Secondly, it could not be used in all the cases because it needs the condition of supersaturation of liquid aluminum with hydrogen which happens only under special situations. For a general purpose, however, the gas contents in aluminum alloys could in some cases be adequately controlled merely by allowing the melt

to stand in air to let hydrogen diffuse away [40]. The percentage of porosity of one inch diameter sand-cast bars of Al-4.5%Cu alloy, shown by Cibula [40], was decreased significantly by only allowing a period of 30 min of quiescence of the melt. This method is usually combined with the use of dry atmosphere free of hydrogen over the melt or lowering the melt temperature to make the absorbed gas in the melt supersaturated with respect to the atmosphere over it [42].

3. Degassing by using a dry atmosphere. This method is quite different in principle from the previous one, as it uses the second mechanism of gas elimination, i.e. the diffusion-adsorption mechanism described in the previous section. As previously mentioned, the dry atmosphere around the melt or above the melt surface will reduce the supply of atomic hydrogen and make the melt supersaturated with hydrogen in respect with the dry atmosphere around it. It is not difficult to understand, however, that the dry atmosphere alone would be slow. Therefore, this method is usually utilized with a device for stirring the melt which will aid diffusion of hydrogen atoms to the dry surface [25,38,40,42]. The dry gas should contain very low moisture. It could be air, nitrogen, helium, etc [38]. In the present investigation, the liquid DURALCANTM was degassed using this method. The dry gas employed was nitrogen dried with CaO.

4. Degassing by solidification and remelting. This method is based on the consideration that hydrogen will precipitate during solidification, as discussed

previously, and is retained in pores in diatomic state which is not readily reabsorbed. If the metal is remelted immediately, that part of hydrogen which comes from the metal surface will be eliminated, and if the metal surface is a big factor in gas absorption, some gas will be removed by using this method. If the situation is such that most of the hydrogen comes from the atmosphere during melting, the process of solidification and remelting will not be very effective. This is also the major disadvantage in principle of the degassing method [38]. In any case, this method of degassing has rarely been seen in the literature review.

5. Vacuum degassing. This is an effective technique for degassing molten metals [25], for aluminum melts, however, it is not widely used [38,42]. In specific situations like the case of liquid DURALCAN™ composites, though, vacuum degassing can be used to avoid loss of reinforcing particles that could otherwise be purged out if the method of bubbling insoluble gas through the melt is used. Vacuum degassing uses the first mechanism of gas elimination where hydrogen precipitates and forms gas bubbles which are removed by pumping system. The elimination of atmospheric pressure over the melt surface facilitates the formation of hydrogen gas bubbles inside the melt [42], since the value of P_E , given in Eqn. (2.16), becomes smaller [38]. It is evident that the rate of vacuum degassing depends upon the rate of nucleation of gas bubbles and the speed of gas bubbles moving to the melt surface. The time required to degas liquid metal of considerable depth to a satisfying gas level, therefore, would be very long if no

external power is used to facilitate these processes . To degas efficiently and rapidly, it is important to form bubbles and to bring them to the melt surface. This could be implemented by pouring metal through vacuum as a thin film or sheet of liquid [25,38] to give maximum exposure to the evacuated surface; or by stirring of the melt to bring the gas-contained metal to melt surface [25,38,42]. The disadvantage of this method of degassing is that the equipment is expensive [38,42,45], and its application could also be limited because of the possible loss of sodium or other modifiers from aluminum-silicon alloys causing coarse silicon particles [38].

6. Degassing by fluxing an insoluble gas through the melt. This method is by far the best developed and the most widely used degassing method in the aluminum industry [3,25,38,42,44]. The principle of this method is, the second mechanism of gas elimination described previously, that hydrogen atoms in liquid diffuse into a gas-liquid interface provided by insoluble gas bubbles within the melt, where no hydrogen is present and where they are desorbed to form diatomic hydrogen inside the bubble. The hydrogen escapes into the atmosphere as the inert gas bubbles rise. Degassing by this method is a physical process thus it does not depend on the composition of the inert gas used [3], provided that the purge gas does not contain water vapour, oxygen, and it does not form insoluble solid nor form films on the bubble surfaces which will block the transfer of hydrogen across the gas-liquid interface [3,38,42]. Any gas or volatile materials could be used for

this purpose if they meet the above requirements [38]. The commonly used purge gases, varying for different circumstances, include pure dry nitrogen, argon, and chlorine. Dry nitrogen is considered the most widely used fluxing agent [44]. It has the advantage of being inert [44], however, the disadvantage of nitrogen is that it produces dross on top of aluminum melt [38]. It forms aluminum nitride ($\text{Al} + \text{N}_2 \rightarrow \text{AlN}$ with the equilibrium constant \mathbf{K} in the order of 10^{11} at 1000 K) which will remain suspended in the melt [44]. Nitrogen is also the least effective fluxing agent [38,44]. Argon is believed more effective than nitrogen, but it is also more expensive [44]. Chlorine is the most effective purge agent [3,38,44]. Its effect is two fold: degassing, and removing inclusions which will exacerbate the effect of hydrogen [3]. However, there are considerable objections to it because of its toxicity and corrosive effects [38,42,44]. It also has disadvantages of coarsening the grain, lowering sodium content of Al-Si alloys, and lowering the magnesium content of the melt [38]. Instead of pure chlorine, various mixtures of inert gas and chlorine are in use [42,44]. This includes the mixtures of nitrogen-chlorine and argon-chlorine with various chlorine concentrations. Mixtures of nitrogen and freon has recently been considered as effective as pure chlorine and in many ways better [42,44]. In addition to gases, there are also solid fluxes which vaporize at high temperature to generate gas bubbles. The most popular of these is hexachloroethane [3,42,44] which decomposes at temperatures above 700 °C. Limitations of this method are dross formation [42] and unpleasant fumes generated by hexachloroethane [42,44]. Since these materials are hygroscopic

[38,42], cares should be taken to keep them dry, otherwise they will introduce hydrogen into the melt rather than remove it. Fluxing gas could be introduced into the melt in many ways. The most referred, however, are the uses of lance, porous plug, or rotary impeller. A water model study shows that a graphite lance can only produce large bubbles, and a rotary impeller can give much finer and dispersed bubbles [42]. The effectiveness of a rotary impeller, therefore, is much higher. A porous plug can produce finer dispersion of bubbles than a straight graphite lance, it is more effective than lance but less effective than rotary impeller [23,42,46]. In modern aluminum industry, in-line degassing is widely employed, which is basically working on the principle of the rotary impeller, and through which aluminum melt is degassed during the transfer from furnace to casting machine [3,15].

2.2.4 Degassing Efficiency and Determining Factors

As indicated previously, the most widely used degassing process in modern aluminum industry is based on the method of gas purging, the degassing efficiency discussed, therefore, would be based on this method of degassing. To evaluate degassing efficiency, it is necessary to have a clear understanding of the whole procedure of gas removal, which could be considered consistent with the following successive steps [10,12,23,42]:

1. Transport of hydrogen atoms in molten aluminum to the surface of purge gas bubbles by

a combination of diffusion and convection.

2. Diffusive transport of hydrogen atoms through a thin stagnant boundary layer of liquid at the bubble surface.
3. Reaction of atomic hydrogen into diatomic hydrogen ($H+H \rightarrow H_2$), adsorption of hydrogen molecules onto and subsequent desorption from the bubble surface.
4. Diffusion of hydrogen molecules inside the bubble of purge gas.
5. Removal of hydrogen at the melt surface.

Varying from different situations, any one of the above steps could be the controlling step of the whole process except steps 4 and 5 [11,12,23,42].

To perform a mathematical analysis of degassing efficiency, we can first take a look at a sketch of the horizontal section of a gas purging control volume shown in Fig. 2-5 with width Δh [11,12,23]. A mass balance could be established, under appropriate assumptions, that the hydrogen leaving this control volume of the melt equals to the hydrogen entering the gas phase, i.e.,

$$\frac{k_t \rho ([\%H] - [\%H]_e) \Delta A}{100 M_H} = 2 \dot{G} \Delta \left(\frac{P_{H_2}}{P_{inert}} \right) \quad (2.20)$$

Where k_t is the total mass transfer coefficient which represents the diffusion through the boundary layer, ρ is melt density, $[\%H]$ is equilibrium hydrogen content, M_H is the molecular

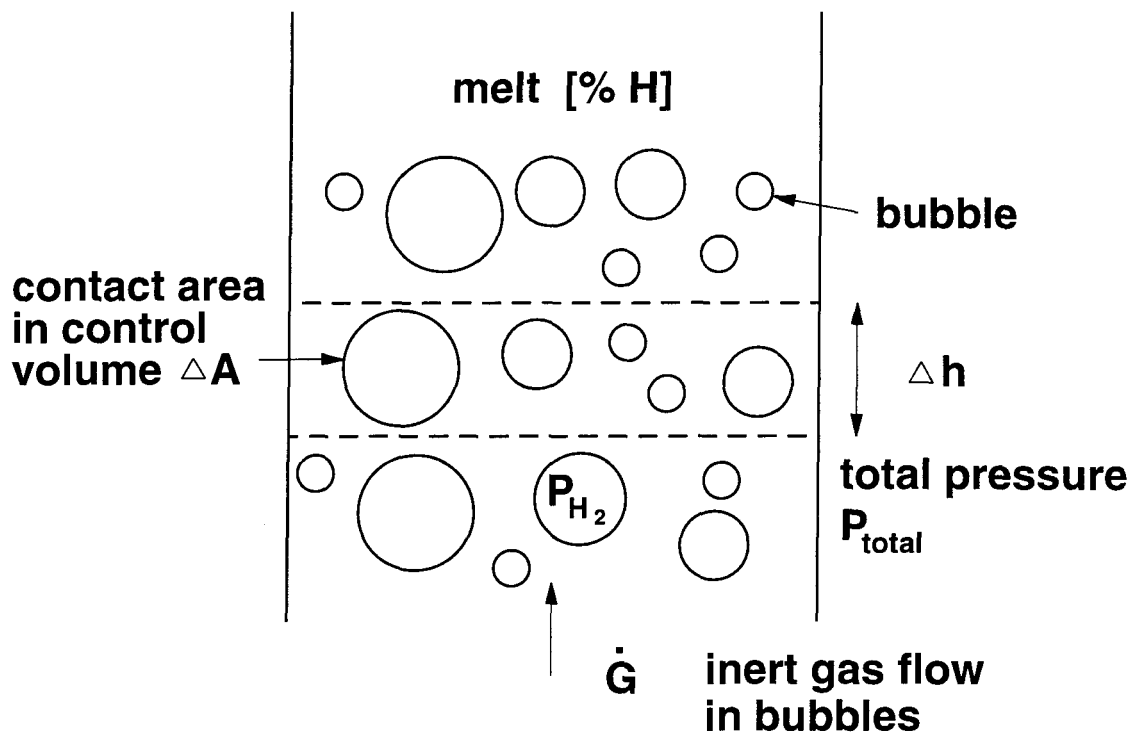


Figure 2-5. Gas purging control volume [23].

weight of hydrogen atom, \dot{G} is the flow rate of inert gas, and p_{H_2} and p_{inert} are hydrogen partial pressure and inert gas partial pressure inside the purging gas bubbles, respectively. Since the degassing ability to reduce the gas content of the melt can be no better than what the thermodynamic solubility will allow, a process of 100 % degassing efficiency could be defined as one in which the partial pressure of hydrogen in the purge gas bubble equals the partial pressure of hydrogen dissolved in the melt [42]. After proper integration and transformation, Eqn. (2.20) becomes [23]

$$\frac{\Psi}{[\%H]} = \int_0^{Z^0} \frac{ZdZ}{(1-Z)} \quad (2.21)$$

Where the left-hand side term of Eqn. (2.21) is called dimensionless contact area,

$$\frac{\Psi}{[\%H]} = \frac{k_i \rho A p_{inert}}{400 M_H \dot{G} f_H^2 [\%H] K_H^2} \quad (2.22)$$

and

$$Z^2 = \frac{P_{H_2}}{f_H^2 [\%H]^2 K_H^2} \quad (2.23)$$

Z^0 is obtained by setting $P_{H_2} = P_{H_2}^0$ in Eqn. (2.23),

$$(Z^0)^2 = \frac{P_{H_2}^0}{f_H^2 [\%H]^2 K_H^2} \quad (2.24)$$

Eqn. (2.21) gives the relationship between degassing efficiency, $(Z^0)^2$, and dimensionless contact area, $\Psi/[\%H]$. This relationship is also shown in Fig. 2-6. It can be seen from Fig. 2-6 that to have a higher degassing efficiency, a bigger value of $\Psi/[\%H]$ is needed. From Eqn. (2.22) we know that a larger total surface area of bubbles, A , will lead to a bigger value of $\Psi/[\%H]$. Consequently, the diameter of the bubbles becomes the most important factor in determining the degassing efficiency [11,12,23,42]. A large number of smaller bubbles will (i) give a larger surface area for a given volume of purge gas; (ii) give a longer time of contact during which they can absorb hydrogen because smaller bubbles rise more slowly; and (iii) be close together and

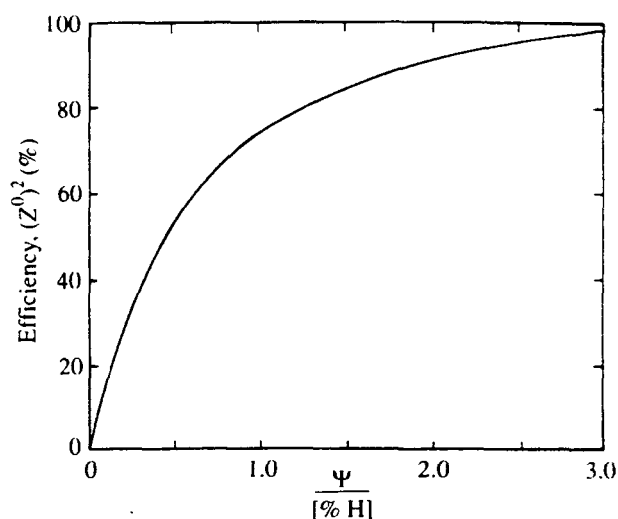


Figure 2-6 Degassing efficiency $(Z^0)^2$ vs the dimensionless bubble contact area $\Psi/[\%H]$ [23].

facilitate hydrogen transport. On the contrary, larger bubbles, for a given flow rate, will (i) give a smaller surface area; (ii) rise more rapidly because they are more buoyant; and (iii) be far apart and take a longer time for hydrogen atoms to diffuse to the bubble surface. Fig. 2-7 shows the effect of bubble size on degassing efficiency, and in Fig. 2-8 degassing efficiencies are compared with three different degassing techniques that give different bubble sizes. Like bubble size, melt temperature plays a role in determining degassing efficiency [11,23,42]. Hydrogen solubility decreases with decreasing melt temperature, i.e. the value of K_H in Eqn. 2.22 is smaller at a lower melt temperature, therefore, the dimensionless contact area $\Psi/[\%H]$ is larger at lower melt temperature. Degassing should be carried out at the lowest melt temperature possible for a particular operation [42].

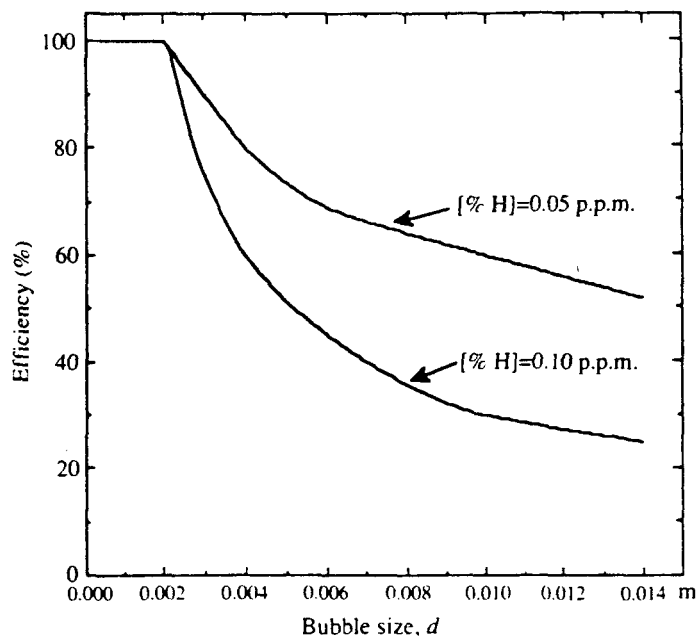


Figure 2-7 Degassing efficiency as a function of purge gas bubble size for two melt hydrogen concentrations [23].

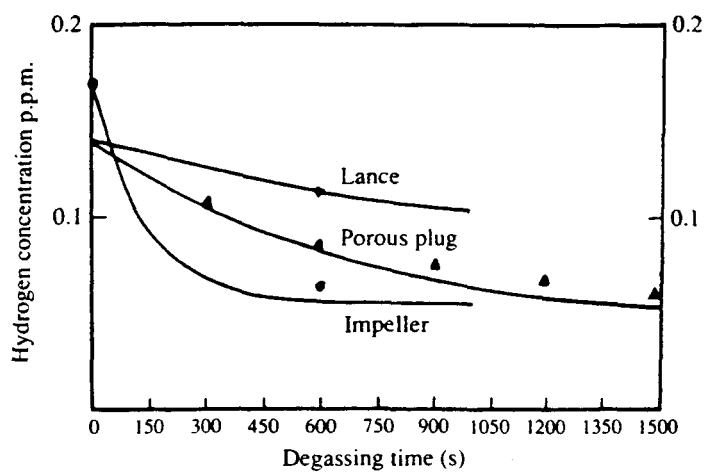


Figure 2-8 degassing performance of a lance, porous plug, and an impeller [23].

2.3 HYDROGEN ABSORPTION IN ALUMINUM MELTS

2.3.1 Introduction

Because of the deleterious effects of hydrogen on the properties of castings of aluminum and its alloys, the knowledge needed to deal with foundry degassing problems cannot be overemphasized. In addition to the study of degassing, which is intended for lowering the level of hydrogen contained in an aluminum melt, a study of hydrogen absorption is of the similar importance, which is to assure a clear understanding of both the mechanisms and the procedure of hydrogen absorption process in aluminum melts, and, further, to find out ways to avoid, to some extent, the occurrence of this process. The absorption of gases in aluminum involves three main processes [38]: (i) adsorption, (ii) diffusion, and (iii) solution. Solution and solubility of hydrogen in liquid aluminum have been discussed earlier in section 2.1. A description of the first two processes and the mechanisms of hydrogen absorption will be given below, and methods to avoid hydrogen absorption will be considered at the end of this section.

2.3.2 Adsorption of Hydrogen on Melt Surfaces

As indicated in section 2.1.3, most hydrogen in molten aluminum comes from the dissociation of hydrogen molecules produced by the reaction of water vapour in the atmosphere and aluminum according to Eqn. 2.11 as follow:



What has not been pointed out is the detailed procedure of hydrogen absorption into an aluminum melt thereafter. The first step of hydrogen absorption is the adsorption of hydrogen onto the metal surface. Adsorption is the condensation of the gas at the metal surface from which it may pass into the interior by diffusion. Hydrogen atoms provided by the dissociation of these hydrogen molecules ($H_2 \rightarrow H + H$), according to Eastwood [38], are adsorbed on the melt surface before diffusion; or as claimed by Engh [23] that it is the water vapour that is adsorbed on the melt surface before the reaction given in Eqn. (2.25) takes place. What is of most importance is that there is an adsorption of hydrogen-atom containing species on top of melt surface before the diffusion of hydrogen atoms into the melt. This completes the first step of hydrogen absorption. This adsorption of hydrogen atoms onto the melt surface is under the category of activated adsorption which has the following features [38]:

1. The amount of activated adsorption increases with temperature to a maximum and then decreases.
2. Inert gases do not undergo this type of adsorption, it being specific between gases and metals, depending on the chemical attraction between the gas and metal.
3. In many cases the gas is dissociated, it being present on the surface in atomic rather than molecular form.
4. It is not reversible with respect to temperature changes, but in some instances it may be reversible with respect to pressure changes if the adsorption is not strong.
5. Activated adsorption increases with the $1/n$ 'th power of the pressure p . At lower

pressures, the adsorption is approximately proportional to pressure, i.e., $1/n$ is unity; at intermediate pressures, $1/n$ is less than unity; and at high pressures, the adsorbed film becomes complete and the adsorption is no longer affected by the pressure.

6. The reversibility and stability of this kind of adsorbed film vary greatly just as the stability of chemical compounds may vary.

2.3.3 Diffusion of Hydrogen in Liquid Metals

Most diffusion studies have been of solid metals. In the case of liquid metals, the problem of predicting, correlating, and extrapolating diffusion data is very difficult because of our lack of understanding of the structure of liquid metals [47]. Eqn. 2.26 still applies in liquids if there is no convection [23],

$$\dot{n} = -D \frac{\partial C_2}{\partial z} \quad (2.26)$$

where \dot{n} is the flux of solute particles and C_2 is their concentration. The remarkable characteristic of diffusion in molten metals is the fact that the values of the diffusion coefficient D are almost all of the same order of magnitude, 10^{-8} - 10^{-9} m²/s, even though their solid state properties differ widely. A convenient equation of predicting diffusion coefficient in liquids is from Einstein equation for Brownian motion [23],

$$D = \frac{\kappa_B T}{3\pi\mu d} \quad (2.27)$$

where κ_B is Boltzmann constant, T is melt temperature, μ is the viscosity of liquid metal, and d is the diameter of diffusion particles. A slightly modified equation was presented, and it was claimed to have a good agreement with experimental values of diffusion in liquid metals [47]:

$$D = \frac{\kappa_B T}{2\pi\mu d} \quad (2.28)$$

In fact D increases with decreasing mass of diffusing atoms, which could be partially explained in terms of interstitial movement between the larger atoms. Taking this factor into account, Einstein's equation becomes [23],

$$D = \frac{\kappa_B T}{2\pi\mu d} \left(\frac{m_1 + m_2}{2m_2} \right)^{\frac{1}{2}} \quad (2.29)$$

For hydrogen in aluminum at 1000 K, the calculated value from Eqn. 2.29, $D = 0.9 \times 10^{-7} \text{ m}^2/\text{s}$, which is in good agreement with experimental value, $D = 10^{-7}$ to $10^{-8} \text{ m}^2/\text{s}$.

2.3.4 Mechanism of Hydrogen Absorption

The mechanism of hydrogen absorption becomes evident with the discussions of adsorption and diffusion previously [38]. Hydrogen atoms produced by the reaction of aluminum with moisture in atmosphere are adsorbed on the melt surface. These adsorbed hydrogen atoms diffuse into the melt and form Al-H solution. New hydrogen atoms supplied by the moisture in atmosphere replace the old ones, and more hydrogen is dissolved in the aluminum melt. This

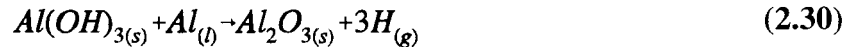
process continues until a thermodynamic equilibrium between the moisture in the atmosphere and the hydrogen content in the melt is established at a given melt temperature. The final hydrogen content in the melt, therefore, depends on:

- (i) The amount of moisture in the atmosphere(The greater the amount of moisture is, the greater the supply of hydrogen atoms, and the greater the quantity and rate of diffusion into the melt);
- (ii) Melt temperature(Hydrogen solubility increases with temperature, higher temperature will lead to more hydrogen content in the melt); and
- (iii) Time(Since diffusion needs time, longer absorption time allows more hydrogen atoms to diffuse into the melt until it is saturated with respect to melt temperature and moisture level in the atmosphere.

Al_2O_3 skin on the melt surface could prevent or slow down hydrogen absorption [14,38]. Its protective effect is probably due to the fact that the reaction with moisture is reduced or prevented, reducing the hydrogen supply, while other factors may also play their part, such as the unlikely adsorption of hydrogen atoms on the oxide surface and the blocking of diffusion.

Moisture could also be introduced under the melt surface by inserting un-preheated tools in the melt. Aluminum reacts with the moisture and produces oxide and hydrogen atoms, which adsorb on the metal-gas interface on the surface of the bubble and diffuse into the melt. As indicated previously, surface gas on ingot or scrap is another source of hydrogen. This may provide hydrogen through sources other than water vapour. One example is the contaminates on

scraps. Partly corroded aluminum can add hydrogen by the decomposition of the corrosion products, aluminum hydroxide, through the reaction [42]:



with its equilibrium constant **K** being in the order of 10^2 at 1000 K.

2.3.5 Method of Avoiding Hydrogen Absorption

It is always best to avoid hydrogen absorption, because a badly gassed melt will need a lot of effective degassing to reduce its gas content to a tolerable level. A regular degassing process can produce a melt of very low hydrogen content if the initial gas content is low.

The sources of hydrogen listed in section 2.1.2 indicate the way in which hydrogen can be absorbed. It also guides foundry workers to keep gas absorption to a minimum. Moisture in the atmosphere is a major source of hydrogen, and it is difficult to control. One means is to introduce dry atmosphere over the melt [38]. There are some methods, though, to avoid absorption of hydrogen from the moisture in the atmosphere [38,42]:

- (a) Care should be taken to break the oxide layer on the melt surface as infrequently as possible, because it is an effective barrier to hydrogen pick-up. The stirring actions or melt additions should be made as gently as possible.
- (b) When pouring, effort should be made to minimize the height of metal fall and turbulence, i.e., to minimize the contact between liquid metal and air, because a degassed melt will re-gas quickly. Therefore, care should be taken in the pouring

operation to keep the pouring point low, near the pouring box on the mold, and no free falls should be permitted. The use of pumps is recommended to pump liquid metal through conduits so all contact with air is minimized during metal transport.

- (c) Sources of hydrogen could be eliminated as much as possible by drying the foundry tools, flux, and mold before the melt operation.
- (d) The gas from the surface of the charge can be avoided by: (i) keeping a minimum of time between the production of ingot and the operation of remelting; (ii) avoiding corrosion of the ingot; (iii) avoiding the accumulation of foundry scrap; and (iv) preheating the ingot before remelting.
- (e) Overheating and prolonged holding should always be avoided because hydrogen solubility increases with temperature and more hydrogen will be absorbed in a longer time.

CHAPTER 3
EXPERIMENTAL PROCEDURE

CHAPTER 3

EXPERIMENTAL PROCEDURE

3.1 MATERIALS

3.1.1 Materials

Two kinds of DURALCAN™ composites and their matrices were selected for this present investigation. They were: the foundry DURALCAN™ composite, F3S.20S (Al-Si-Mg/SiC_(p)); and the wrought DURALCAN™ composite, W6D.22A (6061/Al₂O_{3(p)}). The choice was made based on the order of importance of all the foundry and wrought families of DURALCAN™ composites. All the materials used in this work was supplied by the Dubuc Plant of Alcan International Limited in Québec, Canada.

3.1.2 Description of Materials

The chemical compositions of the matrices of W6D.22A and F3S.20S composites are given in Table 3-1. The reinforcing phase in the W6D.22A composite is calcined aluminum oxide powder. The chemical composition of the powder is at least 98.5% Al₂O₃ and the particle size distribution has a D50 of 20.8 ± 6 μm. The volume percentage of particulate in W6D.22A

composite is 22 ± 2 volume percent. The reinforcing phase in the F3S.20S composite is silicon carbide powder. The chemical composition of the powder is at least 98% SiC and the particle size distribution has a D50 of 12.8 ± 1.0 μm . The volume percentage of particulate in the composite is 20 ± 2 volume percent. Photomicrographs of these two composites are shown in Fig. 3-1.

The materials were available in the form of ingots of about 10 Kg each for composites and about 15 Kg each for the matrix alloys. Fig. 3-2 shows schematically the dimensions of the ingots of the composites and their matrices.

Table 3-1 Chemical Compositions of the Matrices of W6D.22A and F3S.20S

Material	Si	Fe	Cu	Mn	Mg	Cr	Zn	Ti	All Other Elements	Al
W6D.22A*	0.50	0.7	0.19	0.15	0.87	0.10	0.25	0.15	0.15 Tot.	REM.
	0.65	max	0.28	max	1.20	0.15	max	max	0.05 max.	
F3S.20S	8.5	0.20	0.20	0.10	0.45		0.05	0.20	0.10 Tot.	REM.
	9.5	max	max	max	0.65		max	max	0.03 max.	

* same chemistry as Aluminum Association Alloy 6061.

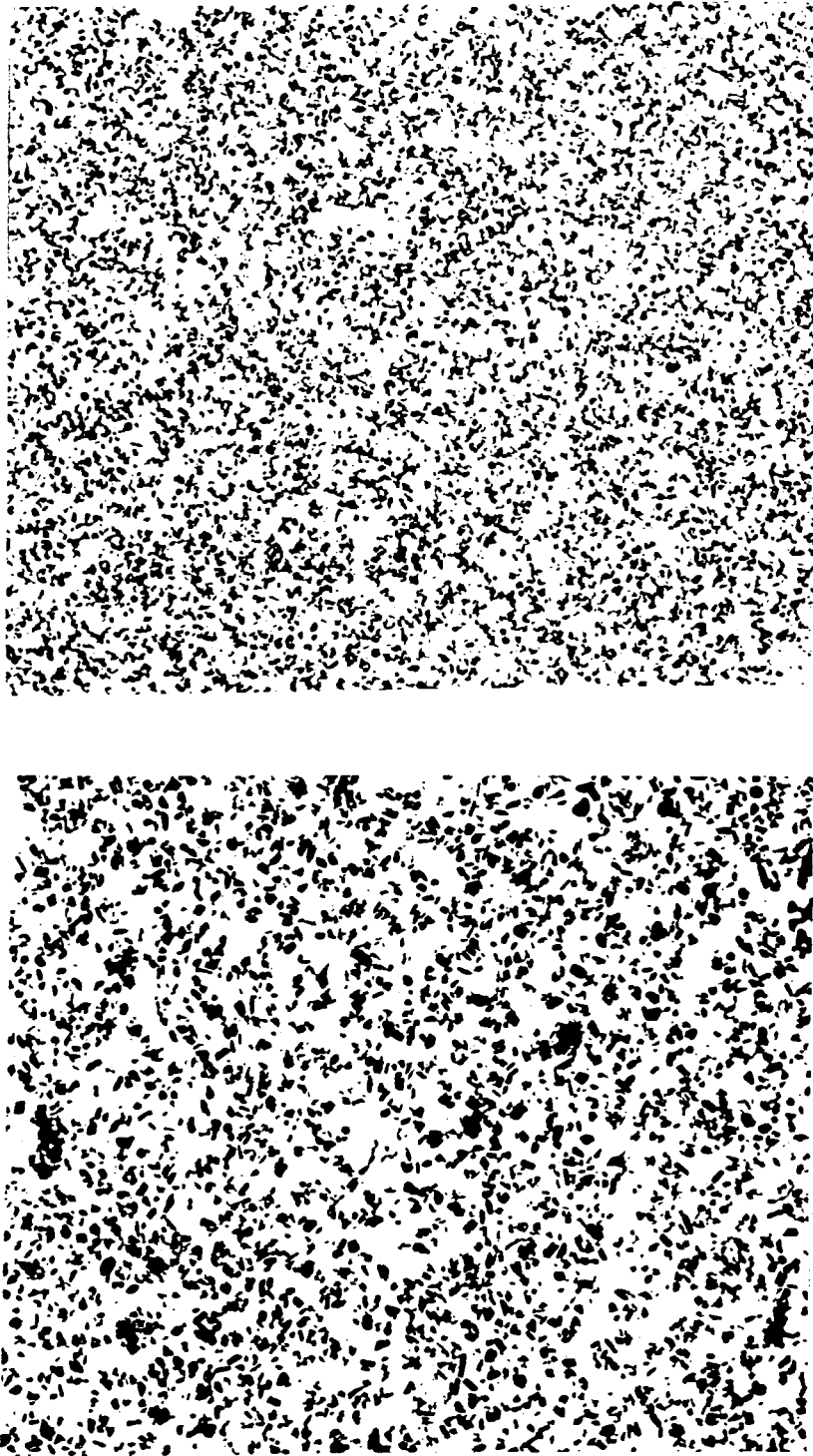


Figure 3-1. Photomicrographs of two DURALCANTM composites, F3S.20S (above), and W6D.22A (below). 50×

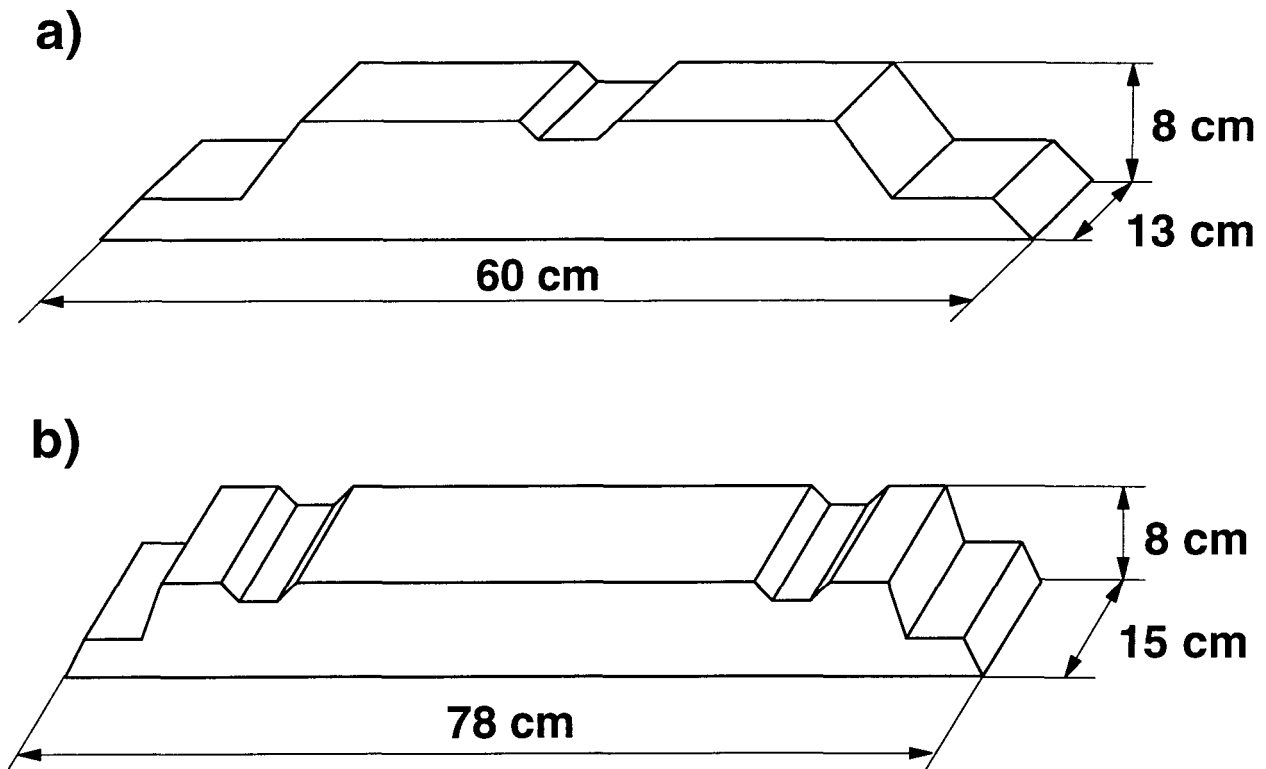


Figure 3-2. The ingots of DURALCANTM composites and their matrices, (a) composites, and (b) matrices.

3.2. DESCRIPTION OF THE EXPERIMENTAL SETUP

3.2.1 The Furnace and the Crucible

One furnace is needed in this investigation for heating and melting the sample, and

holding the liquid metal at a given temperature during the processes of degassing and re-absorption. The furnace used was a PYRADIA electric resistance furnace with a power of 6 kw. The advantages of using this furnace is rapid melting of the alloys and effective temperature control. The liquid metal was contained in a SiC crucible with a capacity of about 10 kg of aluminum. The inner surface of the crucible was coated with a layer of refractory coating to avoid the contamination of the melt. It is safe to assume that hydrogen cannot pass the walls of the crucible. This is equivalent to say that the only interface between the atmosphere and liquid metal is the surface of the melt, and the only source of hydrogen is the reaction with the moisture in the atmosphere on top of the melt surface. This is important especially in the analysis of the effect of the ratio of melt surface to its volume on hydrogen absorption. Temperatures of the furnace and the melt were monitored by two thermocouples and controlled by PID controllers separately. The furnace and the crucible for melting and holding the molten metal are shown schematically in Fig. 3-3.

3.2.2 The Stirrer and the Protection Gas

During the processes of degassing and hydrogen re-absorption of DURALCANTM composites, it is necessary to stir the melt to avoid the sedimentation of ceramic particles. This was implemented in the present investigation by using a mechanical stirrer made of graphite with adjustable rotation speed. In the experiments on the matrix alloys, the stirrer was also used to keep the experimental conditions constant. In the process of degassing, an inert gas was blown in the gap between the melt surface and the cover of furnace to provide a dry atmosphere and

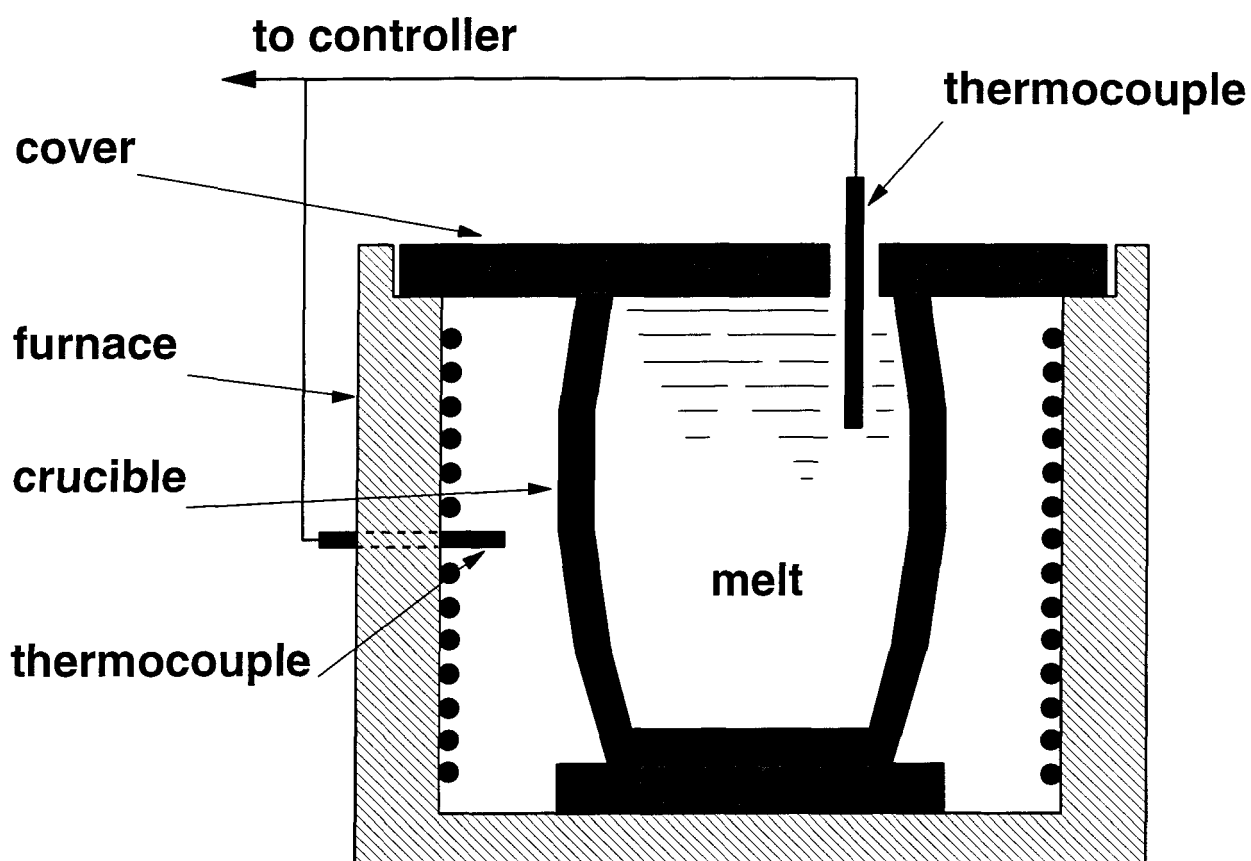


Figure 3-3. A schematic showing the furnace and the crucible used in the experiments.

facilitate degassing. Argon was tried earlier in the investigation, but it had been rejected because of its unwanted effect on Alscan readings. Nitrogen does not have this shortcoming, and it was chosen for this purpose. A flowmeter was used to control the flow rate of nitrogen. The gas was dried by passing through a chamber of CaO before reaching the melt surface. Fig. 3-4 shows the use of stirrer and the nitrogen during degassing.

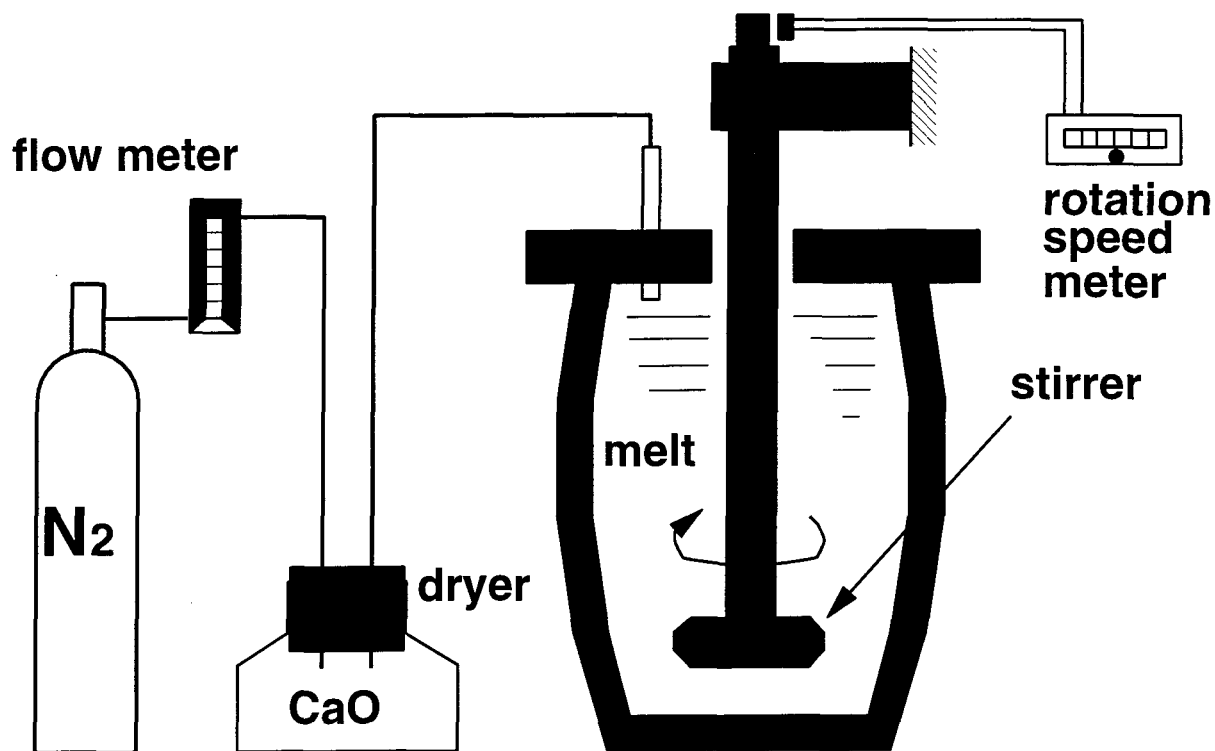


Figure 3-4. The use of stirrer and nitrogen in the experiment.

3.3 DEGASSING AND RE-ABSORPTION

3.3.1 Melting of the Materials

A melt of about 10 kg was needed for each experiment (except for the experiments on the effect of melt surface/volume ratio). The ingots of the right amount were cut into segments small enough to fit the crucible. Every piece of metal were carefully cleaned with water and

thinner, and the scraps were also removed to reduce the initial hydrogen content coming from the metal surface. Metal sample was always dried completely before melting. This is necessary for reducing the possibility of hydrogen absorption before degassing and for avoiding the occurrence of explosion. Some of the pieces could be put in the crucible while heating, they were dried completely before melting. The remaining pieces of metal, in the mean time, were piled up on top of furnace cover where it could be dried before adding into the melt. Once the metal in the crucible was molten, the remaining pieces were put in the melt. They should be added into the melt piece by piece until all the metal samples were molten. After all the metal was molten, the stirrer was immersed into the melt. Care was taken to place it in not too close to the bottom of the crucible and no touching was allowed while it was rotating. Two thermocouples were employed: one for melt temperature control, the other for Alscan. The thermocouples did not have any contact with the stirrer. Before the stirrer and thermocouples were put into the melt, and also before the addition of a new piece of metal, the melt surface was always skimmed to make sure no oxide dross was introduced into the melt. The melt temperature was maintained at about 710 °C where, recommended by industry, most foundry operations are conducted. The melt, at this moment, was ready for the process of degassing.

3.3.2 Degassing of the Aluminum Melt

The whole experiment could be divided into two parts: degassing and re-absorption. It was indicated in chapter 2 that insoluble gas purging is the most commonly used degassing method. In the case of this present investigation, however, this method could not be used because the

ceramic particles in DURALCAN™ composites could possibly be purged out along with hydrogen. Another method using dry atmosphere was employed instead to degas the molten DURALCAN™ composites and their matrix alloys in this investigation. This was performed simply by isolating the melt surface from the atmosphere with an insoluble gas (nitrogen) maintained between a refractory plate and the melt surface at a given flow rate. As described in chapter 2, this degassing method uses diffusion-adsorption model of gas elimination. The use of a stirrer in this work was basically for the purpose of avoiding the sedimentation of ceramic particles in molten DURALCAN™ composites. In the view of degassing, however, the major effect of stirring was to aid the diffusion of hydrogen atoms in molten metal and consequently to facilitate the degassing process. This was important as it allowed the assumption that the hydrogen content was homogeneous throughout the melt during the whole degassing and also during the re-absorption processes. Therefore, the diffusion of hydrogen atoms through the liquid-gas interface was obviously the rate controlling step.

Once the melt was ready, a degassing process could begin, and this process took two to four hours, depending upon the initial hydrogen content in the melt, the environmental condition, and the material, to degas the melt to a satisfactory gas level (0.10 - 0.15 ml/100g). The degassing process is depicted in Fig. 3-5(a). It involved the following steps:

1. Introduce a protection gas (dry N₂ in the present case) on top of the melt surface, and adjust its flow rate to a given value. Three levels of nitrogen flow rate were used: 10, 15, and 25 cfh (cubic foot per hour).

2. Skim the melt surface; put Alscan probe into the melt and start Alscan measurements and data acquisition.
3. Turn the stirrer manually to make sure there is no contact with other objects. Start the stirrer, and increase its rotation speed slowly to a prescribed value of about 100 rpm. The same rotation speed was used for all the experiments in this present investigation.
4. Close the cover of the melt. Adjust the temperature controller to stabilize the melt temperature at about 710 °C.
5. Once the Alscan reading shows that the melt gas content has been lowered to a certain level, stop the degassing process and start re-absorption by removing the protection gas and opening the cover to expose the melt surface to the atmosphere.

3.3.3 Hydrogen Re-absorption of the Melt

The second major step of the experiment was hydrogen re-absorption. When the melt was degassed to a certain level of gas content, it was ready for the process of re-absorption. As indicated in the previous section that the wall of the crucible could be considered non-permeable to moisture or hydrogen atoms, therefore, the main source of hydrogen was the reaction with water vapour in the atmosphere at the liquid-gas interface on top of the melt surface. This was critical to the analysis of hydrogen absorption. It was also important to conduct experiments in days with different levels of humidity, because the humidity level, i.e., the water partial pressure

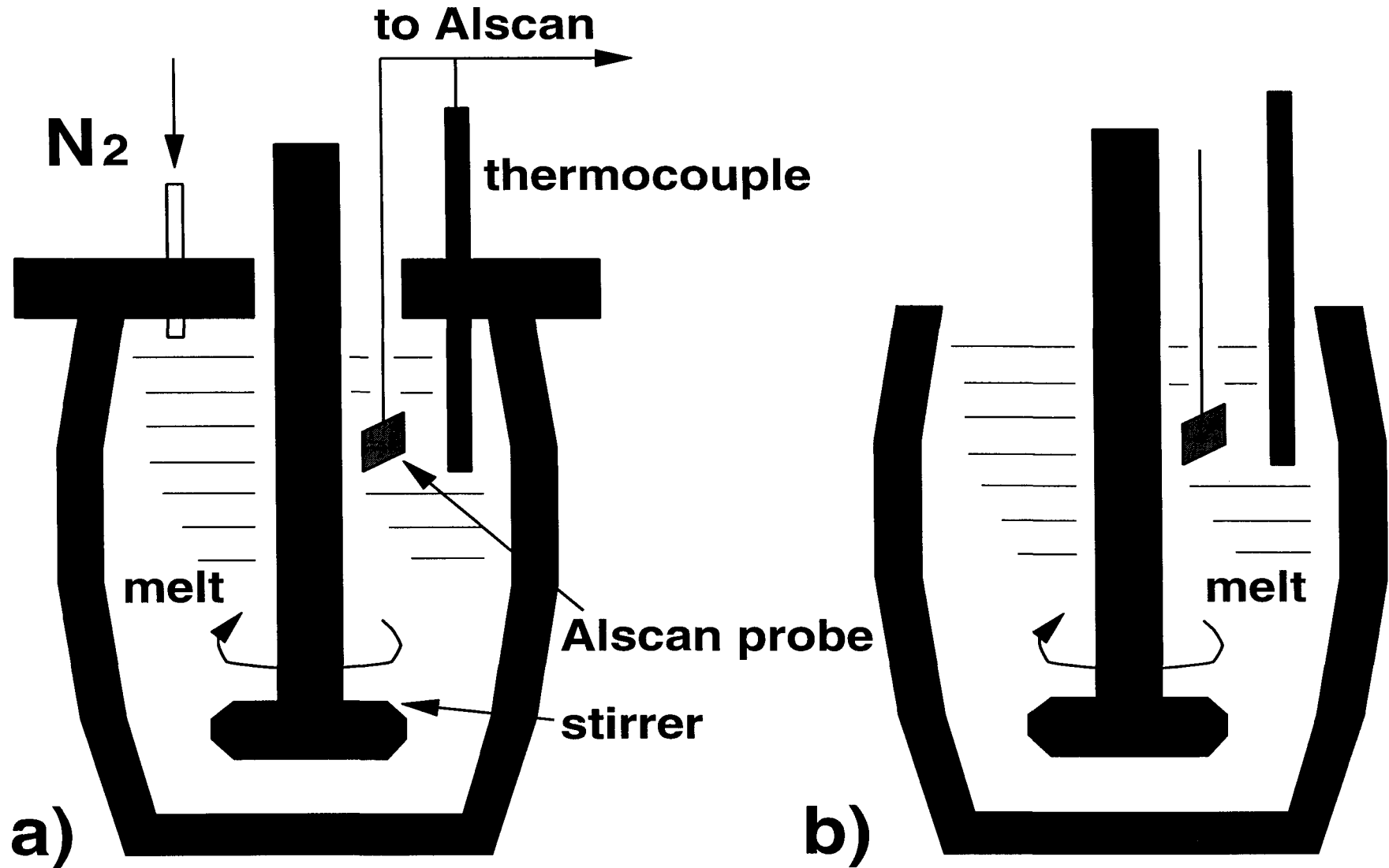


Figure 3-5. A schematic illustration of degassing and hydrogen re-absorption, (a) degassing, (b) re-absorption.

in the atmosphere, is a major factor affecting the behaviour of hydrogen absorption in liquid aluminum, and absorption values measured with various water partial pressures were needed in the analysis. The oxide layer on top of the melt plays an important part in hydrogen re-absorption. Therefore, it was necessary not to destroy this oxide layer during the re-absorption process. Hydrogen re-absorption started immediately after the termination of degassing process. Depending on the environmental condition and the material, it usually took three to five hours to have an equilibrium hydrogen content. This process is schematically shown in Fig. 3-5(b), and following steps were involved:

1. By the end of degassing process, adjust the furnace temperature to minimize the melt temperature fluctuation due to the removal of the cover over the melt surface.
2. Close the protection gas and remove its conduction tubes.
3. Open the cover and let the melt surface completely exposed to the atmosphere.
4. Watch the melt temperature closely, adjust the furnace temperature if necessary to keep the melt temperature stable at 710 ± 5 °C.
5. Monitor the hydrogen content readings given by Alscan until it reaches an equilibrium value, then stop the re-absorption process.
6. Stop the stirrer and Alscan, remove the Alscan probe and the thermocouples. Remove the

stirrer, close the furnace and empty the crucible. Prepare for the next experiment.

3.3.4 Measurement of the Humidity Level

The relative humidity level and room temperature are important because they are directly related to water partial pressure in the atmosphere. The latter is a critical factor affecting the degassing and hydrogen absorption behaviour in liquid aluminum. In this present investigation, relative humidity and room temperature were measured every one hour during the whole degassing and hydrogen re-absorption processes. This was done by using two thermometers, one was dry and the other was wet, the relative humidity value could be evaluated from the difference between the readings of the dry thermometer and the wet one. With the value of relative humidity and the corresponding room temperature, a value of the water partial pressure could be obtained from a table available in a Handbook of Chemistry and Physics [57]. The environmental and other conditions for the experiments in this investigation are summarized in Table 3-2.

3.4 EFFECT OF SURFACE-TO-VOLUME RATIO ON HYDROGEN ABSORPTION

The ratio of the melt surface to its volume, A/V , is of interest in the analysis of hydrogen absorption of liquid aluminum when the main source of hydrogen is the reaction of liquid metal with water vapour at the liquid-gas interface on top of the melt surface. This effect was experimentally evaluated in this present investigation by comparing the hydrogen absorption parameters obtained from experiments with different values of surface area/volume ratio. This

Table 3-2 A Summary of the Experimental Conditions

Material	No	N ₂ Flow Rate (cfh)	Room Temperature	Relative Humidity	P_{H_2O} (mm Hg)
W6D.22A	WC1	~ 15	22 ~ 23 °C	40 ~ 46 %	8.42 ~ 9.12
	WC2	~ 10	26 °C	26 %	6.55
	WC3	~ 10	22 °C	30 %	5.95
	WC4	~ 15	28 °C	53 %	15.03
	WC5	~ 15	23 °C	55 %	11.59
Matrix of W6D.22A	WM1	~ 25	20 ~ 22 °C	20 ~ 17%	3.37 ~ 3.51
	WM2	20 ~ 25	20 °C	23 %	4.03
	WM3	20 ~ 25	20 °C	44 %	7.72
	WM4	~ 15	26 °C	37 %	9.33
	WM5	~ 15	30 °C	50 %	15.91
F3S.20S	FC1	~ 15	19.5 °C	33 %	5.35
	FC2	~ 15	21 °C	32 %	5.97
	FC3	~ 15	20.5 °C	45 %	8.09
	FC4	~ 15	20 °C	18 %	3.16
	FC5	~ 15	22.8 °C	8 %	1.67
Matrix of F3S.20S	FM1	~ 15	20 °C	51 %	8.63
	FM2	~ 15	20 °C	24 %	4.21
	FM3	~ 15	21.5 °C	43 %	8.32
	FM4	~ 15	20 °C	24 %	4.21
	FM5	~ 25	20 °C	24 %	4.21
	FM6	~ 15	19.5 °C	11 %	1.87
	FM7	~ 15	19 °C	9 %	1.48

Note - The following conditions were the same for all experiments:

Sample Charge: ~ 10 Kg
Melt Temperature: ~ 710 °C
Stirrer Rate (rpm): ~ 100

was implemented by three experiments with different amounts of metal. Since the change in surface area of the melt is very small comparing to the change in melt volume with the crucible shown in Fig. 3-3, considerably different surface area/volume ratio can be obtained if different amount of metal is used in experiments. The details of the three experiments are given in Table 3-3. The matrix alloy of F3S.20S composite was used in the experiments with the same experimental conditions, and the same experimental procedure was followed.

Table 3-3 Values of the Ratio of Melt Surface Area to its Volume

No.	Amount of Metal (kg)	Percentage of Total (%)	Area/Volume Ratio (cm)
1	11.09	100	0.0502
2	8.56	77	0.0650
3	7.65	66.7	0.0752

3.5 MEASUREMENT OF HYDROGEN CONTENTS

3.5.1 Introduction

The measurement of hydrogen content in this investigation was of central importance because the parameters of degassing and hydrogen absorption were calculated from the data of hydrogen content in molten DURALCANTM composites and their matrices measured at different times during degassing and absorption processes, respectively. Many techniques have been developed for the measurement of hydrogen content in aluminum and its alloys [48-55]. In the present work, Alscan analyzer was used to measure the hydrogen content in molten

DURALCAN™ composites and their matrices, because Alscan can give a direct measurement of the hydrogen contained in molten aluminum with a short response time which makes it possible to monitor the variation in melt hydrogen content in the course of degassing and hydrogen re-absorption. In the following sections, a brief description of the principles of Alscan and its operations will be given, and the measurement procedure in this investigation will also be presented.

3.5.2 Theory of Operation

Alscan works on the basis of Sieverts' law given in Eqn. (2.4), which can also be written in the following format:

$$C(T, \alpha, p_{H_2}) = K(T, \alpha) \sqrt{p_{H_2}} \quad (3.1)$$

where C represents the amount of hydrogen dissolved in molten aluminum at equilibrium, T is the melt temperature, α represents the alloy chemical composition, K is the equilibrium constant which varies with the melt temperature and chemical composition, and p_{H_2} is hydrogen partial pressure. With a certain degree of approximation, $K(T, \alpha)$ in Eqn. 3.1 could be expressed as a product of two factors, $K_1(T)$, and $K_2(\alpha)$, each depending only on one parameter. Taking into consideration of hydrogen solubility in molten pure aluminum at 700 °C, S_0 , as discussed in chapter 2, Eqn. 3.1 can be re-written as,

$$C(T, \alpha, p_{H_2}) = S_0 \times CF(T) \times CF(A) \times \sqrt{p_{H_2}} \quad (3.2)$$

where **CF(T)** is temperature correction factor, and **CF(A)** is alloy correction factor. **CF(T)** can be easily calculated (as indicated in chapter 2) with the value of melt temperature measured by a thermocouple Alscan is equipped with, and **CF(A)** is provided for every commercial alloy by the supplier of Alscan. The amount of hydrogen dissolved in molten aluminum could be determined by immersing a probe in the melt. An inert gas (nitrogen) circulating in a closed loop collects the hydrogen diffused into the probe from the melt. Hydrogen content could be calculated with Eqn. 3.2 from the amount present in the closed gas loop of the instrument at equilibrium (i.e. the p_{H_2} within the circulation of $N_2 + H_2$ mixture).

3.5.3 A Description of Alscan Analyzer

3.5.3.1 The Probe

One of the most important parts of the instrument is the probe, which is immersed in the molten aluminum during measurement. The probe works as a medium that allows hydrogen diffuse into the nitrogen circulating through the melt. The probe is made of ceramic material which must meet the following requirements: (i) porous, (ii) chemically stable in molten aluminum, and (iii) resistant to thermal and mechanical shocks. The porous part is connected to the recirculation unit by means of stainless tube protected by ceramic coating. A sketch of an

Alscan probe is shown in Fig. 3-6.

3.5.3.2 The Recirculation Loop

The recirculation loop of Alscan analyzer is the central part of this instrument. It measures the hydrogen partial pressure, p_{H_2} , of the H_2/N_2 mixture in equilibrium with the hydrogen in the melt, from which the hydrogen content in the melt is calculated. The recirculation loop consists of diaphragm pump, a gas thermal conductivity measurement cell, probe connectors, and inter-connection tubing. The hydrogen contents in H_2/N_2 mixture is determined continuously by a thermal conductivity cell (catharometer). Hydrogen originating from the melt adds to the nitrogen in the gas loop and increases the thermal conductivity of the gas mixture because of its low molecular weight. This can give an explanation as to why argon was rejected from use as a protection gas during degassing. Argon gas could possibly penetrate into the Alscan probe immersed in the melt and change the thermal conductivity of the gas mixture, and as a result Alscan will give a wrong reading of the melt hydrogen concentration. The recirculation loop is shown in Fig. 3-7. Besides the recirculation loop, an Alscan analyzer also consists of (i) a gas supply that provides high purity nitrogen, (ii) electronic boards for calculation, interface, data acquisition, power supply, and display, and (iii) a recessed keyboard which allows the user to change operation parameters. Fig. 3-8 shows schematically the function of Alscan analyzer.

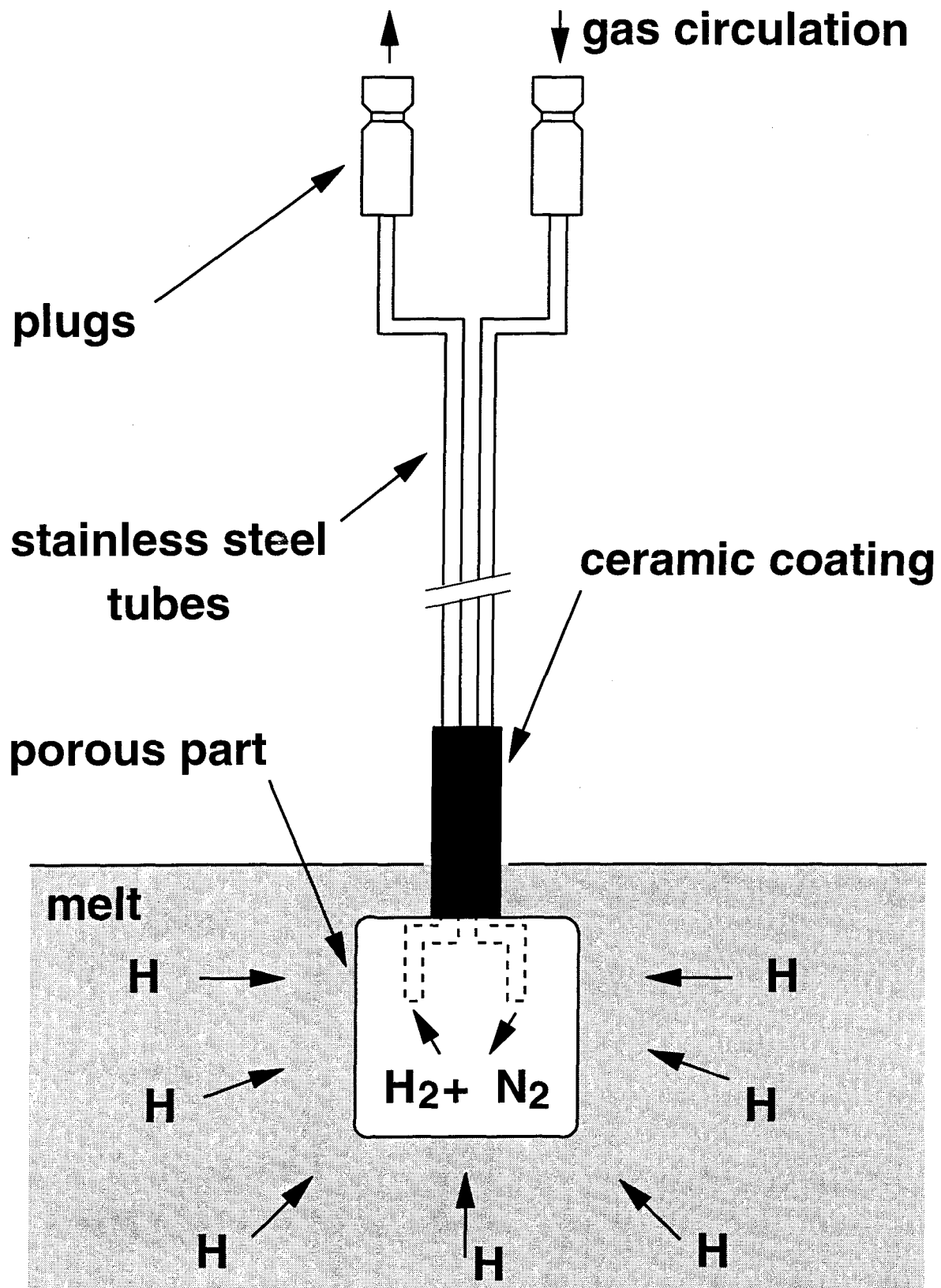


Figure 3-6. A sketch of an Alscan probe [49].

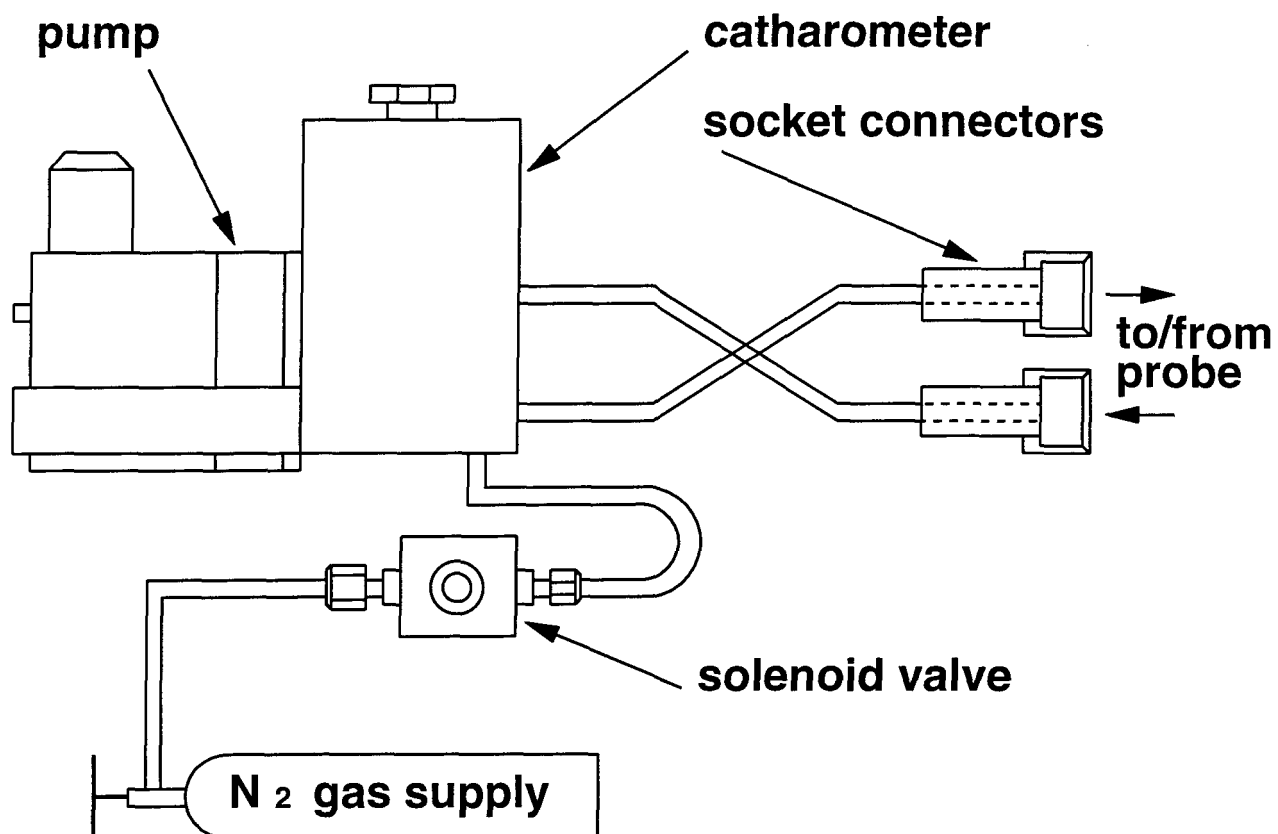


Figure 3-7. The recirculation loop of an Alscan analyzer [49].

3.5.4 Measurement Procedure

The measurement of hydrogen contents in molten DURALCAN™ composites and their matrix alloys was performed in the following order: (1) Set up operation parameters; (2) Install the probe and connect the thermocouple (already immersed in the melt) to the analyzer; (3) Connect the analyzer to data acquisition system with communication cable (as shown in Fig. 3-8) and start the data acquisition software; (4) Immerse the probe in the melt, put the porous part of the probe about 4 cm down the melt surface, and start Alscan; (5) At the end of measurement

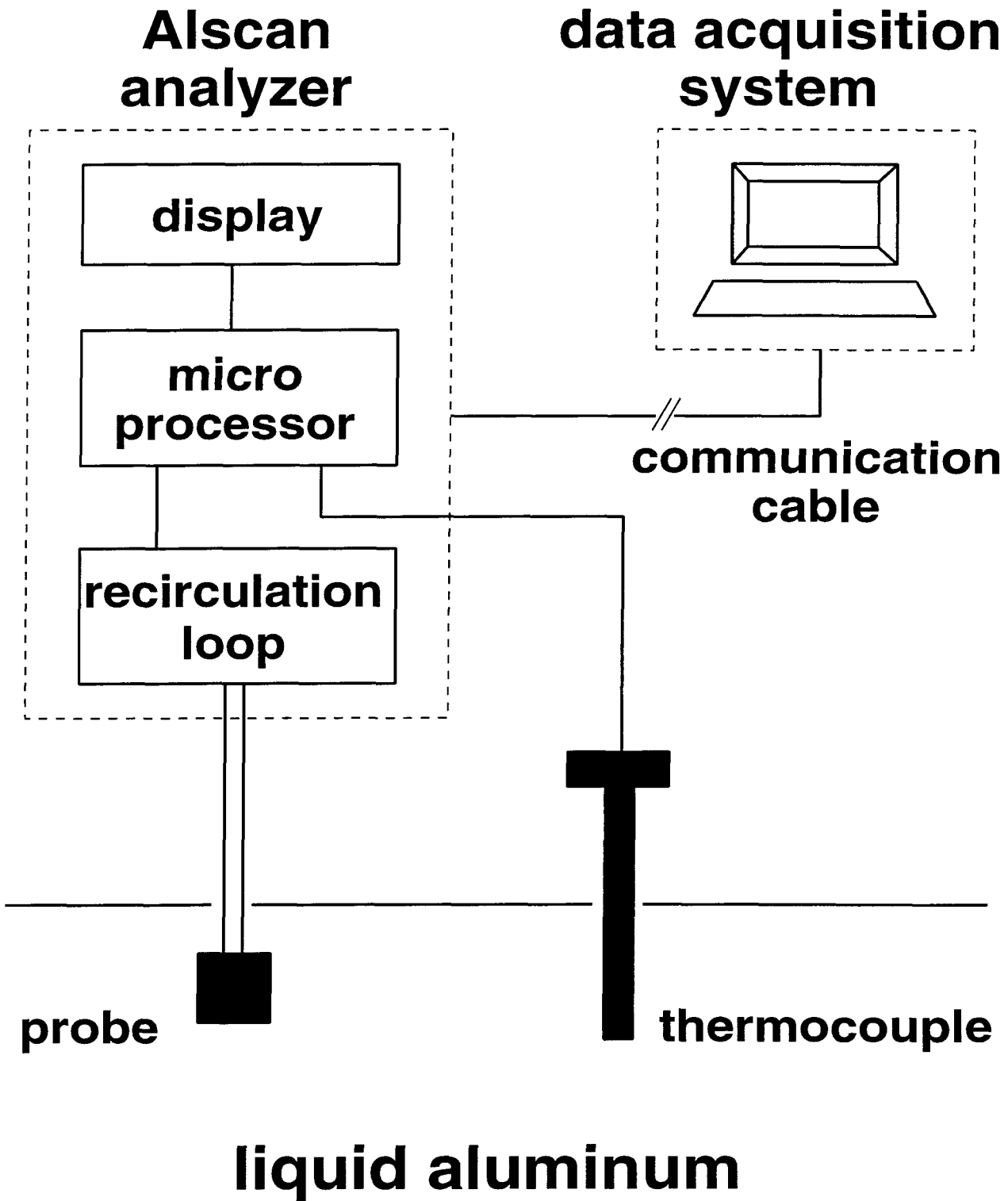


Figure 3-8. A schematic illustration of the function of Alscan analyzer [48,49].

(when the hydrogen re-absorption finishes), stop data acquisition, remove the probe from the melt and stop Alscan. It is conceivable that correct settings of operation parameters are critical to an accurate measurement. Some of the most important operation parameters are discussed below:

1. Alloy Correction Factor. As seen previously, Alscan works on the principle of Sieverts' law and an alloy correction factor, $CF(A)$, is needed in the calculation of hydrogen content in the melt of a certain aluminum alloy. In the present work, two DURALCAN™ composites, W6D.22A and F3S.20S, were investigated with their matrix alloys. An alloy correction factor of 1.01 for the Alloy 6061 given in Alscan user's manual [49] was used for W6D.22A composite and its matrix alloy because they have the same chemical composition. The alloy correction factor for F3S.20S composite and its matrix alloy was calculated according to its chemical composition with the following equation also given in the Alscan user's manual,

$$CF(A) = 10^{(0.0170 \times \%Mg - 0.0269 \times \%Cu - 0.0119 \times \%Si)} \quad (3.3)$$

An alloy correction factor of 0.80 was finally used for F3S.20S and its matrix alloy in the measurement.

2. Alscan Cycle Time. A cycle is the duration of one measurement. It varies between predetermined values of 3, 5, 10, and 15 minutes. One Alscan cycle should be long enough to allow for the establishment of an equilibrium between the hydrogen in the melt and that in the gas recirculation unit. This time varies with chemical composition of the alloys. For pure aluminum, 10 min is sufficient.

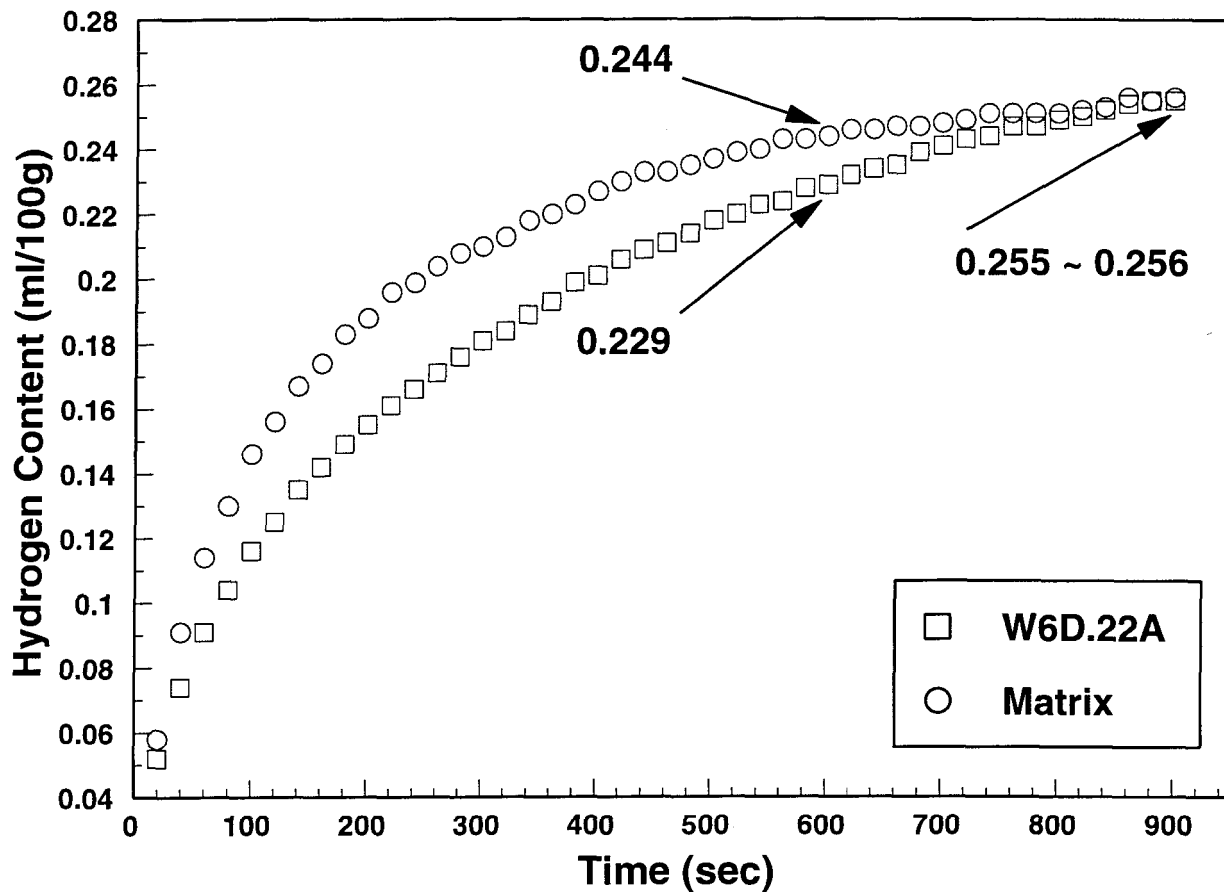


Figure 3-9. Alscan dynamic curves for W6D.22A composite and its matrix alloy.

In the case of DURALCANTM composites, however, 15 min is required to achieve the necessary equilibrium conditions for measurement. Fig. 3-9 shows the Alscan dynamic curves for W6D.22A composite and its matrix alloy. It is seen that the difference between the readings of hydrogen content at 10 min (600 sec) and at 15 min (900 sec, and that the end of the cycle) is over 10 % for W6D.22A composite. This difference should be smaller than about 10 % for a satisfactory measurement. Therefore, a cycle time of 15 min is really necessary for W6D.22A composite. For its matrix alloy, this difference was smaller (about 5 %), but the same cycle time was actually used to keep the experimental condition identical for

all the materials. A 15 min cycle time was also used for F3S.20S composite and its matrix alloy because the shapes of their Alscan dynamic curves were similar.

3. Other Parameters. Apart from the two most important operation parameters discussed above, some other parameters were set in this work as follow: (i) Purge Time was set to 5 sec, i.e., the duration of one purge with pure nitrogen was 5 seconds; (ii) Number of Purges was set to 3, i.e., there were three times purge operations between two measurements; (iii) Sample Interval was set to zero, i.e., there was no interval between measurements; and (iv) Number of Samples was set to 10, i.e., Alscan would execute ten consecutive measurements without stopping.

CHAPTER 4

**APPROACH TO MATHEMATICAL ANALYSIS OF
DEGASSING AND ABSORPTION**

CHAPTER 4
APPROACH TO MATHEMATICAL ANALYSIS OF
DEGASSING AND ABSORPTION

4.1 INTRODUCTION

It has been noted in chapter 2 that the processes of hydrogen absorption and degassing of an aluminum melt are those of hydrogen atoms transport into and out of the liquid aluminum. This includes the diffusion of hydrogen atoms within the melt, the transport of hydrogen atoms through the metal-gas interface, and the diffusion of hydrogen in the gas phase. In this chapter, the kinetics of these processes will be analyzed mathematically. In order to do this, a review of necessary concepts of mass transfer is given and then mathematical models are set for both degassing and hydrogen absorption. The experimental data obtained from this present work will be processed according to this analysis, and the method of data processing is presented at the end of this chapter.

4.2 INTERPHASE MASS TRANSFER

4.2.1 Mixing

It is conceivable that the diffusion of hydrogen atoms within molten aluminum can be accelerated by stirring or mixing the melt. In this present work, mixing was performed by using a mechanical stirrer. In the following discussion on degassing and hydrogen absorption, it will be assumed that stirring is sufficient. This means that the hydrogen concentration in the bulk aluminum melt is constant, and therefore, independent upon spatial coordinates. To characterize mixing, a concept of mixing time τ_m is introduced as [23]:

$$\tau_m \sim 100 \times \left(\frac{L^2}{\dot{\epsilon}} \right) \quad (4.1)$$

where L is the characteristic vessel dimension, and $\dot{\epsilon}$ is the energy dissipation which characterizes turbulence. In the present investigation, the energy dissipation could be estimated to be $\dot{\epsilon} \sim 1.5 \text{ W/kg} = 1.5 \text{ m}^2/\text{s}^3$, and L , the diameter of the crucible, is about 0.2 m. Eqn. (4.1) gives $\tau_m = 20 \text{ s}$. Since the duration of the processes of degassing and hydrogen absorption usually lasts several hours, it is evident that the melt is completely mixed. This also means that the resistance to the transfer of hydrogen atoms inside the bulk metal could be ignored.

In the case of the present investigation, there are two phases: a liquid phase of the

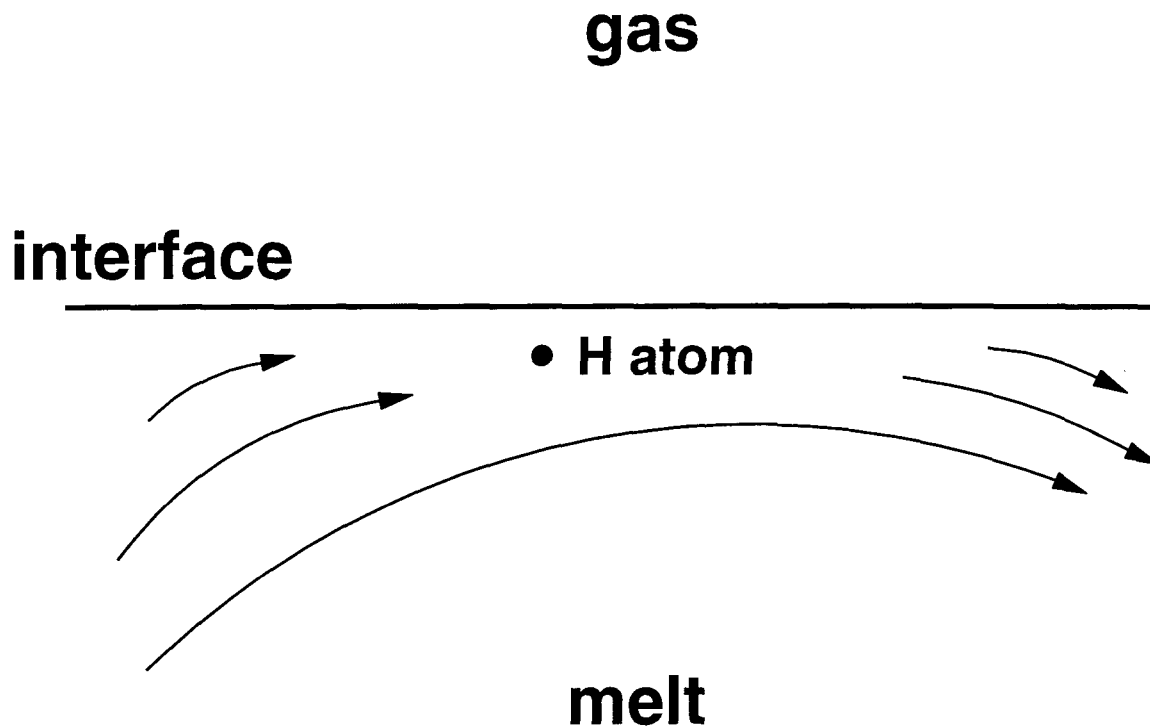


Figure 4-1. Velocities are low along the interface so that the transfer of H atoms depends on the slow mechanism of diffusion [23].

aluminum melt and a gas phase of the atmosphere. At the interface, the surface of the melt, the movement of hydrogen atoms is parallel to the interface and not normal to it, as illustrated in Fig. 4-1. The main mechanism of transport of hydrogen atoms is no longer convection or turbulent eddies, but a slow mechanism of diffusion. Then a mass transfer coefficient, k , for the melt boundary layer (not for the bulk melt) is important in the description of the transport of hydrogen atoms. Actually for a transfer between two phases it is necessary to take into account the resistance to transfer on both sides of the interface. This will be discussed in the following section.

4.2.2 The Mass Transfer Coefficient

In the study of hydrogen absorption and degassing of liquid aluminum, which are processes controlled by the transport of hydrogen atoms into and out of an aluminum melt, it is convenient to introduce the concept of mass transfer coefficient. For the sake of being general, here we consider a species A (not necessarily hydrogen atom in liquid aluminum) and its molar flux in the x-direction, N_{Ax} , as the sum of a diffusive contribution, $\mathbf{j}_{Ax} = -CD_A \partial X_A / \partial x$, and a bulk flow contribution, $C_A \mathbf{v}_x^*$, expressed as follow [47]:

$$N_{Ax} = -CD_A \frac{\partial X_A}{\partial x} + C_A v_x^* = C_A v_{Ax} \quad (4.2)$$

where C is the total molar concentration in the solution, D_A is diffusivity, \mathbf{v}_x^* is the local molar average velocity in the x-direction, and \mathbf{v}_{Ax} is the velocity of A in the x-direction. However, a mass transfer coefficient for transfer of A into or out of a phase is defined in terms of diffusive contribution normal to the interface:

$$k_M = \frac{j_A^0}{C_A^0 - C_{A\infty}} = - \frac{D_A (\partial C_A / \partial x)_{x=0}}{C_A^0 - C_{A\infty}} \quad (4.3)$$

The superscript 0 refers to quantities evaluated at the interface, and $C_{A\infty}$ to the bulk concentration of A within the fluid. It should be noted that at interfaces involving a fluid phase, there could be an additional contribution to mass transfer caused by bulk flow. The mass transfer coefficient in Eqn. (4.3) is defined only in term of diffusive contribution rather than of the total flux N_A^0 , because it is expected to have the diffusion flux approximately proportional to a concentration difference as indicated in Eqn. (4.3), whereas the bulk flow contribution can be relatively

independent of any concentration difference. Actually, in the present investigation, as indicated previously, the bulk melt flow itself is less important to the transport of hydrogen atoms at the interface. This difference in concentration represents a driving force for the mass transfer. In the case where the bulk flow term is negligible, then,

$$k_M = \frac{N_A^0}{C_A^0 - C_{A\infty}} \quad (4.4)$$

Eqns. (4.3) and (4.4) are only definitional, it must be evaluated by means of various analytical expressions for the flux under particular circumstances. As an example, the coefficient of mass transfer of A into a falling film of liquid is [47]:

$$k_{M,z} = \frac{N_{Ax}|_{x=0}}{C_A^0 - C_{A\infty}} = \sqrt{\frac{D_A v_{\max}}{\pi z}} \quad (4.5)$$

where z is the direction of falling of the liquid film, $N_{Ax}|_{x=0}$ is the mass flux at the surface, and v_{\max} is maximum velocity of the falling liquid.

4.2.3 Mass Transfer in a Two-phase System

In the present investigation, as indicated previously, the main source of hydrogen for the molten DURALCAN™ composites and their matrix alloys is water vapour in the atmosphere. Therefore, the processes of degassing and hydrogen absorption involve the transport of hydrogen atoms in two phases (a liquid phase of the aluminum melt and a gas phase of the atmosphere) and through their interface. In experimental determination of the rate of mass transfer, it is

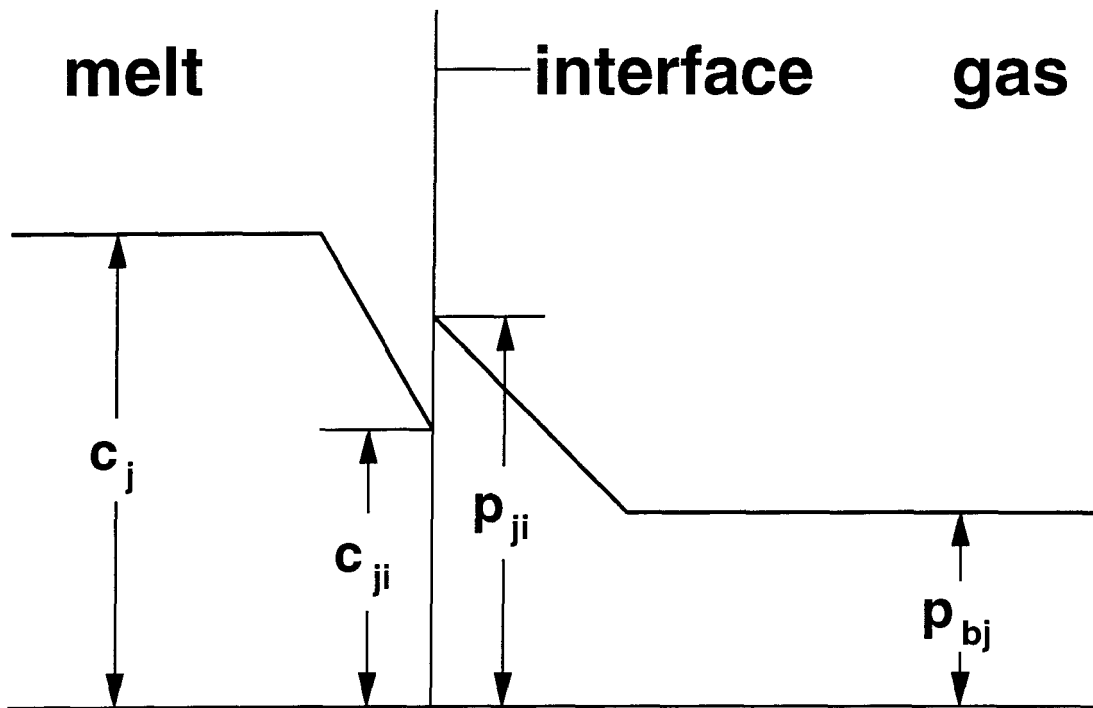


Figure 4-2. A melt-gas system shows the concentrations c_j and c_{ji} in the melt and pressures p_{ji} and p_{bj} in the gas phase [23].

possible to determine hydrogen concentration in the bulk melt and the partial pressure of water vapour in the atmosphere, but it is usually difficult to determine the hydrogen concentration at the interface, because the boundary layer is extremely thin on either side of the interface. In this case it is required to relate the rate of mass transfer to the difference of the two bulk concentrations, and it is convenient to introduce the concept of a total mass transfer coefficient, k_t . For a general melt-gas system depicted in Fig. 4-2, where c_j is the concentration of component j in the bulk melt, c_{ji} is the concentration of j at the melt boundary layer, p_{ji} is the partial pressure of j at the gas boundary layer, and p_{bj} is the partial pressure of j in the bulk gas. The

partial pressure in the gas in equilibrium with the melt is

$$p_j = \gamma_j K_j c_j \quad (4.6)$$

where γ_j is activity coefficient, and K_j is the equilibrium constant. If this pressure is not equal to the partial pressure at the gas boundary layer p_{ji} , there will be a net flux to or from the interface as follow [23],

$$\dot{n}_j = \frac{(p_j - p_{ji})}{RT} \left(\frac{RT}{2\pi M_j} \right)^{\frac{1}{2}} \quad (4.7)$$

or, employing Eqn. (4.6),

$$\dot{n}_j = (\gamma_j K_j c_{ji} - p_{ji}) \frac{1}{\sqrt{2\pi M_j RT}} \quad (4.8)$$

where M_j is the molecular weight of j . It can be seen that if the pressure in the gas phase boundary layer, p_{ji} , and the concentration in the melt phase boundary layer, c_{ji} , are not in equilibrium, there is a net flux of j , and the flux \dot{n}_j has to pass through resistances both in melt phase boundary layer and the gas phase boundary layer on the two sides of the melt-gas interface. That is for melt phase,

$$\dot{n}_j = k(c_j - c_{ji}) \quad (4.9)$$

and for gas phase,

$$\dot{n}_j = \frac{k_g (p_{ji} - p_{vj})}{RT} \quad (4.10)$$

where k and k_g are the mass transfer coefficients for j in the melt and in the gas phase,

respectively. As mentioned above, due to the difficulty in the measurement of c_{ji} and p_{ji} in experiment, it is usually required to obtain \dot{n}_j in terms of the total driving force from the melt with concentration c_j to the gas with concentration p_{bj}/RT for degassing, or from the gas to the melt for absorption. Then Eqns. (4.8)-(4.10) can be rewritten in terms of driving forces:

$$\begin{aligned} \dot{n}_j/k &= c_j - c_{ji} \\ \dot{n}_j \sqrt{2\pi M_j RT} / K_j \gamma_j &= c_{ji} - p_{ji} / K_j \gamma_j \\ \dot{n}_j RT / k_g K_j \gamma_j &= p_{ji} / K_j \gamma_j - p_{bj} / K_j \gamma_j \end{aligned} \quad (4.11)$$

Summation of the two sides of the three equations above yields,

$$\dot{n}_j \left(\frac{1}{k} + \frac{\sqrt{2\pi M_j RT}}{K_j \gamma_j} + \frac{RT}{k_g K_j \gamma_j} \right) = c_j - \frac{p_{bj}}{K_j \gamma_j} \quad (4.12)$$

The total mass transfer coefficient, k_t , can be defined as,

$$\frac{1}{k_t} = \frac{1}{k} + \frac{\sqrt{2\pi M_j RT}}{K_j \gamma_j} + \frac{RT}{k_g K_j \gamma_j} \quad (4.13)$$

$1/k_t$ is equal to the sum of the three resistances from the melt boundary layer, the evaporation, and the gas boundary layer, respectively. The combination of Eqns. (4.12) and (4.13) give the rate of mass transfer for j as follow:

$$\dot{n}_j = k_t \left(c_j - \frac{p_{bj}}{K_j \gamma_j} \right) \quad (4.14)$$

where $p_{bj}/(K_j \gamma_j)$ is the hypothetical concentration in the melt in equilibrium with the partial pressure p_{bj} in the bulk gas. Eqn. (4.14) relates the flux \dot{n}_j to the parameters c_j and p_{bj} which

are experimentally determinable.

4.2.4 Effect of the Ratio of Surface Area to Melt Volume

The area of interface is an important factor in the kinetics of a chemical reaction at the interface of two phases. In the present investigation of hydrogen absorption and degassing of molten aluminum, it is the ratio of the surface area to melt volume that affects the reaction rate, and the transport of hydrogen atoms across the melt surface into or out of the melt is the only way for hydrogen to be absorbed in or removed out of the melt. Therefore, the melt surface, the interface between liquid aluminum and the atmosphere, is the reaction site for degassing and hydrogen absorption. In the definition of mass transfer coefficient and the discussion of mass transfer in a two-phase system given earlier, the effect of the ratio of interface area to melt volume was not presented. In fact, the rate of transport of species A, j_A^0 , shown in Eqn. (4.3), taking into account the ratio of surface area to melt volume, should be expressed as follow [13,56],

$$j_A^0 = k_M \frac{A}{V} (C_A^0 - C_{A\infty}) \quad (4.15)$$

where A is the area of interface, and V is the melt volume. Eqn. (4.15) shows evidently that the transport rate increases with increasing ratio of surface area to volume. In the present work, the effect of this ratio was experimentally evaluated by the experiments listed in Table 3-2. Different values of Area/Volume ratio were used in the experiments with the matrix alloy of F3S.20S composite, and the corresponding rates of degassing and hydrogen absorption were measured,

which will be presented later. In other experiments, a constant value of this ratio was used and the term, kA/V , as a whole was employed in the evaluation of kinetic parameters of degassing and hydrogen absorption. Eqn. (4.15) can be applied to the transport of hydrogen atoms in the melt boundary layer, melt-gas interface, and gas boundary layer expressed in Eqn. (4.11). With respect to the total mass transfer coefficient, we can have an equation, corresponding to Eqn. (4.14), to describe the overall rate of mass transfer as follow,

$$\dot{n}_j = k_t \frac{A}{V} \left(c_j - \frac{P_{bj}}{K_j \gamma_j} \right) \quad (4.16)$$

4.3 MATHEMATICAL MODELS FOR HYDROGEN ABSORPTION AND DEGASSING

4.3.1 Melt-Side and Gas-Side Mass Transfer Resistances

The mass transfer of hydrogen atoms at the melt-gas interface is of particular importance in the present investigation, as mentioned above, because the melt surface is the reaction site for both degassing and hydrogen absorption. Therefore, an analysis is required of the atomic mass transfer in a melt-gas system before establishing the mathematical models for degassing and hydrogen absorption of molten aluminum. Since the melt was well stirred, it is safe to assume that the melt-side mass transfer is dominated by the melt boundary layer and the gas-side mass transfer is dominated by the gas boundary layer.

From Eqn. (4.13), a useful concept can be introduced of the ratio, λ , between resistance in the gas phase and in the melt phase as follow,

$$\lambda = \frac{kRT}{k_g K_j \gamma_j} \quad (4.17)$$

and this ratio has the order of magnitude of [23],

$$\lambda \sim \frac{10^5}{K_j \gamma_j} \quad (4.18)$$

It can be seen from Eqn. (4.18) that only if the value of $K_j \gamma_j$ is so high that it is greater than 10^5 , the resistance of the gas boundary layer can be neglected. For a diatomic gas like H_2 , as in the case of the present work, the mass transfer equations can be written in analogy with Eqns. (4.9) and (4.10) for the melt boundary layer,

$$\dot{n}_j = k(c_j - c_{ji}) \quad (4.19)$$

and for the gas boundary layer,

$$\dot{n}_j = \frac{2k_g}{RT}(p_{ji} - p_{bj}) \quad (4.20)$$

Here, the equilibrium at the interface is given by

$$c_{ji}^2 K_j^2 \gamma_j^2 = p_{ji} \quad (4.21)$$

From Eqns. (4.19) and (4.20), the interfacial concentration c_{ji} and pressure p_{ji} can be eliminated by using Eqn. (4.21), and yields,

$$\frac{\dot{n}_j}{kc_j} = 1 + \frac{\lambda}{2c_j} - \sqrt{\left(\frac{\lambda}{2c_j}\right)^2 + \frac{P_{bj}}{K_j^2 \gamma_j^2 c_j^2} + \frac{\lambda}{c_j}} \quad (4.22)$$

where λ is the ratio of mass transfer resistance in gas boundary layer to that in melt boundary layer for a diatomic gas, i.e.,

$$\frac{\lambda}{c_j} = \frac{kRT}{2k_g K_j^2 \gamma_j^2 c_j} \quad (4.23)$$

If

$$\frac{\lambda}{c_j} = \frac{kRT}{2k_g K_j^2 \gamma_j^2 c_j} \ll 1 \quad (4.24)$$

Eqn. (4.22) can be simplified to

$$\dot{n}_j = k(c_j - c_{je}) \quad (4.25)$$

where c_{je} is the hypothetical concentration in the melt in equilibrium with the bulk concentration in the gas, $c_{je} = \sqrt{P_{bj}} / (K_j \gamma_j)$. Eqn. (4.25) indicates that the total mass transfer coefficient k_t would

be equal to the mass transfer coefficient for the melt boundary layer if Eqn. (4.24) is satisfied.

By comparison of Eqns. (4.17) and (4.18) we can see that Eqn. (4.24) is fulfilled if

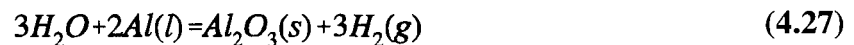
$$\frac{10^5}{2K_j^2 \gamma_j^2 c_j} \ll 1 \quad (4.26)$$

For hydrogen in pure aluminum at 1000 K, the value of $K_H^2 \gamma_H^2 c_H$ is 3.8×10^{11} [%H] [23]. This

means Eqn. (4.24) can be satisfied with a practical value of hydrogen content [%H], and the resistance to mass transfer is greater on the melt side than on the gas side.

4.3.2 Pick-up of Hydrogen from Water Vapour

It is seen from previous discussions that the mass transfer of hydrogen atoms is limited by the resistance in the melt boundary layer, and hydrogen partial pressure at the interface can be regarded as equal to the pressure in bulk gas. In the case of the present work, however, the main hydrogen source is the chemical reaction of liquid aluminum with water vapour in the atmosphere, and now the pressure at the interface should be determined to perform the mass transfer calculation. The chemical reaction at the melt surface was given in Eqn. (2.11) as follow,



As indicated previously, the standard free energy change for this reaction is highly negative ($\Delta G^0 = -187807$ cal/mole at 700 °C). This implies that the complete conversion to hydrogen of all traces of water vapour in contact with the melt, and the hydrogen partial pressure at the interface could consequently be regarded as equal to water partial pressure in the bulk gas. This can also be obtained from the following analysis. The various steps, together with their corresponding rate equations, involved in the mass transfer of hydrogen atoms across the interface are listed below, and some of them are illustrated in Fig. 4-3 [23,56].

1. Water vapour diffuses through the gas boundary layer to the melt surface,

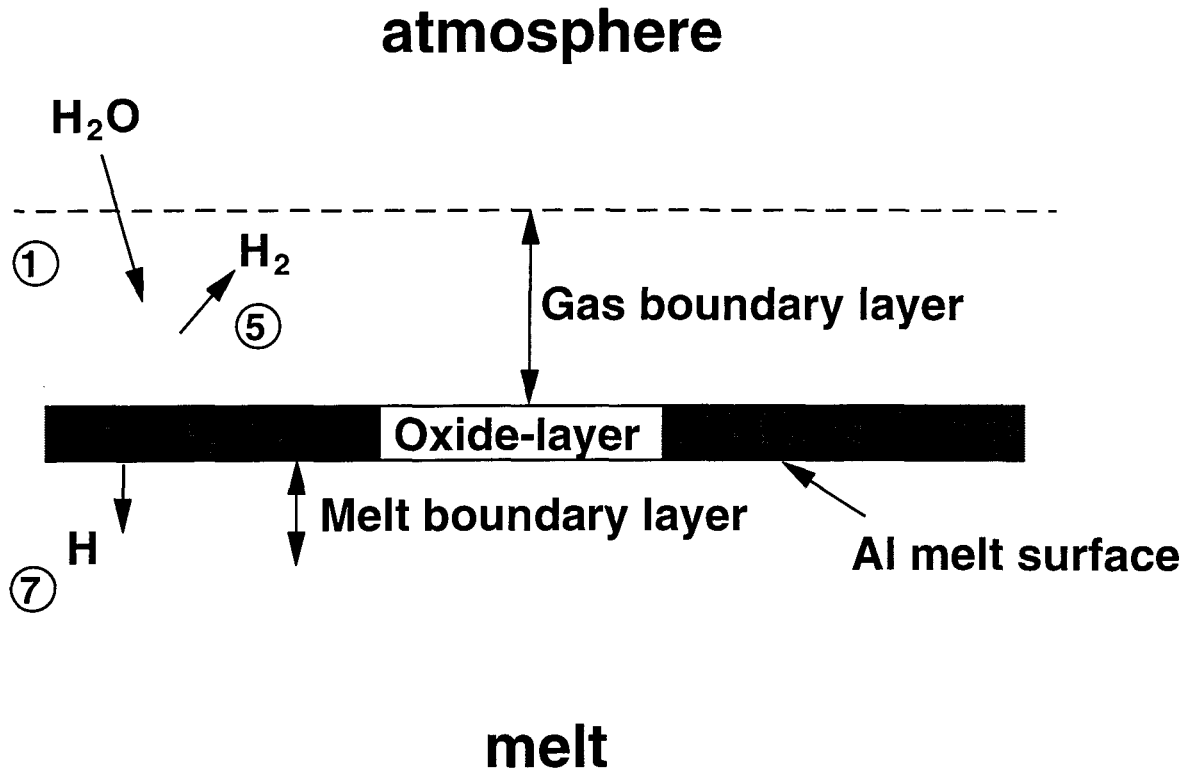
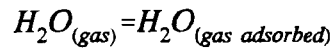


Figure 4-3. Some of the steps involved in the transfer of H across the aluminum melt-gas interface. [23]

$$r = \frac{k_{H_2O}}{RT} (p_{H_2O(b)} - p_{H_2O(i)}) \quad (4.28)$$

2. The water molecules are adsorbed at the melt surface. The reaction is,



and the rate of the reaction is

$$r = k_{ad} C_s (p_{H_2O(eq)} - p_{H_2O}) \quad (4.29)$$

where C_s is the concentration of surface sites available for the adsorption of molecules of hydrogen, $p_{H_2O(eq)}$ is the equilibrium water pressure, and p_{H_2O} is the water pressure in equilibrium with the hydrogen concentration in the melt.

3. The adsorbed water molecules react with aluminum according to Eqn. (4.27).

4. Hydrogen molecules are desorbed from the surface to the atmosphere by the reaction,

$$H_{2(gas\ adsorbed)} = H_{2(gas)} \quad (4.30)$$

and the rate of reaction is

$$r = k_{de} C_s (p_{H_2} - p_{H_2(eq)}) \quad (4.31)$$

5. Hydrogen molecules diffuse back out of the gas boundary layer,

$$r = \frac{k_{H_2}}{RT} (p_{H_2(i)} - p_{H_2(b)}) \quad (4.32)$$

6. Hydrogen molecules dissociate into atoms on the melt surface. One additional surface site is required to accommodate the two atoms of hydrogen released by

the dissociation of each H₂ molecule. Then,

$$r = k_{ds} C_s^2 (p_{H_2} - p_{H_2(eq)}) \quad (4.33)$$

7. Hydrogen atoms diffuse through the melt boundary layer. The rate is

$$r = k_H (c_{H(i)} - c_{H(b)}) \quad (4.34)$$

where

$$K_H^2 \gamma_H^2 c_{H(i)} = p_{H_2(i)} \quad (4.35)$$

Under the assumptions that the chemical reactions, dissociation, adsorption, and desorption are rapid, only the steps 1, 5, and 7, shown in Fig. 4-3, would be considered in the analysis. A mole balance for hydrogen for the reactions that take place at the surface is presented as,

$$2\dot{n}_{H_2O} = \dot{n}_{H_2} + 2\dot{n}_H \quad (4.36)$$

and the equilibrium hydrogen content in the melt is proportional to the square root of water partial pressure in the bulk gas, i.e.,

$$c_{H(e)} = K \sqrt{p_{H_2O(b)}} \quad (4.37)$$

where **K** is the equilibrium constant of the reaction given in Eqn. (2.1).

4.3.3 Mathematical Models for Hydrogen Absorption and Degassing

Under the consideration that the summation of the resistances to a mass transfer on both sides of the interface can be represented by a total mass transfer coefficient, k_t , the rate of hydrogen absorption can be expressed in analogy to Eqn. (4.14) as follow,

$$\frac{d[H]}{dt} = k_a ([H]_e - [H]) \quad (4.38)$$

where $[H]$ is hydrogen content in the melt, k_a is the mass transfer coefficient for hydrogen absorption, and $[H]_e$ is the hydrogen content in equilibrium with water partial pressure in the bulk gas. It should be noted that here the ratio of melt surface area to melt volume, A/V , is not included. It is considered constant except in the analysis of its effect on hydrogen absorption and degassing. Eqn. (4.38) can be integrated as follow,

$$\int_{[H]_0}^{[H]} \frac{d[H]}{[H]_e - [H]} = \int_0^t k_a dt \quad (4.39)$$

where $[H]_0$ is the initial hydrogen content after degassing for hydrogen re-absorption process and t is absorption time. Consequently,

$$[H] = [H]_e - ([H]_e - [H]_0) e^{-k_a t} \quad (4.40)$$

or simply

$$[H] = [H]_e - \Delta[H] e^{-k_a t} \quad (4.41)$$

where $\Delta[H] = ([H]_e - [H]_0)$ represents the driving force for hydrogen absorption of the aluminum melt. Derivation of Eqn. (4.41) gives the relationship of hydrogen absorption rate to the

absorption time,

$$\frac{d[H]}{dt} = \Delta[H]k_a e^{-k_d t} \quad (4.42)$$

Substituting Eqn. (4.37) into Eqns. (4.41) and (4.42) yields the expressions describing all the influencing factors on the process of hydrogen absorption,

$$[H] = KP_{H_2O(b)}^{1/2} - \left(KP_{H_2O(b)}^{1/2} - [H]_0 \right) e^{-k_d t} \quad (4.43)$$

and

$$\frac{d[H]}{dt} = \left(KP_{H_2O(b)}^{1/2} - [H]_0 \right) k_a e^{-k_d t} \quad (4.44)$$

In the present work, degassing was performed by using the mechanism of adsorption-diffusion model of gas elimination, which means that hydrogen was removed by the diffusion of hydrogen atoms across the melt surface out of the liquid metal. Therefore, the degassing process could be regarded as the inverse process of hydrogen absorption, and it could be described by Eqns. (4.41) and (4.42) except for a replacement of k_a by a degassing mass transfer coefficient k_d , i.e.,

$$[H] = [H]_e - \Delta[H]e^{-k_d t} \quad (4.45)$$

and

$$\frac{d[H]}{dt} = \Delta[H]k_d e^{-k_d t} \quad (4.46)$$

From the equations (4.43) through (4.46), it can be seen that the hydrogen content and the mass

transfer rate are correlated to both thermodynamic parameter \mathbf{K} and kinetic parameters \mathbf{k}_a and \mathbf{k}_d for hydrogen absorption and degassing, respectively. Eqns. (4.41), (4.42) and Eqns. (4.45), (4.46) are mathematical models for the processes of hydrogen absorption and degassing, respectively, and the curve fitting to these equations of the experimental data of hydrogen content at different times during degassing and hydrogen re-absorption allows the evaluation of the kinetic parameters \mathbf{k}_a and \mathbf{k}_d , which will be presented in the next section.

4.4 DATA PROCESSING

4.4.1 Curve Fitting with the Least-Square Method

Values of the kinetic parameters \mathbf{k}_a and \mathbf{k}_d are required to describe the kinetic behaviour of hydrogen absorption and degassing of the molten DURALCANTM composites. In this present investigation, experimental data of hydrogen content were measured at different times during the processes of degassing and hydrogen re-absorption, and the above kinetic parameters were evaluated from the experimental data according to their mathematical models developed previously. This evaluation was performed by fitting the data to the equations using least-square method. For hydrogen absorption, Eqn. (4.41) could be rewritten in terms of simple mathematical symbols as follow

$$Y=A-Be^{Cx} \tag{4.47}$$

For a single experiment, we have a set of data (X_i, Y_i) ($i = 1, \dots, n$). In order to determine the

values of coefficients **A**, **B**, and **C**, Eqn. (4.47) were rearranged and rewritten in logarithmic form

$$\ln(A - Y) = \ln B + CX \quad (4.48)$$

and the following transformations were made

$$Y_T = \ln(A - Y), \quad C_0 = \ln B, \quad C_1 = C \quad (4.49)$$

Then, we have a linear equation

$$Y_T = C_0 + C_1 X \quad (4.50)$$

The curve fitting of a straight line with least-square method is a simple matter. Here for Eqn. (4.50), we have

$$C_1 = \frac{\sum_{i=1}^n X_i Y_{Ti} - \bar{Y}_T \sum_{i=1}^n X_i}{\sum_{i=1}^n X_i^2 - \bar{X} \sum_{i=1}^n X_i}, \quad C_0 = \bar{Y}_T - \bar{X} C_1 \quad (4.51)$$

The coefficients **B** and **C** in Eqn. (4.47) can simply be calculated from Eqn. (4.49) as

$$B = e^{C_0}, \quad C = C_1 \quad (4.52)$$

The value of coefficient **A** could be determined by a method of trial and error, until the best fitted curve was found with the experimental data for a single experiment. The values of parameters $[\mathbf{H}]_e$, $\Delta[\mathbf{H}]$, and k_a in Eqn. (4.41) were determined since we know that $[\mathbf{H}]_e = \mathbf{A}$, $\Delta[\mathbf{H}] = \mathbf{B}$, and $k_a = -\mathbf{C}$. The residual and precision of the curve fitting could also be calculated according to the following equations:

$$R_0^2 = \sum_{i=1}^n Y_i^2 - \frac{1}{n} \left(\sum_{i=1}^n Y_i \right)^2, \quad R^2 = \sum_{i=1}^n (Y_i - \hat{Y}_i)^2, \quad r^2 = 1 - R^2/R_0^2 \quad (4.53)$$

where \hat{Y} is the calculated value, and Y is the observed value. The fittingness of experimental data to its mathematical model is indicated by the value of coefficient of regression, r^2 . The closer to unity of r^2 , the better the fitness of the experimental data. The parameters in Eqn. (4.45) for degassing could be determined in a similar manner.

4.4.2 A Description of the Program

The kinetic parameters of degassing and hydrogen absorption were calculated by a program written in FORTRAN running on Sun Sparc station. For each experiment, a data file was prepared in advance. The program read the experimental data, hydrogen contents at different times during degassing or absorption, and calculate the required parameters and the coefficient of regression with a method of least-square curve fitting. The flow chart of the program is shown in Fig. 4-4, and a list of the program is given in the Appendix.

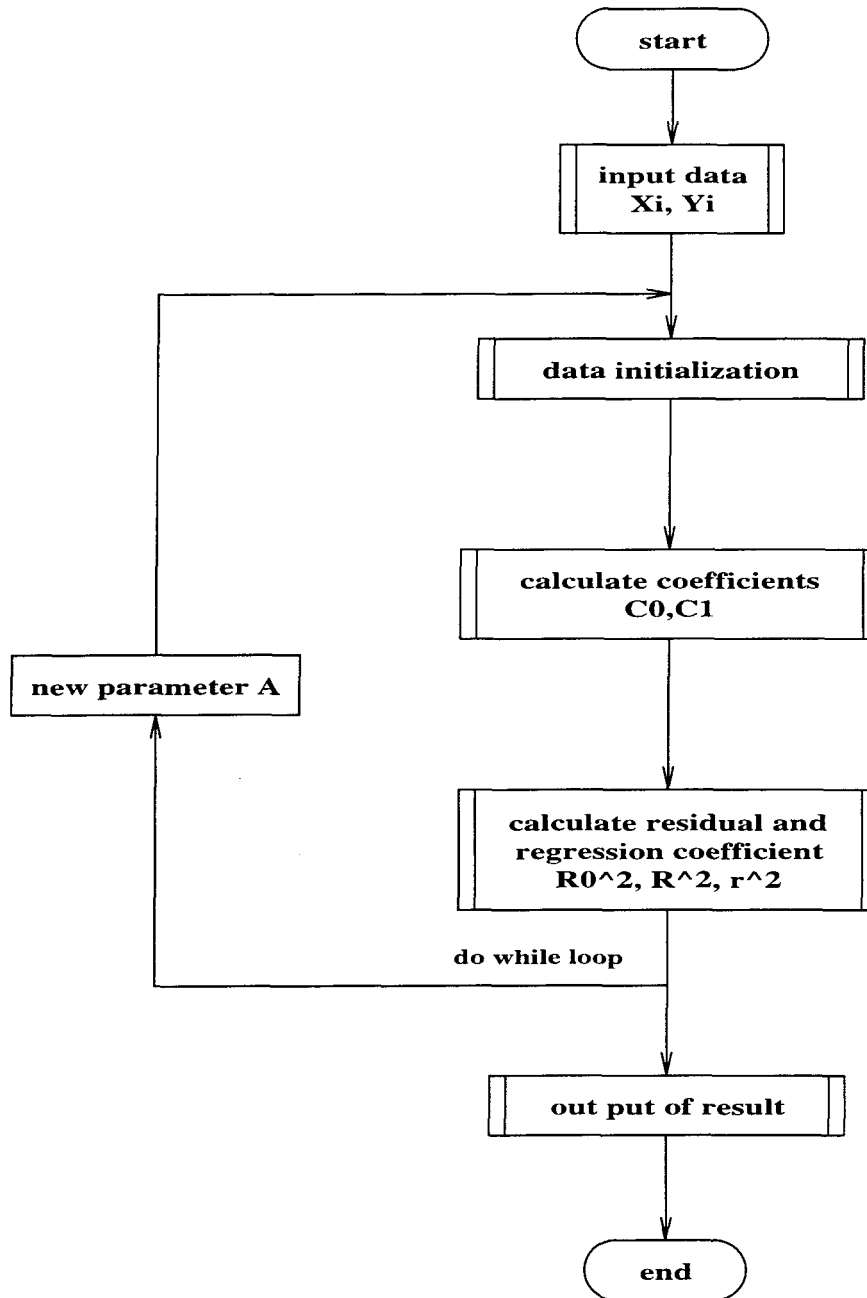


Figure 4-4. Flow chart of the program.

CHAPTER 5
RESULTS AND DISCUSSIONS

CHAPTER 5

RESULTS AND DISCUSSIONS

5.1 EXPERIMENTAL RESULTS

5.1.1 Characteristics of the Variation of Hydrogen Concentration

Experiments on DURALCAN™ composites W6D.22A and F3S.20S and their matrix alloys have been conducted under various atmospheric conditions. In the experiments, hydrogen concentration in the liquid metals was monitored continuously by Alscan during the entire processes of degassing and hydrogen absorption. The change of hydrogen content in molten DURALCAN™ composites and their matrix alloys are shown in Figs. 5-1 through 5-4. All the values of Alscan readings in each cycle are shown in these figures, only the last reading of each cycle, however, was regarded as the value of the hydrogen content at that time and this value was used in curve fitting. The Alscan readings for one single cycle is shown in Fig. 3-9. If the Alscan readings at the end of each cycle is selected and plotted against time, we have corresponding Figs. 5-5 through 5-8 which give a better view of the hydrogen content variation during the processes of degassing and absorption. It can be seen that the hydrogen content decreases during

degassing and reaches an equilibrium region where it changes little with degassing time. In the process of absorption, hydrogen concentration increases rapidly at the beginning and eventually reaches a plateau which is in equilibrium with the atmosphere where the experiment was conducted. In a kinetic study of degassing and hydrogen absorption, the absolute values of hydrogen equilibrium concentration during degassing and absorption are not necessarily equal for each experiment. It is the rate of change of these values that is under consideration. As we can see from the figures, the values of hydrogen concentration decrease with time in degassing and increase in absorption. The equilibrium values for both degassing and absorption differ from each experiment. Actually these values varied with the atmospheric conditions of the day when the experiment was conducted. From Figs. 5-2, 5-6 and Figs. 5-3, 5-7 we can see that the first one or two Alscan readings at the beginning of degassing were unreasonably low. This had occasionally happened in the experiments, and the search for its reason was beyond the scope of the present investigation. These readings were not considered in the curve fittings for degassing. In the whole degassing and hydrogen absorption processes, the melt temperature was kept at about 710 °C where most of the melt treatments are carried out in practice. A fluctuation, however, can be observed at the end of degassing and the beginning of absorption because of the sudden removal of the cover of crucible at that moment.

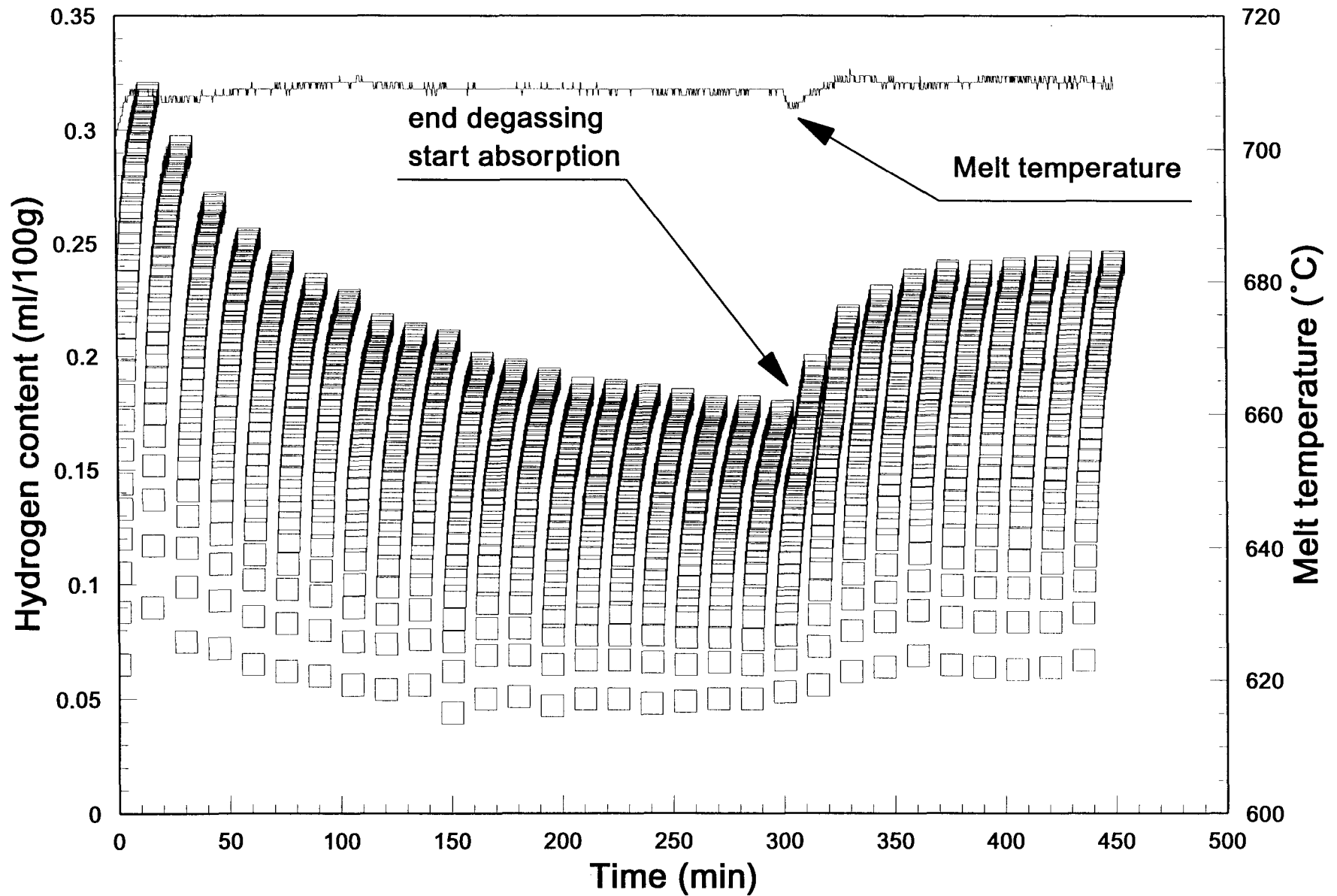


Figure 5-1 Alscan readings of hydrogen concentration of W6D.22A composites during degassing and hydrogen re-absorption (Experiment No. WC1).

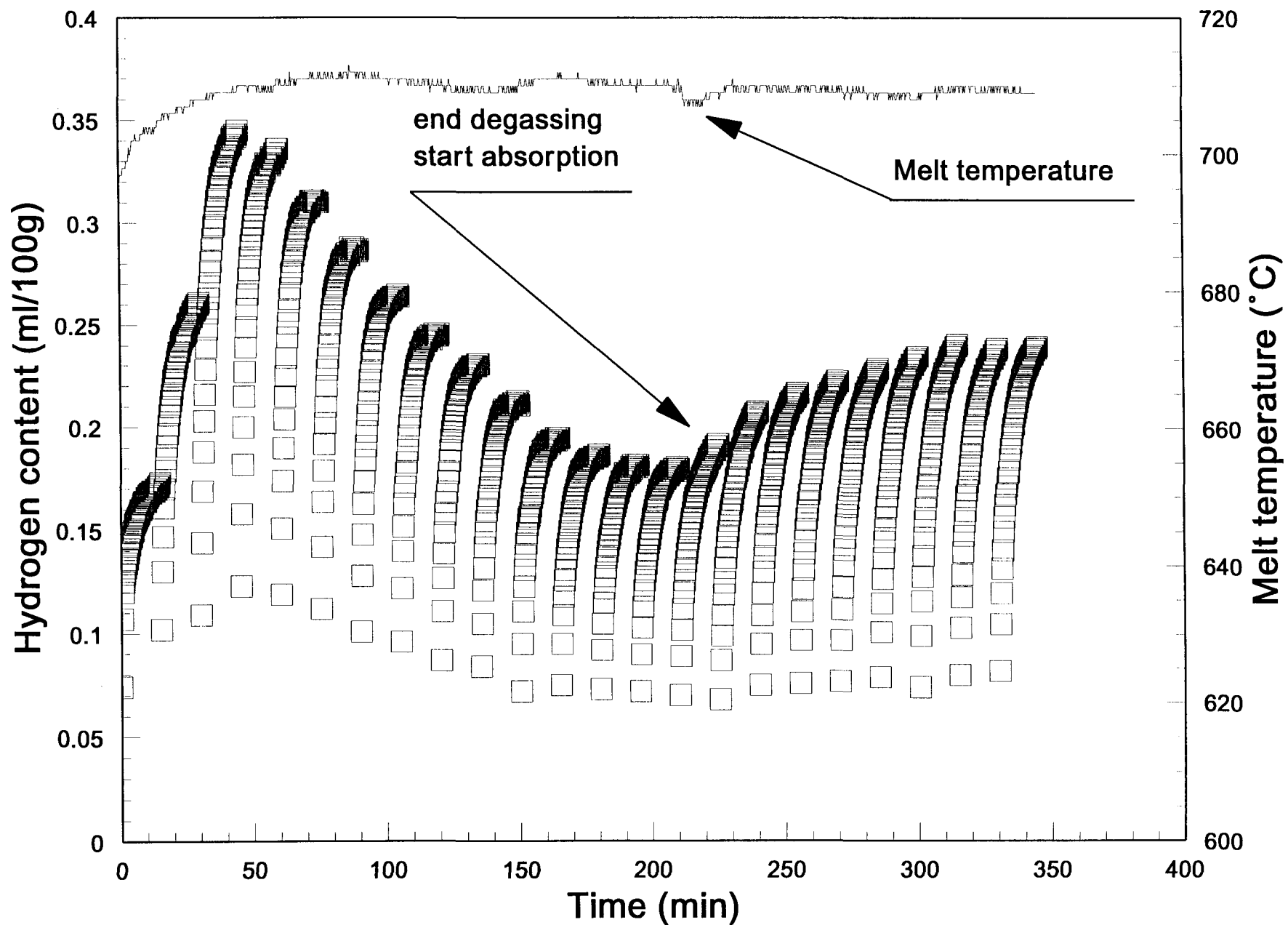


Figure 5-2. Alscan readings of hydrogen concentration of the matrix alloy of W6D.22A (Experiment No. WM3).

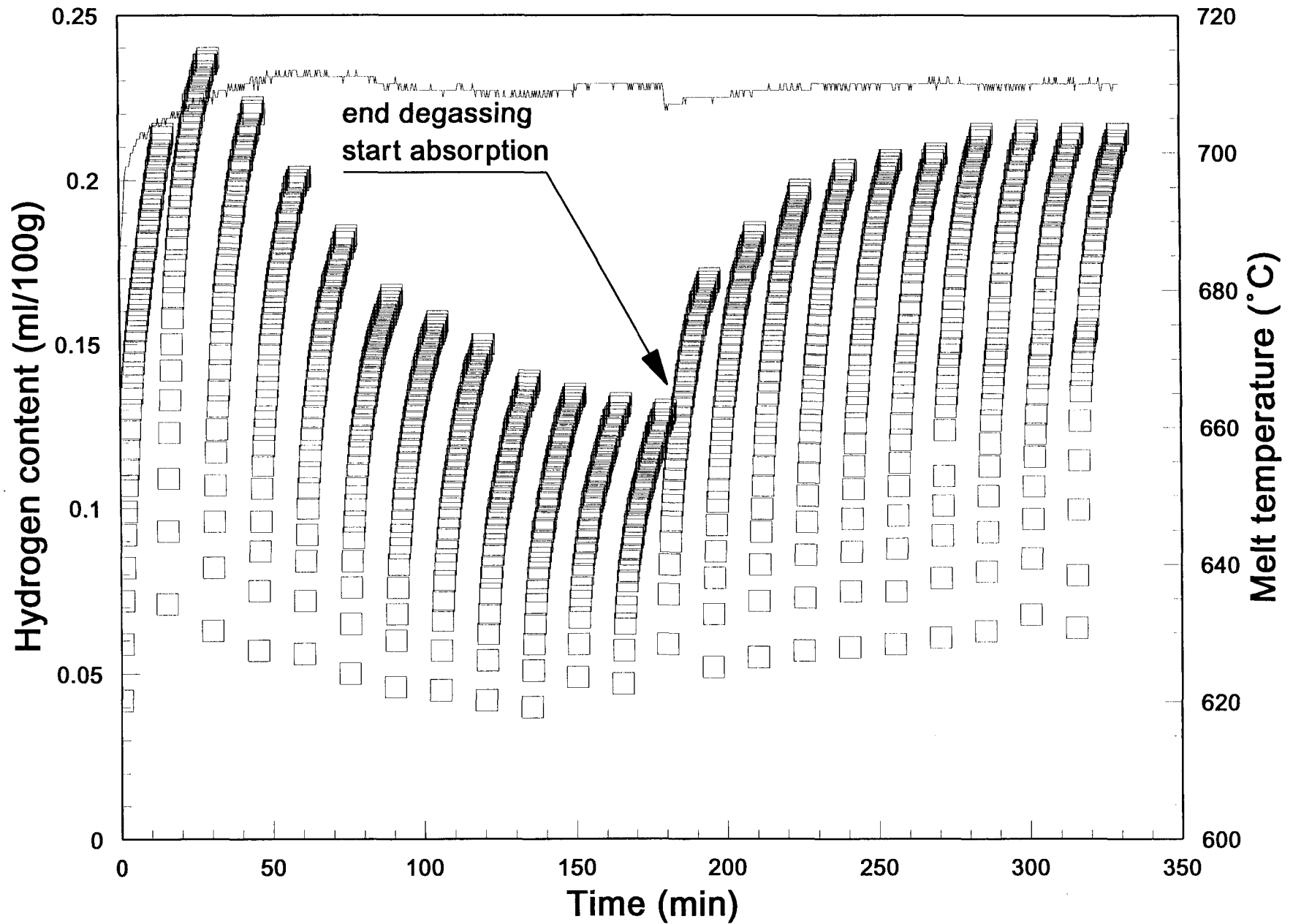


Figure 5-3. Alscan readings of hydrogen concentration of F3S.20S composite during degassing and hydrogen re-absorption (Experiment No. FC3).

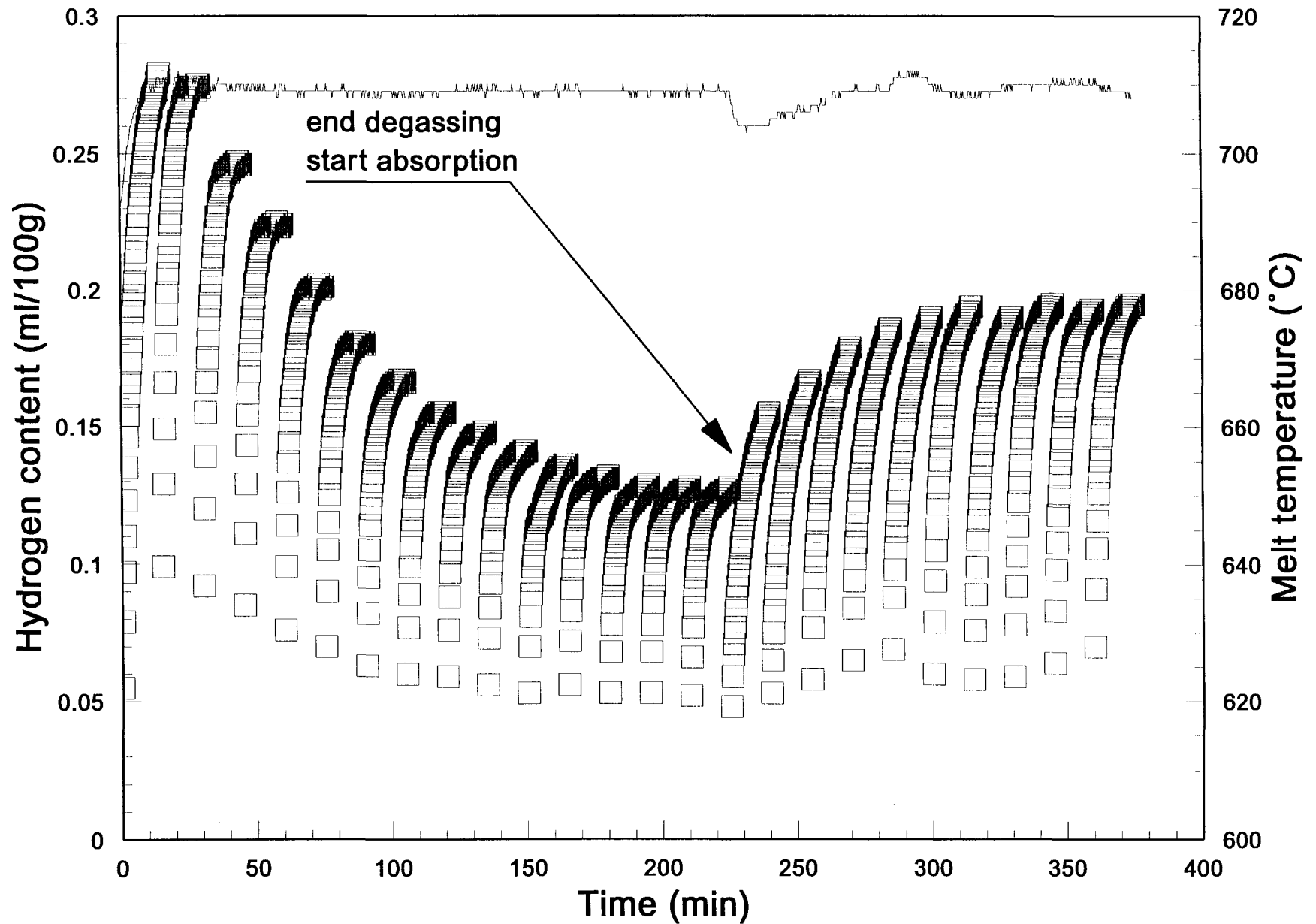


Figure 5-4. Alscan readings of hydrogen concentration of the matrix alloy of F3S.20S composite (Experiment No. FM2).

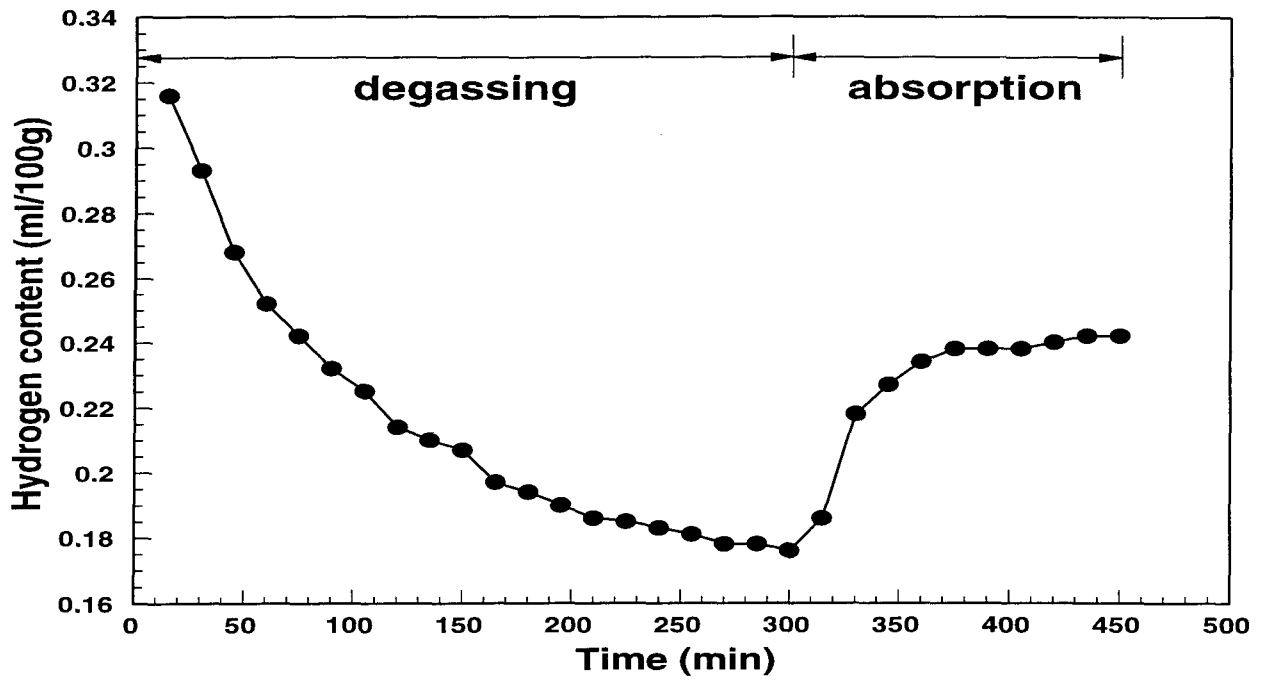


Figure 5-5. The end cycle Alscan readings of hydrogen concentration of W6D.22A composite (Experiment No. WC1).

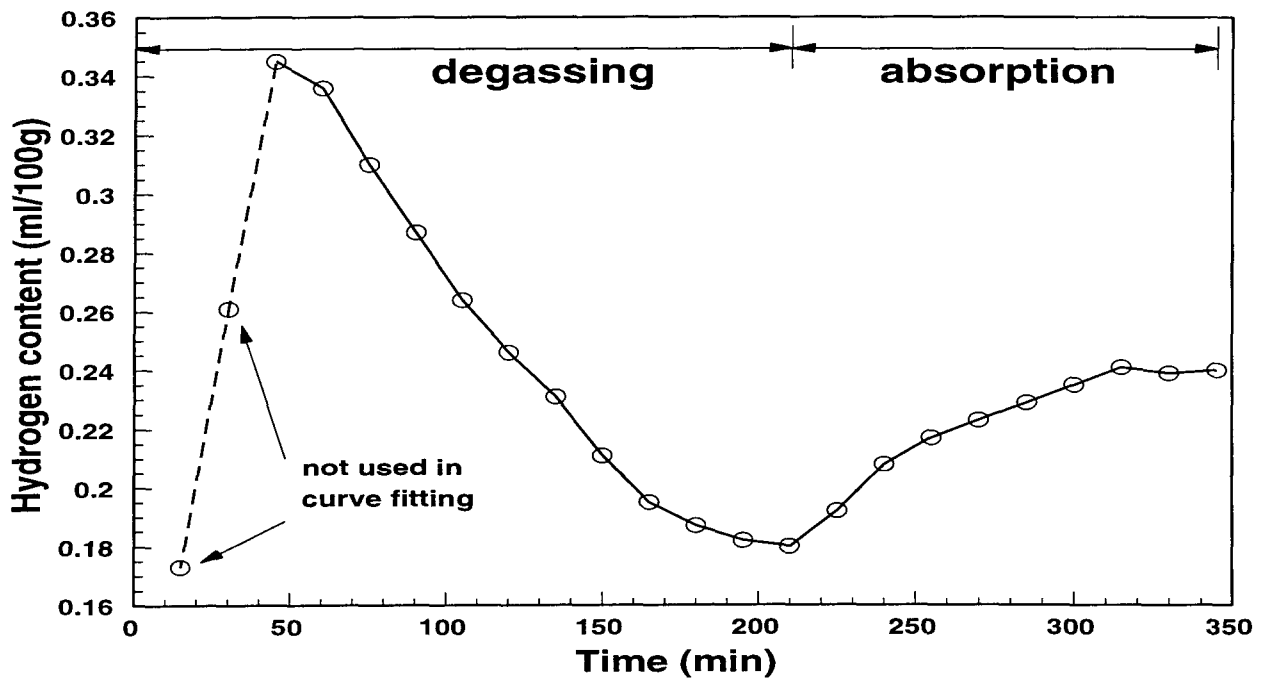


Figure 5-6. The end cycle Alscan readings of hydrogen concentration of the matrix alloy of W6D.22A composite (Experiment No. WM3).

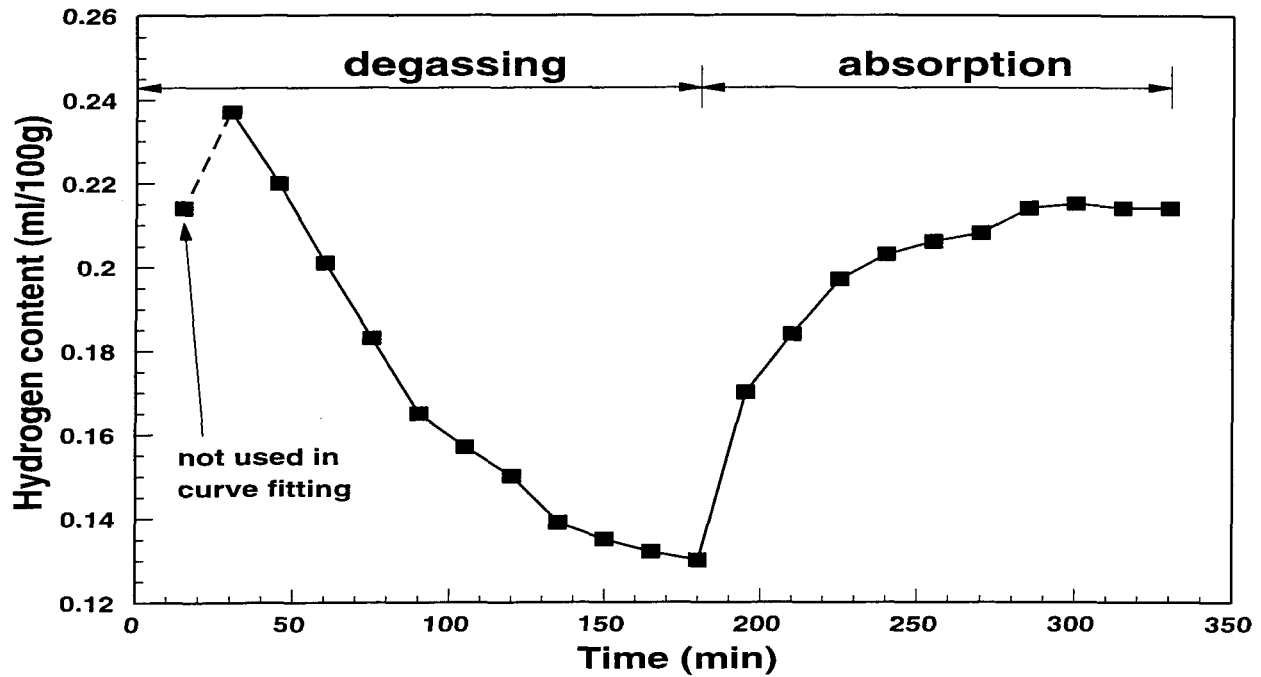


Figure 5-7. The end cycle Alscan readings of hydrogen concentration of F3S.20S composite (Experiment No. FC3).

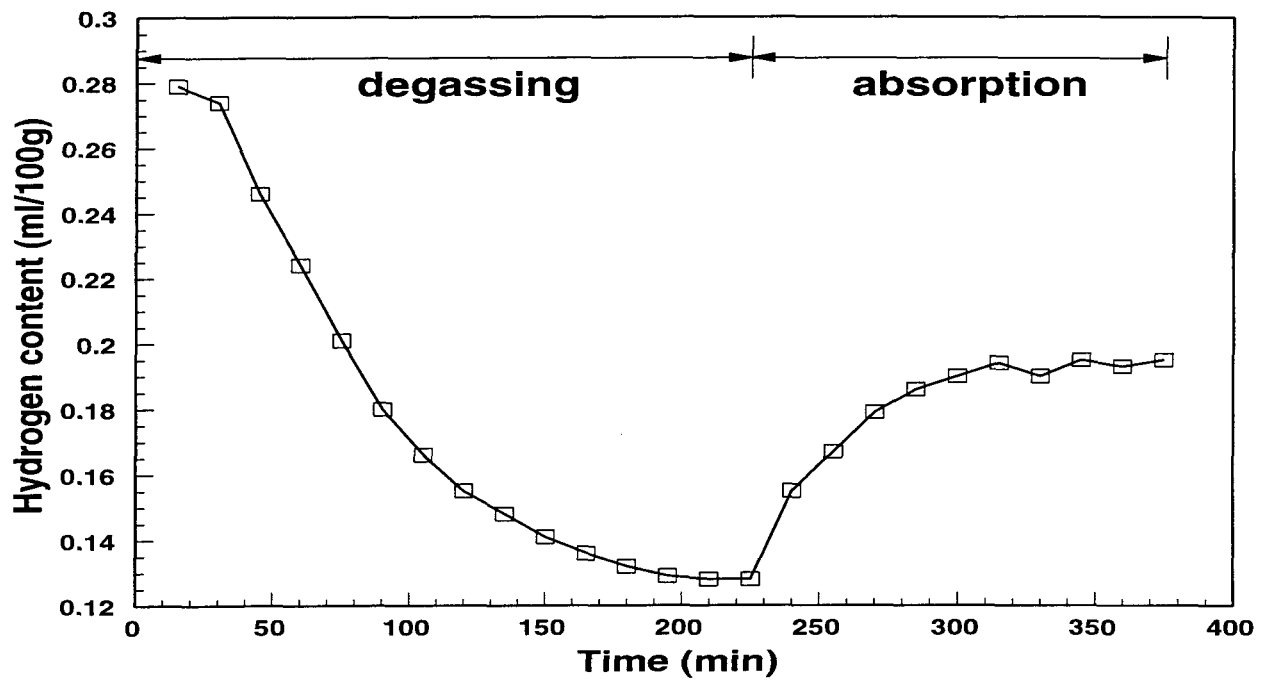


Figure 5-8. The end cycle Alscan readings of hydrogen concentration of the matrix alloy of F3S.20S composite (Experiment No. FM2).

5.1.2 The Kinetic Parameters

The most important task of this present investigation is to study the kinetic behaviour of degassing and hydrogen absorption in molten DURALCANTM composites, and this could only be fulfilled by the evaluation of kinetic parameters for these processes under certain experimental conditions. As indicated previously in chapter 4, the kinetic parameters for degassing and hydrogen re-absorption can be evaluated through the curve fitting of the experimentally measured values of hydrogen concentration at different times during degassing and hydrogen re-absorption according to their given mathematical models. With the measured values of hydrogen content versus scanning time during hydrogen absorption, curve fitting was carried out for hydrogen absorption according to Eqn. (4.41) for each experiment.

$$[H]=[H]_e-\Delta[H]e^{-k_d t} \quad (4.41)$$

The fitted curves for hydrogen re-absorption, together with the observed values of hydrogen content, are shown in Figs. (5-9) and (5-10) for W6D.22A composite and its matrix alloy, and in Figs. (5-11) and (5-12) for F3S.20S composite and its matrix alloy. It can be seen from these curves that the observed values agree very well with Eqn. (4.41), which in turn proves the correctness of the mathematical model used. The values of water partial pressure (in mm Hg) were also given in the figures for each experiment, and it can be seen that the equilibrium hydrogen content was related to the water partial pressure of the day the experiment was conducted. Higher values of water partial pressure give higher equilibrium hydrogen content, and a lower water partial pressure results in lower equilibrium hydrogen content. This also indicates that the moisture in the atmosphere is the major source of hydrogen in this investigation. Curve

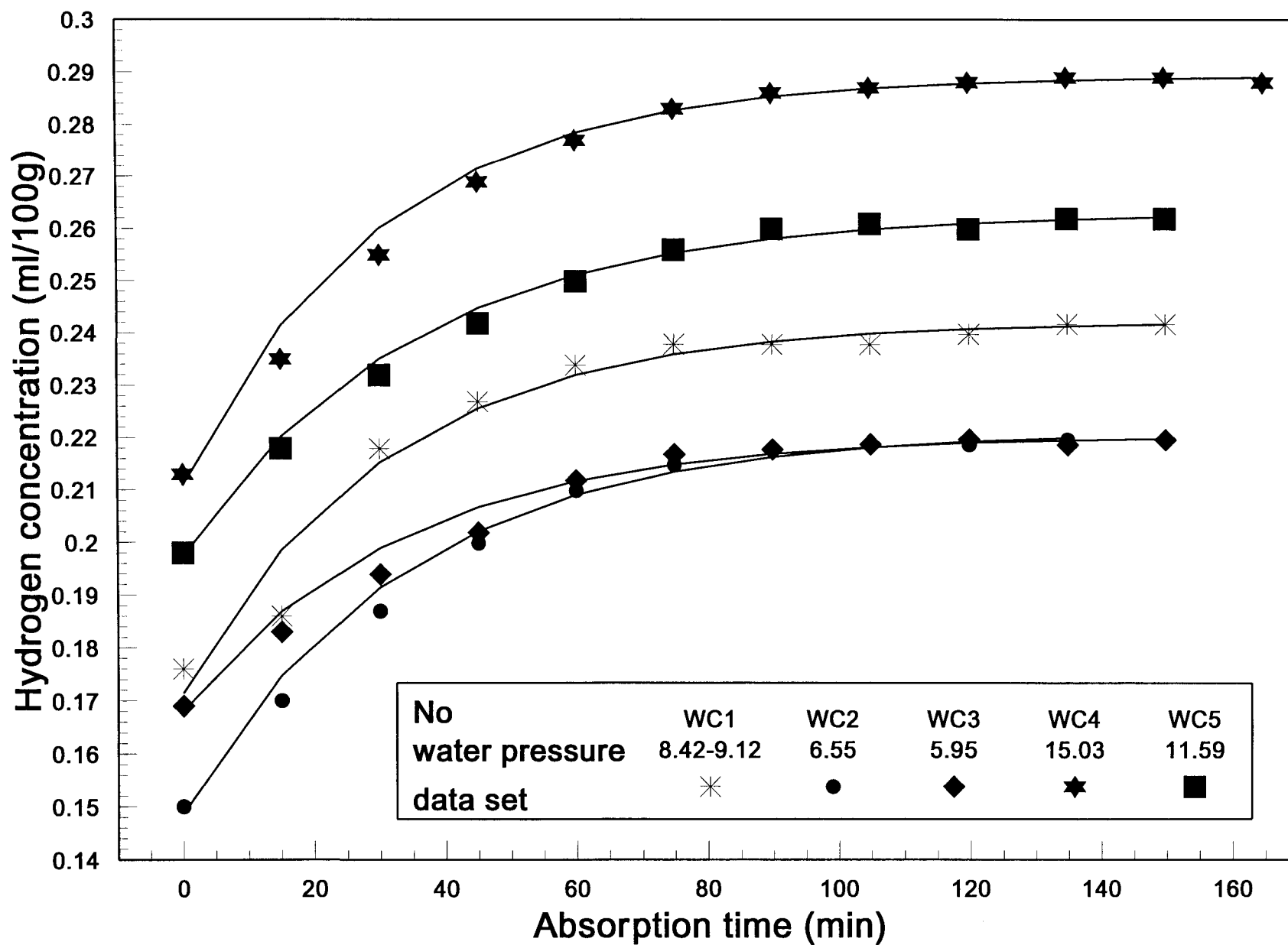


Figure 5-9. The fitted curves for hydrogen absorption in W6D.22A composite under different environmental conditions.

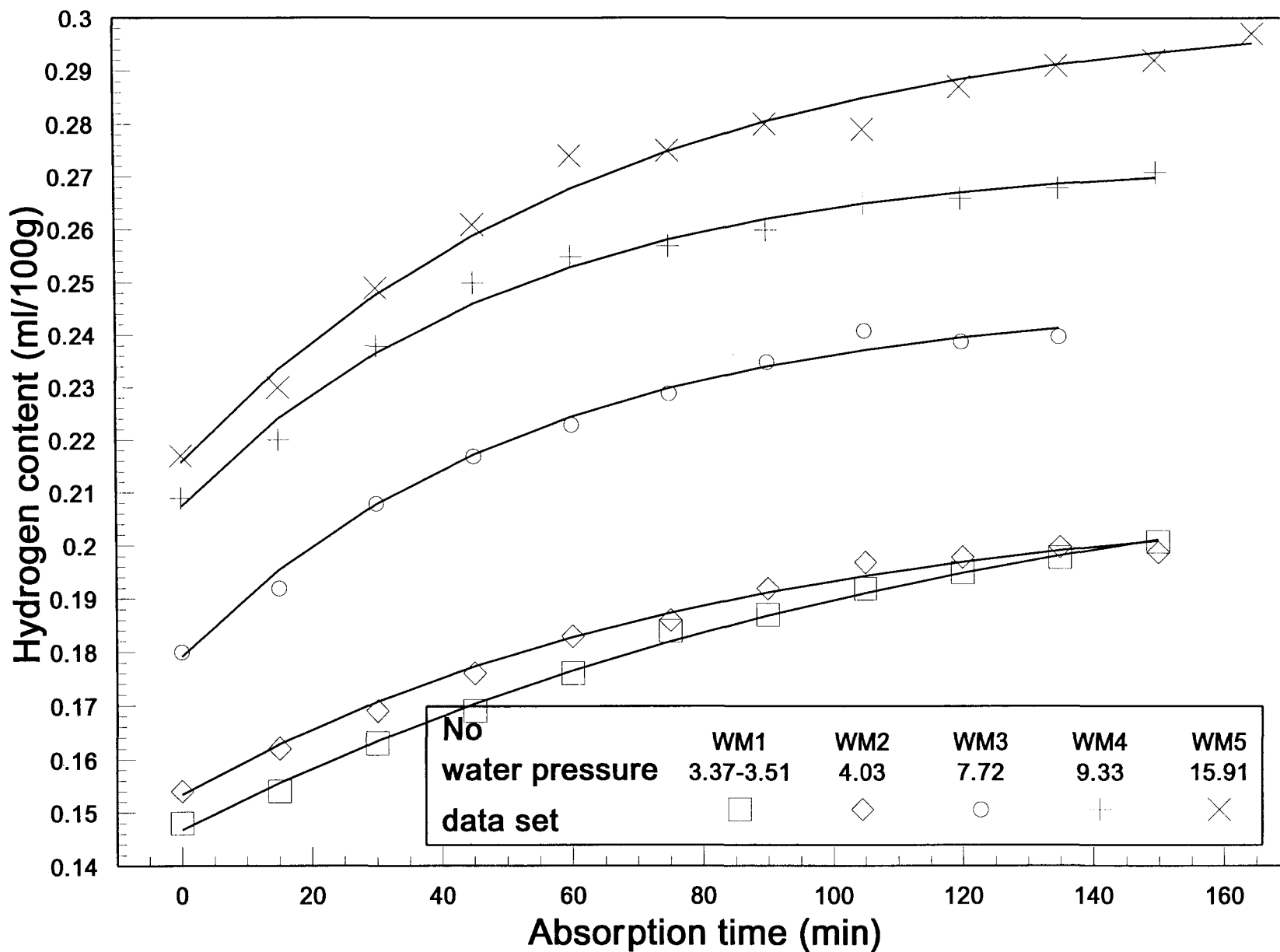


Figure 5-10. The fitted curves for hydrogen absorption of the matrix alloy of W6D.22A under different environmental conditions.

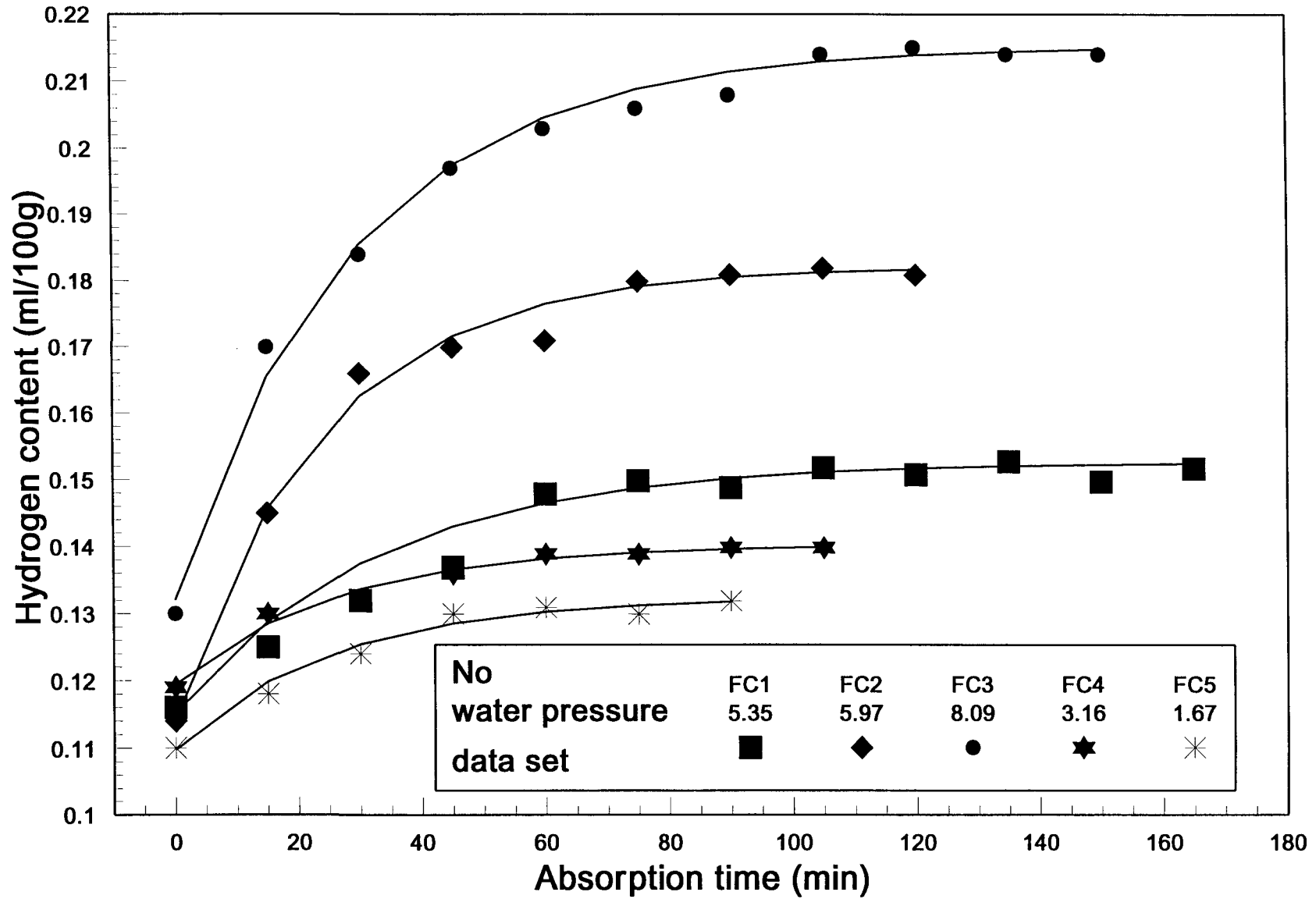


Figure 5-11. The fitted curves for hydrogen absorption of F3S.20S composite under different environmental conditions.

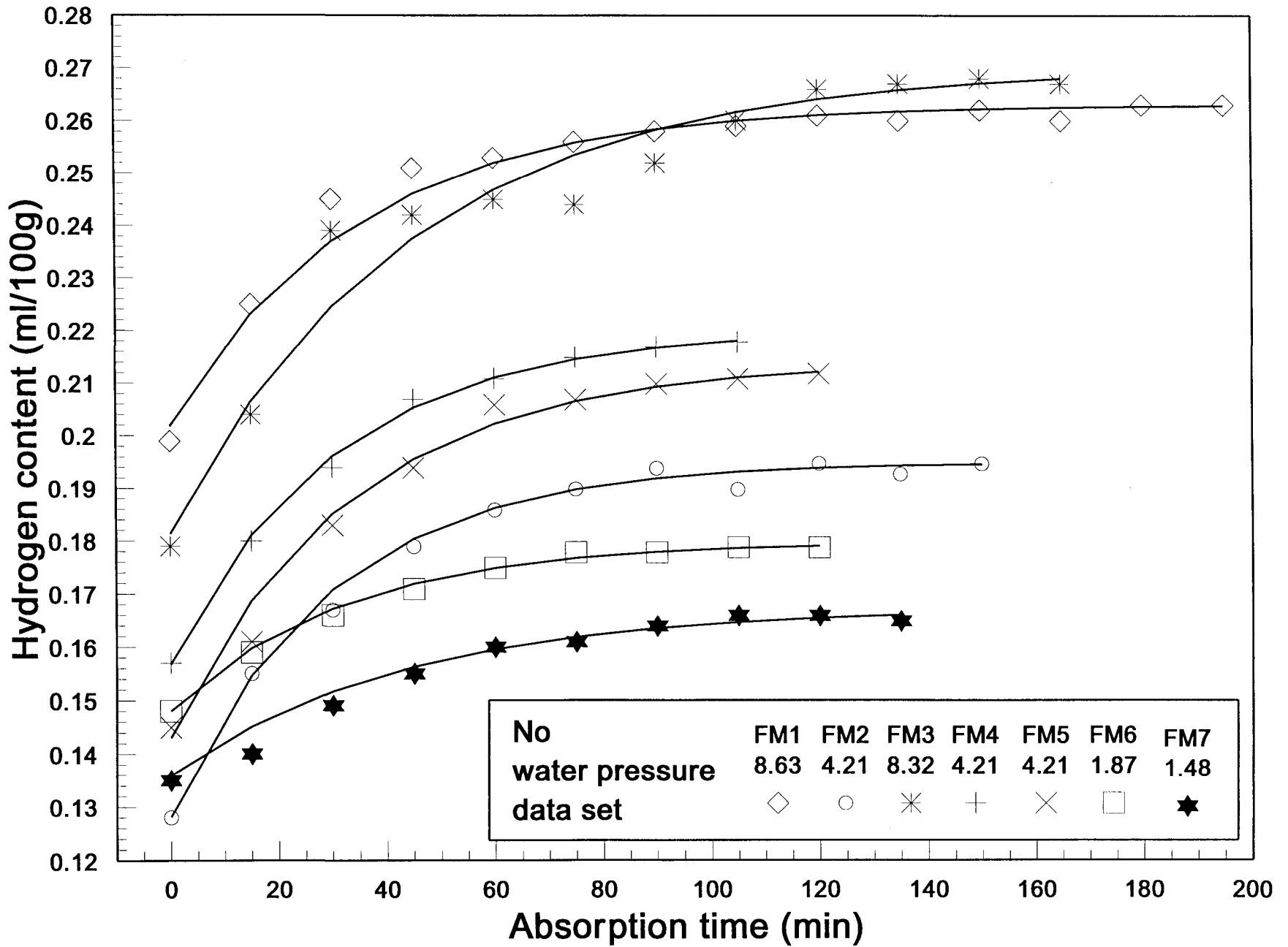


Figure 5-12. The fitted curves for hydrogen absorption of the matrix alloy of F3S.20S under different environmental conditions.

fittings were also performed for the process of degassing for each experiment according to its mathematical model expressed in Eqn. (4.45). The fitted curves are shown together with the measured values of hydrogen content in Figs. (5-13) and (5-14) for W6D.22A composite and its matrix alloy, and in Figs. (5-15) and (5-16) for F3S.20S composite and the matrix alloy. It can also be seen from these curves that the model developed agrees well with the degassing process. The equilibrium hydrogen content of degassing seems to be influenced by the environmental conditions of the day the experiment was conducted. If the day was dry, the melt was likely easier to be degassed to a lower hydrogen level. If the day was humid, it seemed harder to degas the melt, since in general a higher value of equilibrium hydrogen content corresponds to a higher water partial pressure, and a lower equilibrium hydrogen content to a lower water partial pressure no matter what their initial hydrogen levels are. Another potential factor in degassing is the flow rate of the protection gas blown on top of the melt surface, which will be discussed later.

The parameters in Eqns. (4.41) and (4.45) were evaluated by curve fitting and they are listed in Tables 5-1 and 5-2 for hydrogen absorption and degassing, respectively. Attention should be given to the values of the initial hydrogen content $[H]_0$. For hydrogen absorption (given in column 4 of Table 5-1), the $[H]_0$ values listed were the ones actually measured at the end of degassing and at the start of absorption; for degassing (given in column 4 of Table 5-2), however, the $[H]_0$ values were extrapolated ones from the fitted curves for degassing because of the unreasonably low readings given by Alscan at the beginning of degassing. These erroneous readings have not been considered in the curve fittings as shown in Figs. (5-6) and (5-7).

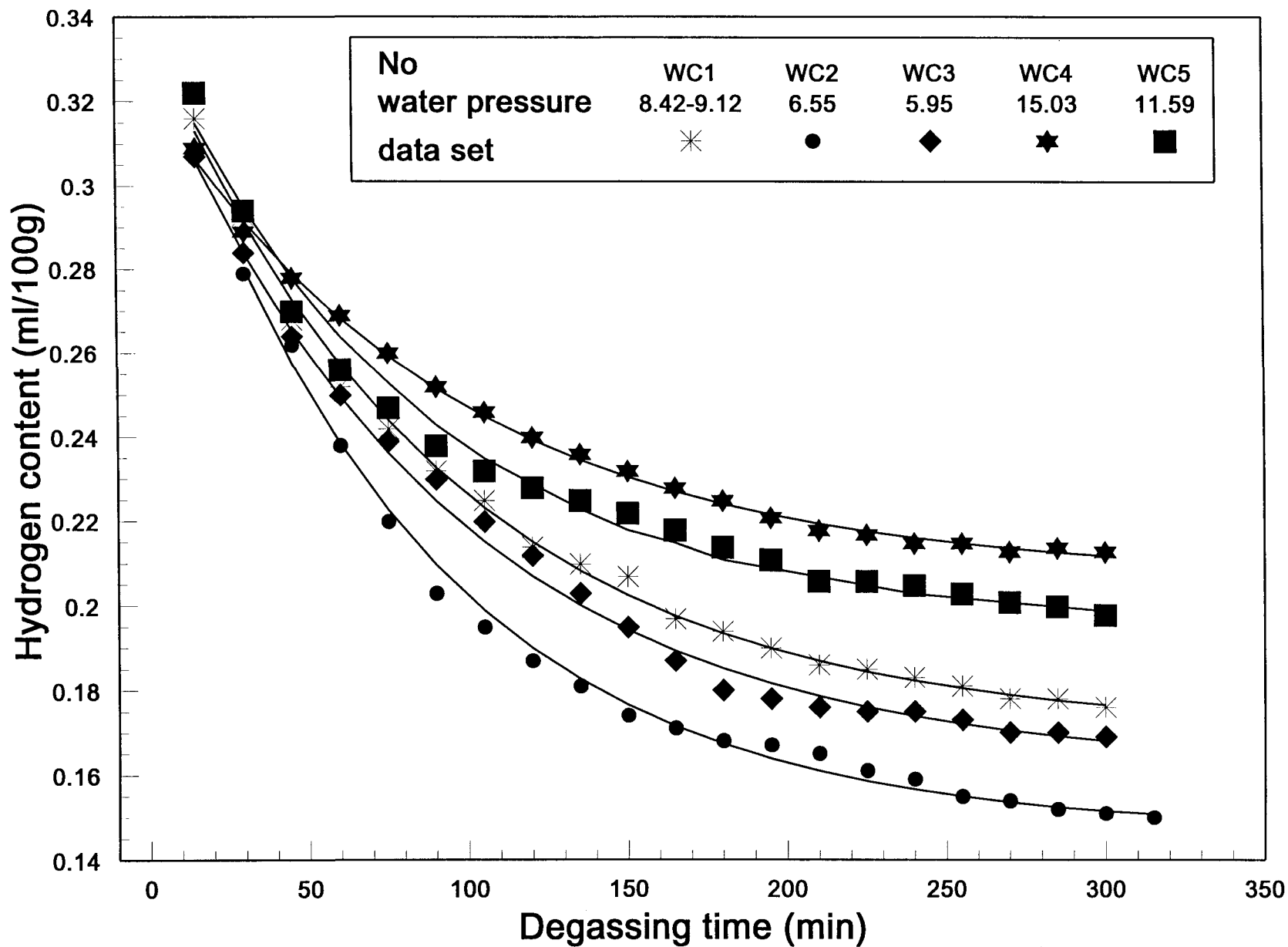


Figure 5-13. The fitted curves for degassing of W6D.22A composite under different environmental conditions.

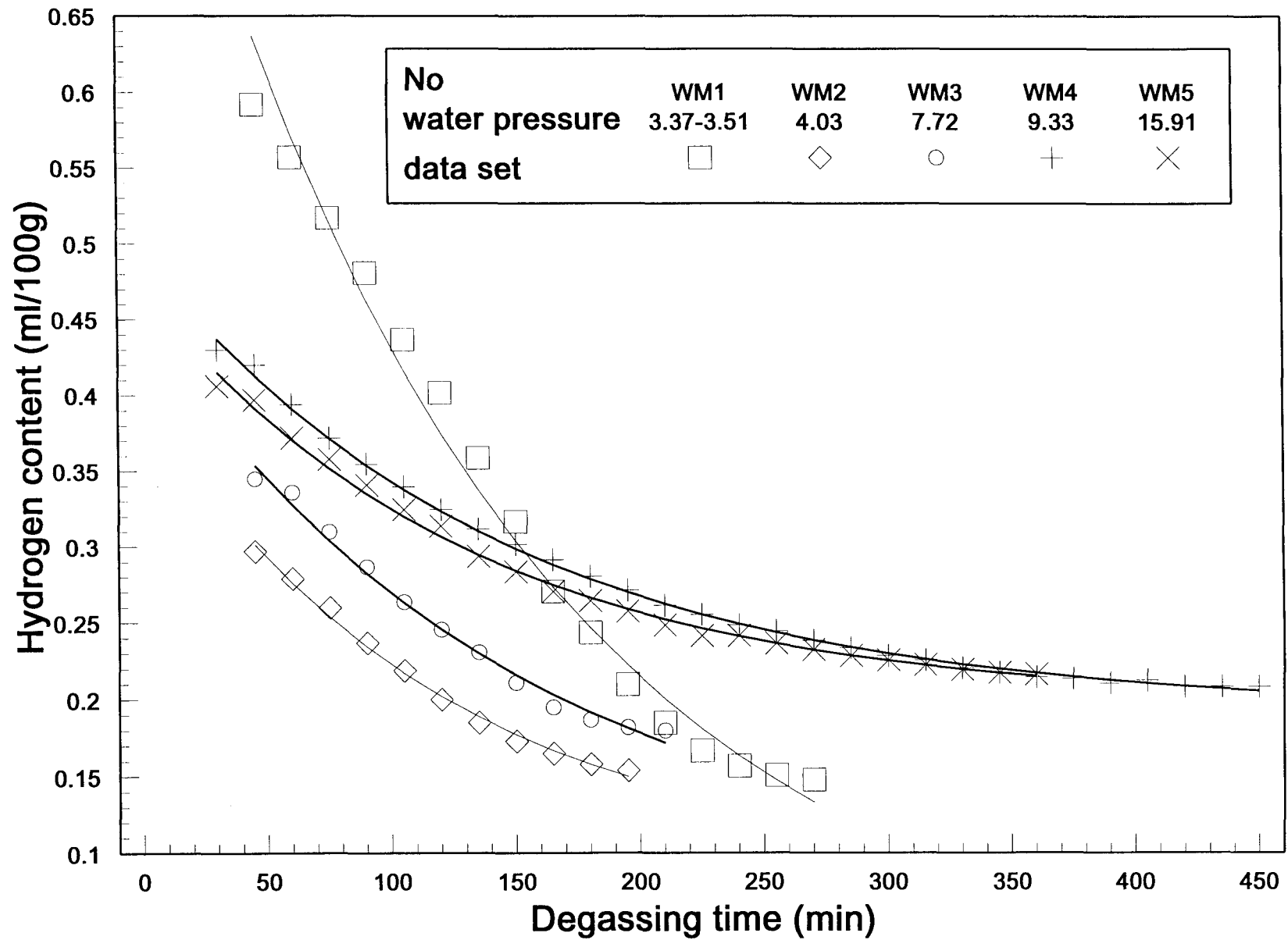


Figure 5-14. The fitted curves for degassing of the matrix alloy of W6D.22A under different environmental conditions.

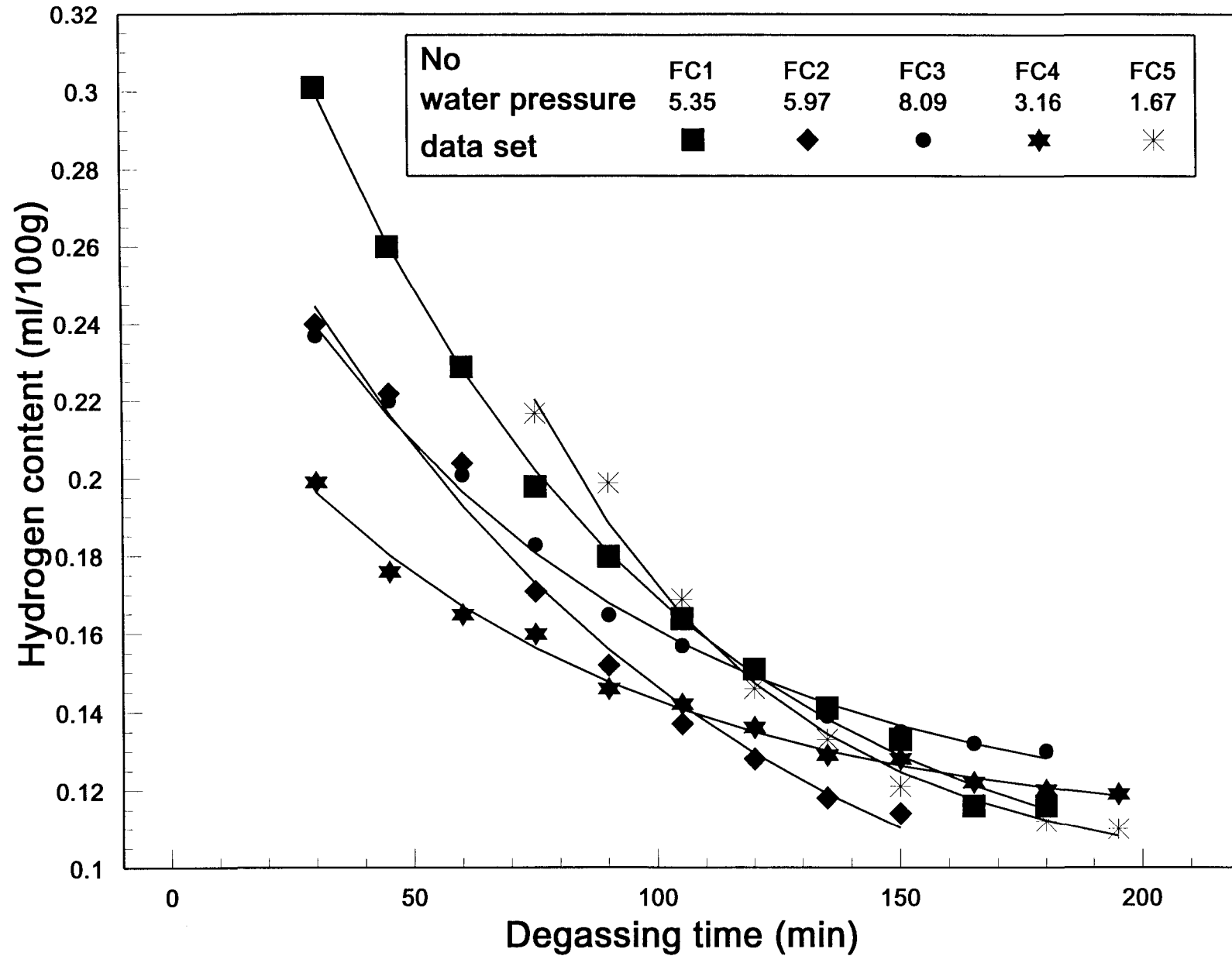


Figure 5-15. The fitted curves for degassing of F3S.20S composite under different environmental conditions.

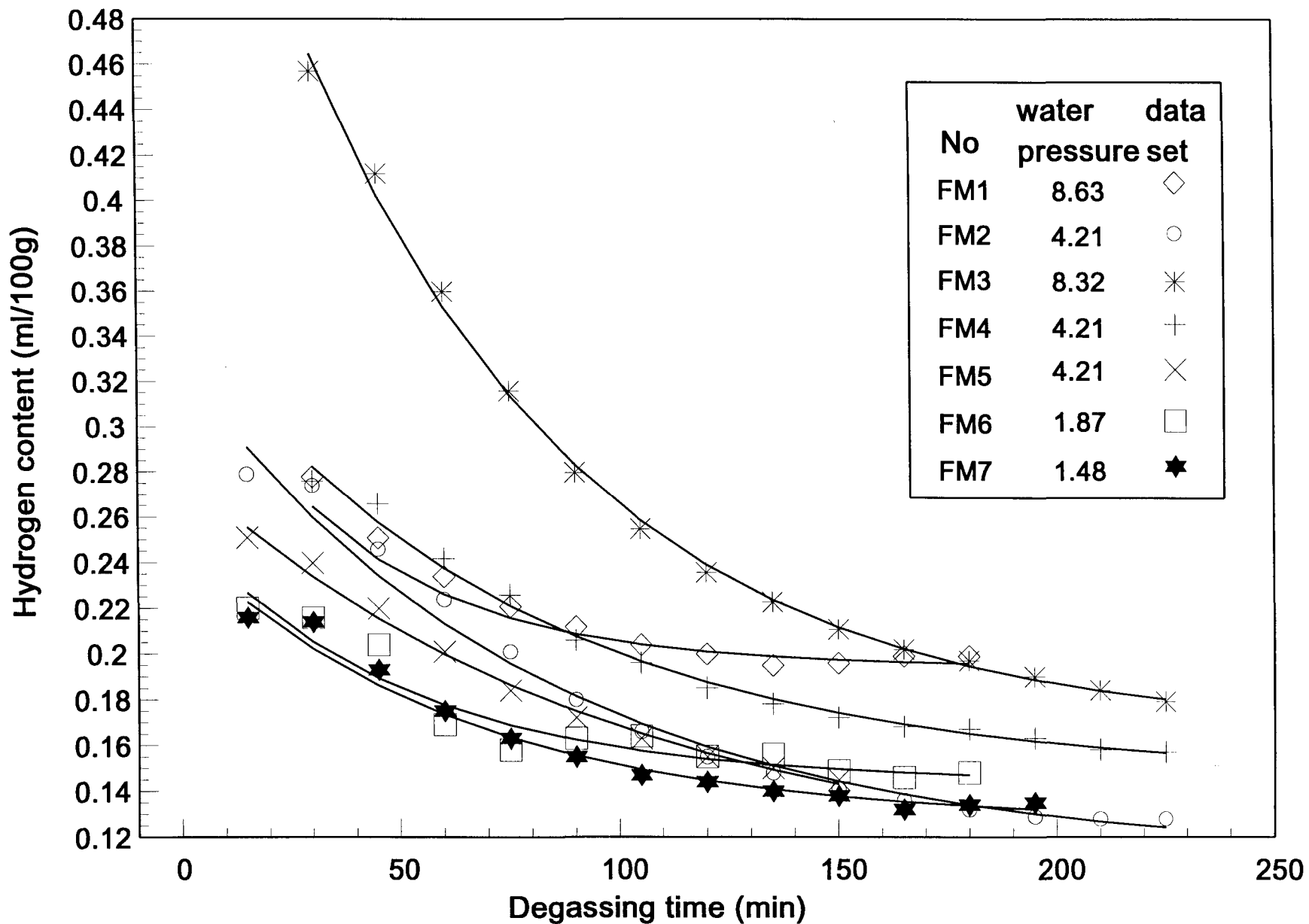


Figure 5-16. The fitted curves for degassing of the matrix alloy of F3S.20S under different environmental conditions.

The value of $\Delta[\mathbf{H}]$, given in column 6 of Table 5-1 and Table 5-2, is the difference between the equilibrium hydrogen value and the initial hydrogen value ($[\mathbf{H}]_e - [\mathbf{H}]_0$), which represents the driving force for the processes of absorption and degassing. It should be noted that this value is positive for hydrogen absorption and negative for degassing, and this value is one of the two factors determining the rate of the processes as expressed in Eqns. (4.42) and (4.46). Another factor is the kinetic parameters k_a and k_d , which are more important in describing the kinetic behaviour of the processes of hydrogen absorption and degassing.

The equilibrium values of hydrogen content, $[\mathbf{H}]_e$, are listed in column 5 of Tables 5-1 and 5-2 for absorption and degassing, respectively. Since the moisture in the atmosphere is the only source of hydrogen considered in the present investigation, it is easy to understand that the equilibrium hydrogen concentration of the melt in absorption was determined by water partial pressure in the atmosphere (given in column 3 of the tables). That is, a higher value of equilibrium hydrogen content should correspond to a higher water partial pressures, and a lower equilibrium hydrogen concentration to a lower water partial pressure. However, a generally similar relationship between the equilibrium hydrogen concentration and water partial pressure could also be found in the process of degassing from Table 5-2 and Figs. 5-13 through 5-16. This may be explained by the possibility that the melt surface could not be completely isolated from the atmosphere during degassing even though N_2 was blown on top of it, therefore the gas side of the melt-gas interface was not moisture free especially on the day when the water partial pressure was high. Consequently, there was always a hydrogen supply at the melt-gas interface during degassing making the melt more difficult to degas.

Table 5-1 Evaluated Hydrogen Absorption Parameters

Material	No	P_{H_2O} (mmHg)	$[H]_0^*$	$[H]_e$	$\Delta[H]$	k_a (1/min)	\bar{k}_a	s_{k_a}
W6D.22A	WC1	8.42-9.12	0.176	0.243	0.0682	0.0322	0.0304	0.00179
	WC2	6.55	0.150	0.222	0.0730	0.0293		
	WC3	5.95	0.169	0.221	0.0528	0.0294		
	WC4	15.03	0.213	0.289	0.0786	0.0329		
	WC5	11.59	0.198	0.263	0.0658	0.0283		
Matrix of W6D.22A	WM1	3.37-3.51	0.148	0.225	0.0784	0.00798	0.0146	0.00419
	WM2	4.03	0.154	0.211	0.0572	0.0121		
	WM3	7.72	0.180	0.247	0.0683	0.0182		
	WM4	9.33	0.209	0.274	0.0662	0.0195		
	WM5	15.91	0.217	0.302	0.0862	0.0155		
F3S.20S	FC1	5.35	0.116	0.153	0.0378	0.0297	0.0363	0.00399
	FC2	5.97	0.114	0.182	0.0680	0.0413		
	FC3	8.09	0.130	0.215	0.0832	0.0343		
	FC4	3.16	0.119	0.141	0.0211	0.0375		
	FC5	1.67	0.110	0.133	0.0228	0.0387		
Matrix of F3S.20S	FM1	8.63	0.199	0.263	0.0613	0.0284	0.0285	0.00406
	FM2	4.21	0.128	0.195	0.0672	0.0336		
	FM3	8.32	0.179	0.270	0.0890	0.0222		
	FM4	4.21	0.157	0.220	0.0636	0.0322		
	FM5	4.21	0.145	0.214	0.0713	0.0297		
	FM6	1.87	0.148	0.180	0.0321	0.0305		
	FM7	1.48	0.135	0.168	0.0326	0.0230		

* Measured initial hydrogen content before absorption.

Table 5-2 Evaluated Degassing Parameters

Material	No	P_{H_2O} (mmHg)	$[H]_0^*$	$[H]_e$	$\Delta[H]$	k_d (1/min)	\bar{k}_d	S_{k_d}
W6D.22A	WC1	8.42-9.12	0.339	0.170	-0.169	0.0110	0.0115	0.000753
	WC2	6.55	0.342	0.147	-0.194	0.0126		
	WC3	5.95	0.332	0.162	-0.170	0.0110		
	WC4	15.03	0.324	0.208	-0.116	0.0108		
	WC5	11.59	0.339	0.196	-0.143	0.0123		
Matrix of W6D.22A	WM1	3.37-3.51	0.876	0.008	-0.868	0.00717	0.00746	0.000641
	WM2	4.03	0.398	0.0920	-0.307	0.00856		
	WM3	7.72	0.451	0.0851	-0.366	0.00685		
	WM4	9.33	0.494	0.193	-0.301	0.00694		
	WM5	15.91	0.471	0.199	-0.273	0.00770		
F3S.20S	FC1	5.35	0.409	0.0883	-0.321	0.0138	0.0144	0.00294
	FC2	5.97	0.316	0.0614	-0.255	0.0110		
	FC3	8.09	0.305	0.112	-0.193	0.0137		
	FC4	3.16	0.240	0.109	-0.131	0.0137		
	FC5	1.67	0.706	0.0968	-0.609	0.0199		
Matrix of F3S.20S	FM1	8.63	0.350	0.195	-0.156	0.0265	0.0164	0.00504
	FM2	4.21	0.328	0.112	-0.217	0.0126		
	FM3	8.32	0.642	0.165	-0.476	0.0155		
	FM4	4.21	0.349	0.146	-0.203	0.0133		
	FM5	4.21	0.281	0.107	-0.174	0.0104		
	FM6	1.87	0.256	0.144	-0.112	0.0201		
	FM7	1.48	0.249	0.127	-0.122	0.0161		

* Extrapolated values from the fitted degassing curves.

Column 7 of Tables 5-1 and 5-2 gives the values of mass transfer coefficients, k_a and k_d , for the processes of hydrogen absorption and degassing, respectively, which are the most important parameters in describing the kinetic behaviour of hydrogen in liquid aluminum. Theoretically, the mass transfer coefficient (or rate constant), k_a or k_d , is independent of the environmental conditions. It is only a function of material and melt temperature. Since a similar value of melt temperature (710 °C) was used in all the experiments of the present investigation, for one material the values of k_a (or k_d) should be constant in every experimental run no matter what the water partial pressure is. In order to study the effect of reinforcing particles and chemical compositions on the kinetic behaviour of hydrogen in liquid DURALCAN™ composites and their matrices, an average value and a value of standard deviation of k_a and k_d for each material were calculated and listed in the last two columns of tables 5-1 and 5-2.

5.2 ANALYSES AND DISCUSSIONS

5.2.1 Rates of Degassing and Hydrogen Absorption

The central purpose of this present investigation is to study the kinetic behaviour of hydrogen absorption in molten DURALCAN™ composites. It is believed that the composites will show particular characteristics in hydrogen absorption other than their matrices due to the presence of the reinforcing ceramic particles. In this present investigation, experiments were conducted on hydrogen absorption and degassing of two typical DURALCAN™ composites: W6D.22A from the wrought alloy family and F3S.20S from the foundry alloy family as well as

their matrices. These experiments, as described in chapter 3, allow an evaluation for these materials of the rate constants of the processes of hydrogen absorption and degassing, k_a and k_d . In this section, an analysis will be presented on the rate of these two processes molten DURALCAN™ composites and their matrices.

An absolute value of hydrogen absorption rate is usually of great interest in practice. Under the present experimental conditions, the rate of hydrogen absorption was expressed in Eqn.

(4.42):

$$\frac{d[H]}{dt} = \Delta[H]k_a e^{-k_a t} \quad (5.1)$$

It can be seen from the above equation that the value of hydrogen absorption rate, $d[H]/dt$, is dependent upon two parameters: $\Delta[H]$, which represents a driving force for the process; and k_a , which is a rate constant or a total mass transfer coefficient for the process. With the evaluated values of the driving force $\Delta[H]$ and the rate constant, k_a , as given in Table 5-1, absolute values of hydrogen absorption rate could be calculated from Eqn. (5.1) for each experiment at different times during the process of hydrogen absorption. Comparisons of hydrogen absorption rates as a function of absorption time were made between W6D.22A and F3S.20S composites and their respective matrix alloys, and the results are graphically illustrated in Figs. 5-17 and 5-18.

It can be seen clearly from Figs. 5-17 and 5-18 that the hydrogen absorption rate was at the highest level at the beginning of the process and gradually became smaller and finally tended to zero when the process reached an equilibrium state. Since hydrogen absorption rate is

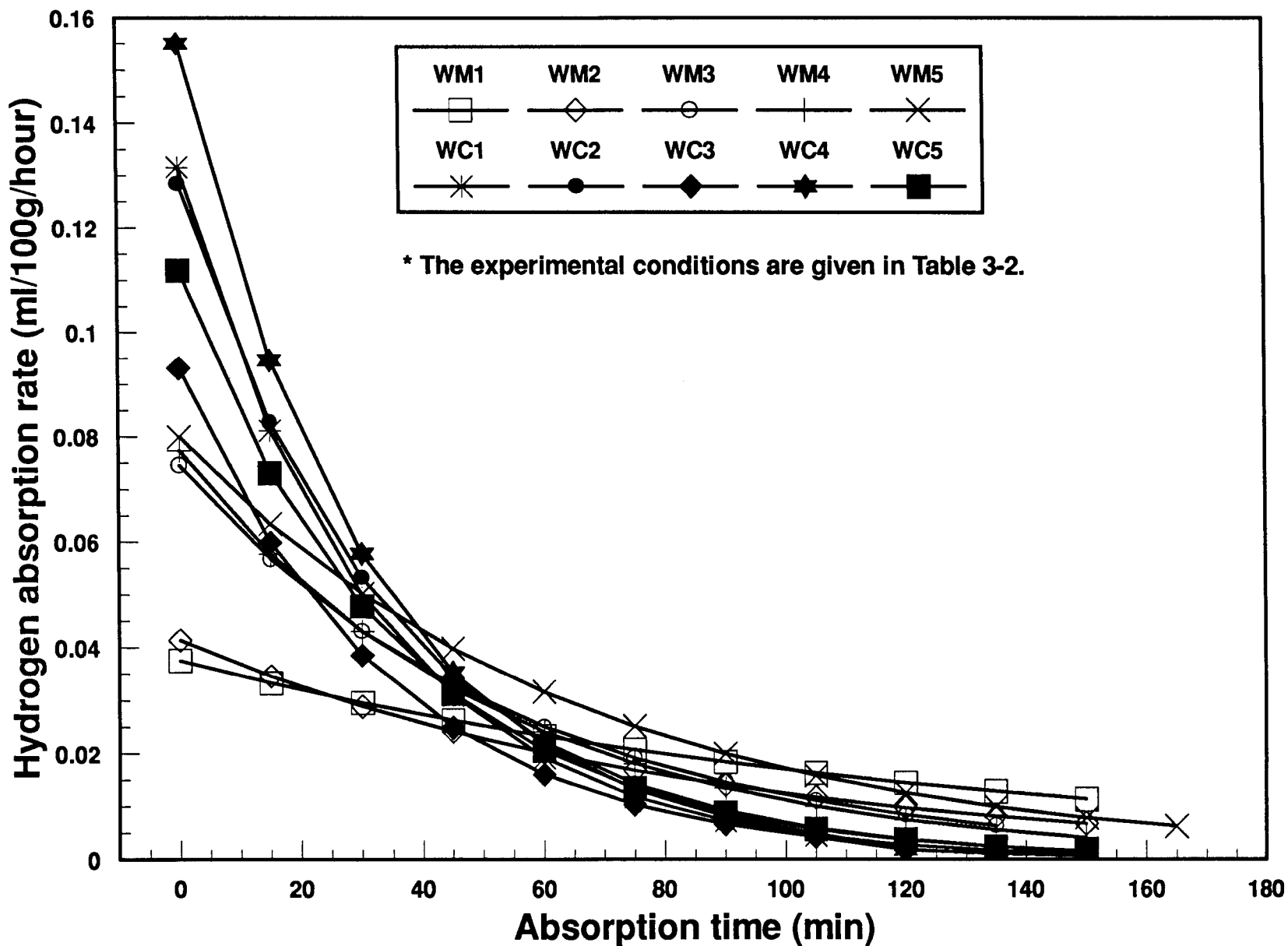


Figure 5-17. The hydrogen absorption rate of W6D.22A and its matrix alloy at different times during the process of absorption.

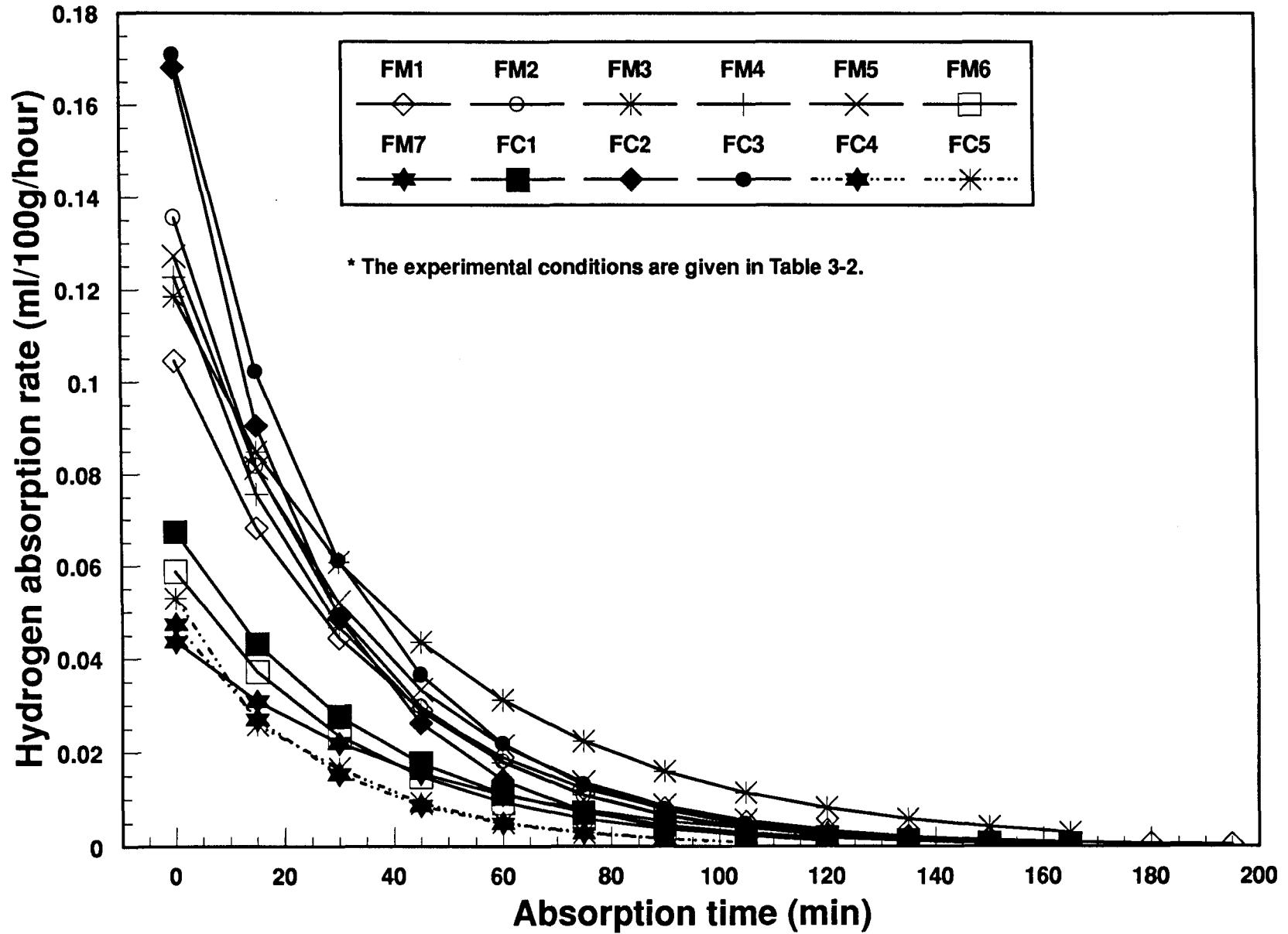


Figure 5-18. The hydrogen absorption rate of F3S.20S composite and its matrix alloy at different times during the process of absorption.

determined by the driving force, $\Delta[H]$, and the rate constant, k_a , when the product of these two factors was bigger for one experiment than others, the initial hydrogen absorption rate was higher for that experiment. This relationship could be easily found out from Figs. 5-17 and 5-18 and Table 5-1 where the evaluated parameters are listed. It could also be noted that the rate of hydrogen absorption is not directly dependent upon environmental conditions. This means that a higher initial hydrogen absorption rate would not necessarily need a higher water partial pressure on the day of the experiment, or vice versa. The atmosphere could become effective through its effect on the equilibrium value of hydrogen content of absorption, and indirectly affect the hydrogen absorption rate by changing the value of driving force $\Delta[H]$. The material also would take its effect on the rate of hydrogen absorption through the value of rate constant, k_a , which is a function of material and melt temperature.

A similar relationship between the degassing rate and the values of driving force, $\Delta[H]$, and rate constant, k_d , was given in Eqn. (4.46),

$$\frac{d[H]}{dt} = \Delta[H]k_d e^{-k_d t} \quad (5.2)$$

and a comparison of degassing rates from some of the experiments is graphically shown in Fig. 5-19. Due to the fact that unreasonably low readings of hydrogen content were occasionally given by Alscan at the beginning of degassing process and that these erroneous readings were not considered in the curve fittings as shown in Figs. 5-6 and 5-7, extrapolated values of hydrogen content from the fitted curves instead of actually measured hydrogen contents were used in the calculation of the driving force, $\Delta[H]$. Therefore, the real degassing rate at the start of degassing

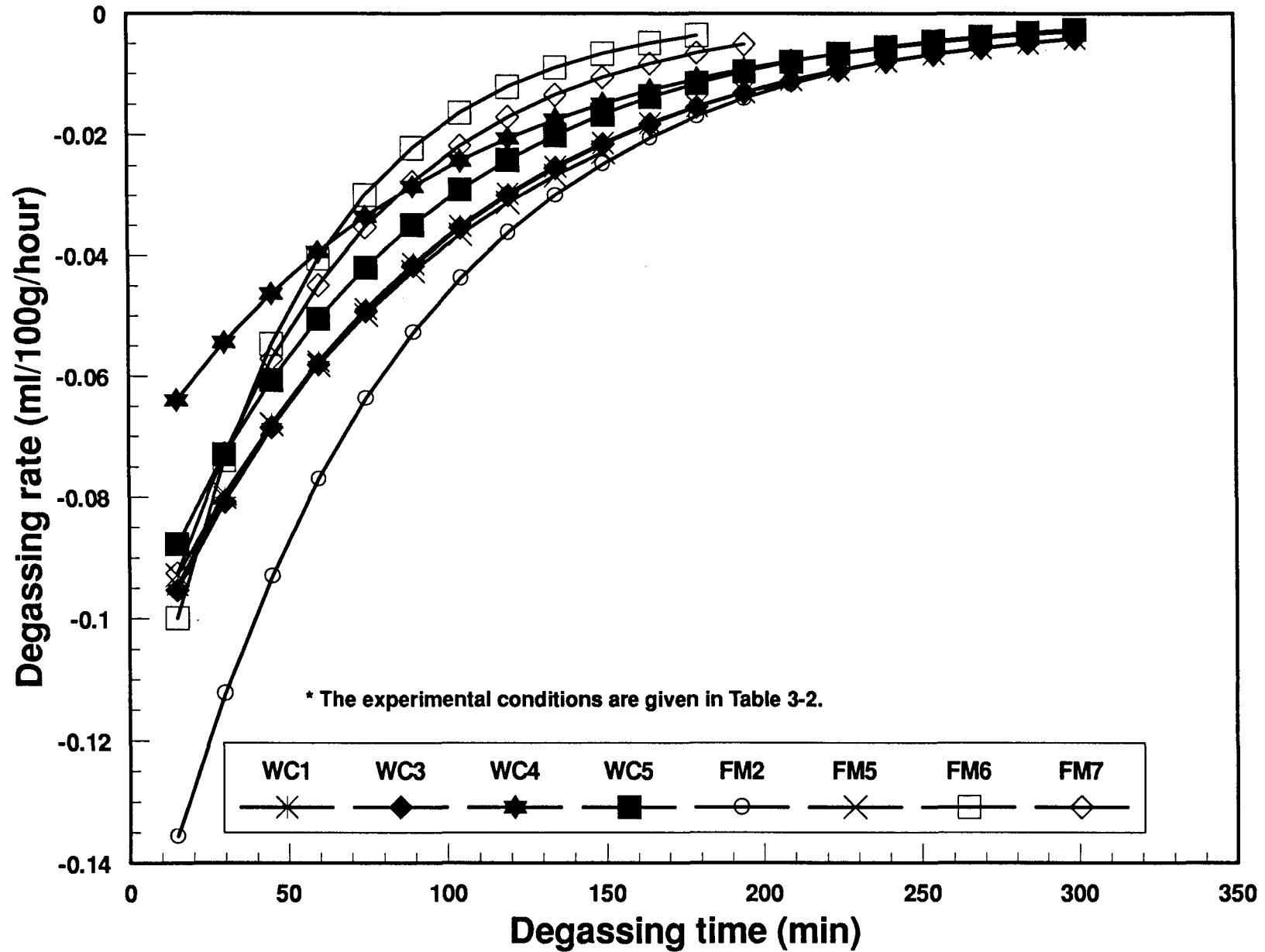


Figure 5-19. The rate of degassing for some of the experiments at different times during the degassing process.

process could not be expressed properly by the rate values calculated from the extrapolated values of driving force, even though the part thereafter of the process could be perfectly described by the mathematical model, as shown in Figs. 5-13 through 5-16. Unlike the case of the rate of hydrogen absorption (Figs. 5-17 and 5-18), only the degassing rates from the experiments with reasonable Alscan readings at the beginning of degassing process were shown in Fig. 5-19. It can be seen from Fig. 5-19, the absolute value of degassing rate, like that of hydrogen absorption, was at the highest level at the beginning of the process, and decreased and approached to zero at the end of the process. It also could be found out from Fig. 5-19 and table 5-2 that a larger value of the product of driving force, $\Delta[\mathbf{H}]$, and rate constant, \mathbf{k}_d , will give a higher initial degassing rate, and vice versa, which is in accordance with the mathematical expression given in Eqn. (5.2). It also should be noted that the rate of degassing is negative indicating that the hydrogen level of the melt is decreasing during the degassing process compared to the increase in the hydrogen level which is seen during the process of hydrogen absorption. The rate of the latter process is positive as shown in Figs. 5-17 and 5-18. In the case of degassing, the environmental condition is even less important than in the case of hydrogen absorption because of the uncertainty of its effect on the value of equilibrium hydrogen content and the value of driving force. This can be seen from Table 5-2. The effect of material on degassing rate, like the case of hydrogen absorption, is through the value of rate constant, \mathbf{k}_d . The effects of atmosphere and material on the rates of the processes will be discussed separately in the following sections.

5.2.2 Effects of the Reinforcing Particles

The kinetic behaviour of hydrogen absorption and degassing of molten DURALCANTM composites is of great concern in the production and processing of these materials. It is believed to be different from their matrix alloys due to the presence of a large volume percent of ceramic particles. This kinetic behaviour, however, has not been well understood because of the lack of a quantitative analysis of the processes, which makes this present work necessary. In the present investigation, experiments were so designed that it is possible to evaluate the kinetic parameters, k_a and k_d , under various environmental conditions for the composites and their matrices as well. Therefore, the effects of the reinforcing particles on the kinetics of hydrogen absorption and degassing could be seen by a comparison of the values of k_a and k_d of the composites with those of the matrices, which were given numerically in Tables 5-1 and 5-2 and shown graphically in Figs. 5-20 for the rate constant of hydrogen absorption, k_a , and 5-21 for degassing rate, respectively.

From Table 5-1 and Fig. 5-20, it can be found that the difference in k_a values was evident between the composites and their matrices. This difference was more significant for W6D.22A composite, reinforced by alumina, being 108% higher in the mean value of k_a than its matrix alloy. Compared to this, F3S.20S, reinforced by silicon carbide, was only 27% higher than its matrix. This indicates that the presence of the ceramic particles make it easier for molten DURALCANTM composites to absorb hydrogen from the atmosphere, at least under the experimental conditions of the present investigation. Furthermore, there exists a difference

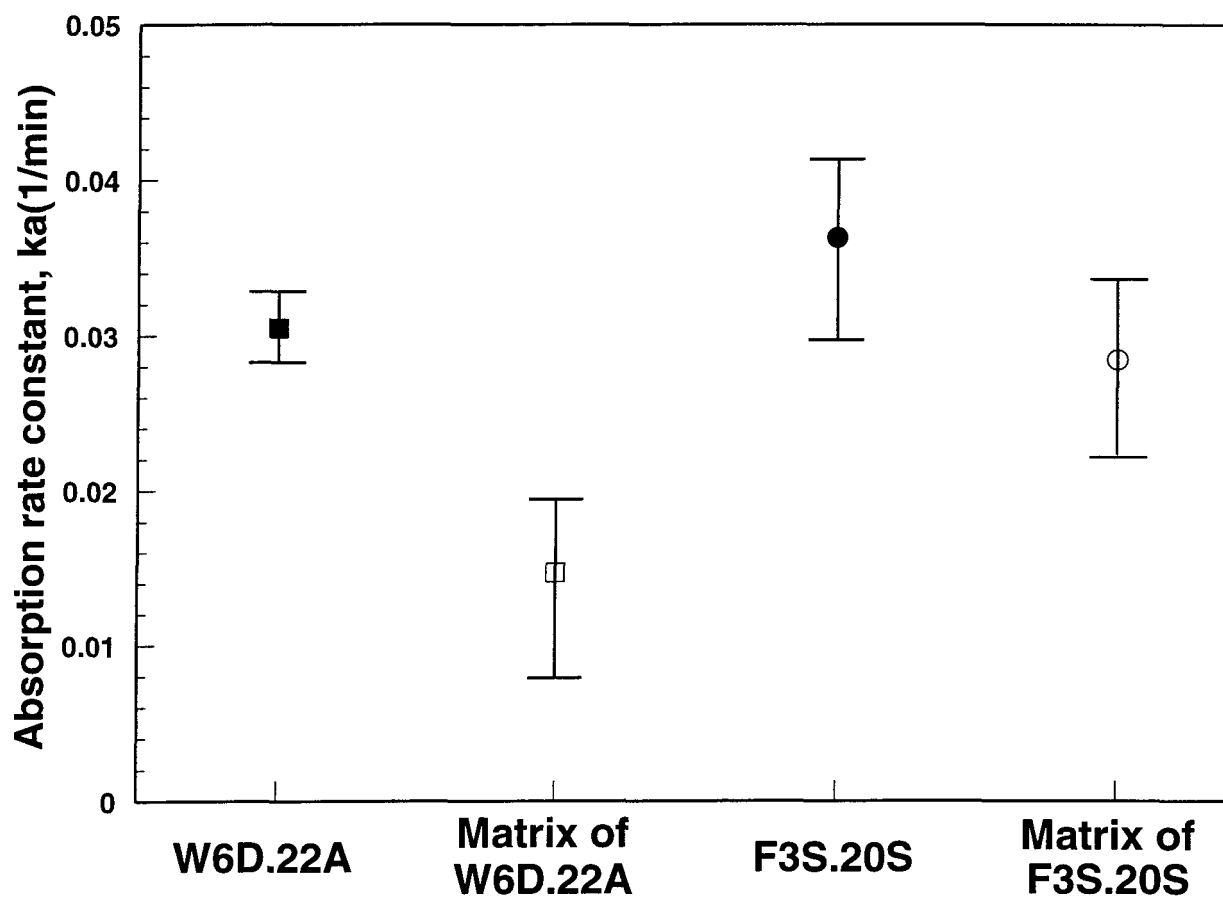


Figure 5-20. A comparison of the rate constant of hydrogen absorption, k_a , for different materials (markers represent the mean values).

between the effects of the two different particles of alumina and silicon carbide, i.e., the effect of alumina seems stronger than that of silicon carbide.

In order to analyze the effects of the reinforcing particles on the rate of hydrogen absorption in molten DURALCAN_{TM} composites, let's recall the definition of the total mass transfer coefficient, k_t , given in Eqn. (4.13):

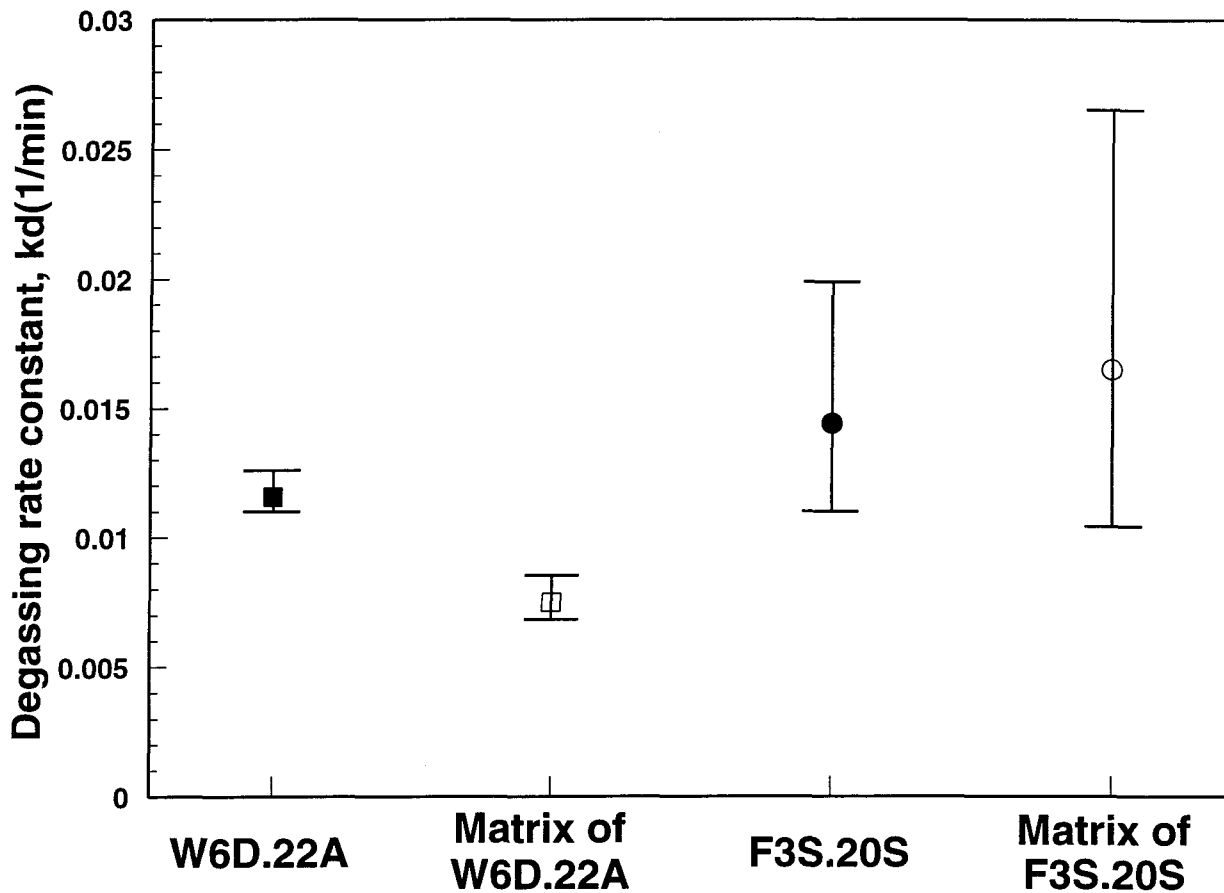


Figure 5-21. A comparison of the degassing rate constant, k_d , for different materials (markers represent the mean values).

$$\frac{1}{k_t} = \frac{1}{k} + \frac{\sqrt{2\pi M_j RT}}{K_j \gamma_j} + \frac{RT}{k_g K_j \gamma_j} \quad (5.3)$$

This total mass transfer coefficient, k_t , was used in the mathematical analysis as the rate constant, k_a , for the process of hydrogen absorption, and k_d , for the process of degassing. The three terms at the right-hand side of Eqn. (5.3) represent the three resistances against the mass transfer in the processes. These are the melt boundary layer, the evaporation, and the gas boundary layer, respectively. It is evident that no influence can be found of liquid metal on the values of the last two terms on the right-hand side of Eqn. (5.3). The melt could take its effect on the total mass

transfer coefficient only through the value of k , the first term at the right-hand side of Eqn. (5.3), which is the mass transfer coefficient for the melt boundary layer. Under the present experimental condition where the melt is thoroughly stirred, k could be expressed as [23],

$$k = \frac{D}{2\delta_2} \quad (5.4)$$

where D is diffusion coefficient and δ_2 is the thickness of the melt boundary layer. No evidence has been found that the presence of ceramic particles have significant influence on the values of either the diffusion coefficient D of liquid metal or the thickness of melt boundary layer δ_2 , which means that ceramic particles have no significant effect on the value of mass transfer coefficient k for the melt boundary layer.

It seems, based on the above analysis, that the rate of hydrogen absorption of molten aluminum should have nothing to do with the composition of the liquid metal. This is obviously wrong because the results of our experiments show that there does exist a difference in the rates of the processes of hydrogen absorption and degassing between the composites and their matrices. Actually, in the definition of the total mass transfer coefficient and the development of mathematical models for the processes, there is one parameter that has not been taken into account, which is the oxide layer on the top of the melt. The fact that the oxide layer has not been considered in the mathematical models does not affect the accuracy of the models, which could be proved by the fitted curves shown in Figs. 5-9 through 5-12 for hydrogen absorption and Figs. 5-13 through 5-16 for degassing. However, the oxide layer does play a role in the kinetics of these processes [13,14,23]. The mechanisms of the formation of oxide layer of molten

DURALCAN™ composites and their matrices and those of the transport of hydrogen through this layer are beyond the scope of the present investigation. What we could know is that due to the presence of a large volume percent of ceramic particles, molten DURALCAN™ composites can form an oxide layer with a different structure other than their matrices, and hydrogen will transport through these different oxide layers with different rates. This is reasonable since in the process of hydrogen absorption the melt was completely open to the atmosphere and a thick layer of oxide was formed and it was not destroyed during the whole absorption process. The difference in the effects of the two different ceramic particles could also be explained by the possibility that different oxide layers were formed, resulting from the possible interactions between the reinforcing particles and the matrix alloys.

The case for degassing process was different, because the melt was isolated from the atmosphere by a layer of N₂ gas blown in between the melt surface and a cover of refractory plate. Little, if any, oxide was formed during the whole degassing process. Consequently, the effect of oxide layer was much less important for the process of degassing, as it can be found from Fig. 5-21 and Table 5-2 where the k_d value is 54% higher for the W6D.22A than its matrix alloy compared to a 108% difference in the values of k_d . The value of k_d for the F3S.20S composite is even smaller than that of its matrix alloy by 12%.

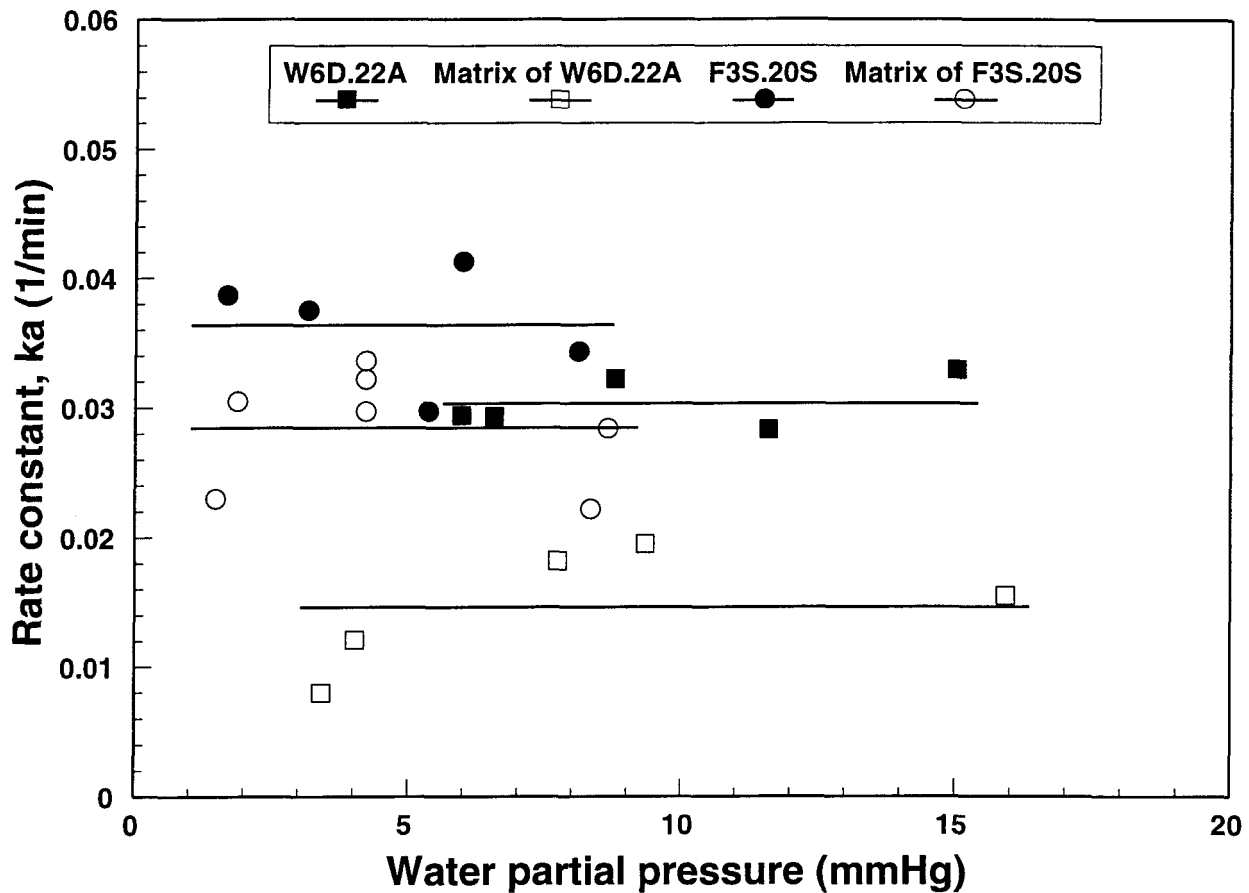


Figure 5-22. A diagram showing that k_a is constant with the water partial pressure in the atmosphere.

5.2.3 Effects of the Atmospheric Conditions

As indicated previously, the values of the rate constants for hydrogen absorption, k_a , and that for degassing, k_d , have nothing to do with environmental conditions. They are functions of material and melt temperature only. This relationship could be seen from the definition of the mass transfer coefficient given in Eqn. (4.3) and that of the total mass transfer coefficient given in Eqn. (4.13) which were used as the rate constants for the processes. An experimental

examination of such a relationship helps to prove the correctness of the models of hydrogen absorption and degassing. This is shown in Fig. 5-22 where the evaluated values of k_a of each experiment were plotted against the water partial pressure of the day when that experiment was conducted. It can be seen from Fig. 5-22 that the k_a values were roughly constant with the observed values of water partial pressure in the atmosphere. A certain degree of scattering exists, though, which may be caused by fluctuations of the experimental conditions and the measuring devices. Similarly, during the process of degassing, the dry atmosphere on the top of the melt was provided by N_2 gas blown in between the melt surface and a refractory cover, therefore, the atmospheric condition could be represented by the flow rate of N_2 . The k_d values of W6D.22A and its matrix alloy were plotted versus the values of N_2 flow rate (column 3 of Table 3-2) in Fig. 5-23, from which we can see that k_d was constant with the flow rate of N_2 and there is no correlation between them. Such a relationship indicates that the atmosphere conditions and the rate constants, k_a and k_d , are independent parameters that play different roles in influencing the rate of hydrogen absorption and degassing.

However, as mentioned previously, the environmental conditions do have their effect on the rates of the processes of degassing and hydrogen absorption by changing the values of the driving force, $\Delta[H]$, of the processes. Actually the value that is influenced directly by the environmental conditions is the equilibrium hydrogen content of the processes. For hydrogen absorption, the relationship between the equilibrium hydrogen content and the water partial pressure in the atmosphere has been given in Eqn. (4.43), which could be simplified as,

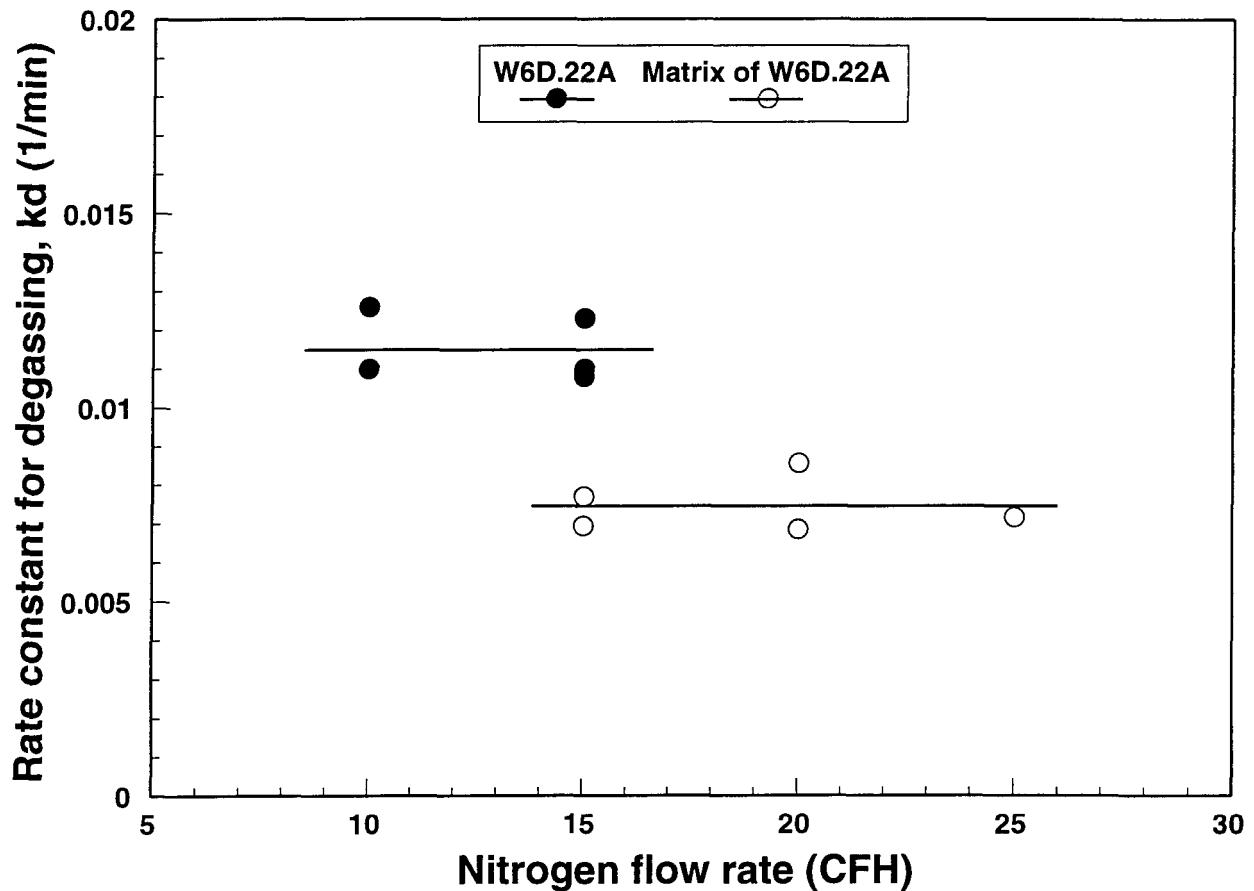


Figure 5-23. A diagram showing that the k_d values were constant with the flow rate of N_2 .

$$[H]_e = K\sqrt{p_{H_2O}} \quad (5.5)$$

where K is a constant. Eqn. (5.5) indicates that the equilibrium hydrogen content for the process of hydrogen absorption is proportional to the square root of water partial pressure in the atmosphere. In order to have a clear view of this relationship, the equilibrium values of hydrogen content (given in column 5 of Table 5-1) for hydrogen absorption of the composites and their matrices are plotted in Fig. 5-24 against the observed values of the square root of water partial pressure (given in column 3 of Table 5-1). It can be seen from Fig. 5-24 that the equilibrium hydrogen content increases with increasing water partial pressure, and a good linear relationship

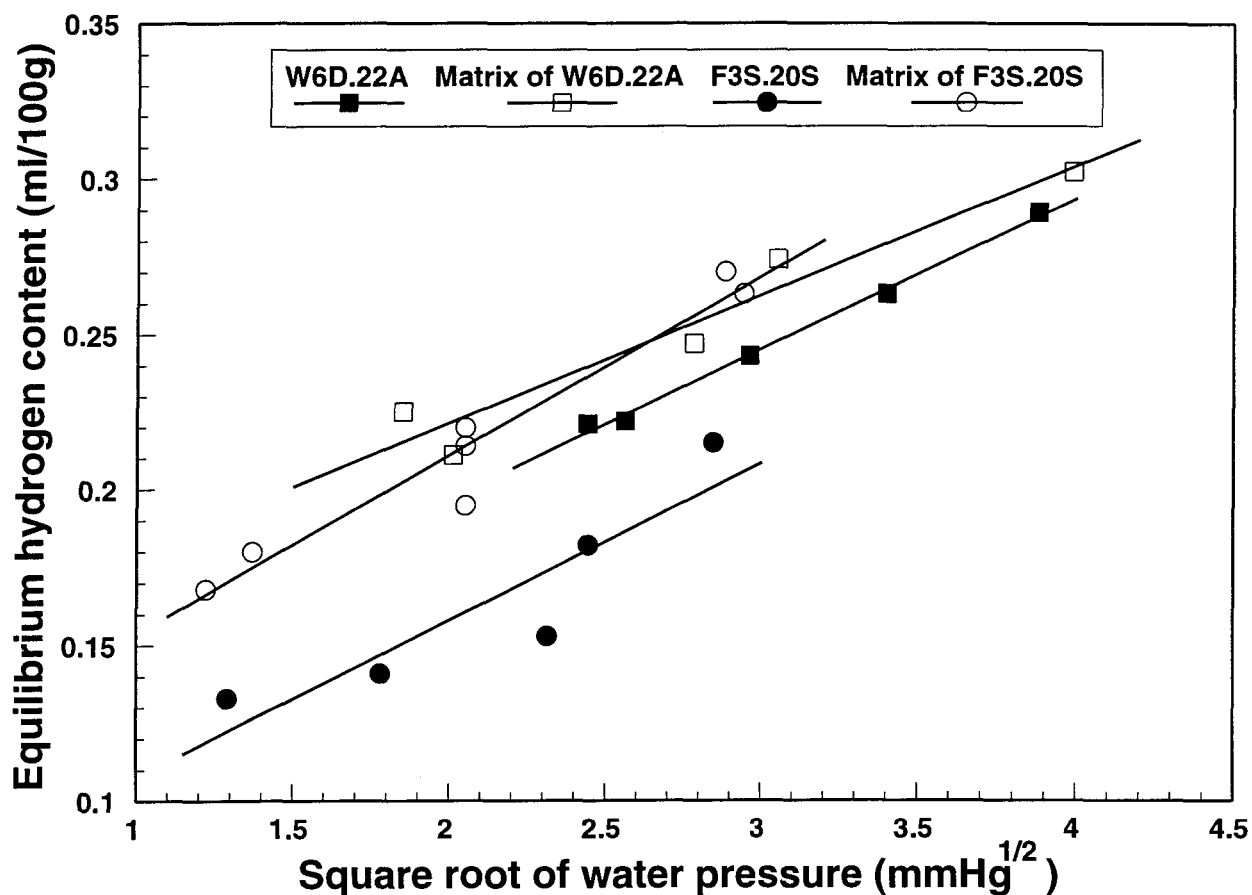


Figure 5-24. Relationship of the equilibrium hydrogen content of absorption and the water partial pressure in the atmosphere.

between $[H]_e$ and $\sqrt{p_{H_2O}}$ was obtained for each alloy, which indicates that the Sieverts' law

expressed in Eqn. (5.5) were generally obeyed.

It should also be noted from Fig. 5-24 that the equilibrium values of hydrogen contents of the composites were always smaller than those of their matrices under the same environmental conditions. These relatively low Alscan readings for the composites are not believed to be caused by the effect of reinforcing particles on hydrogen solubility of these materials but by something

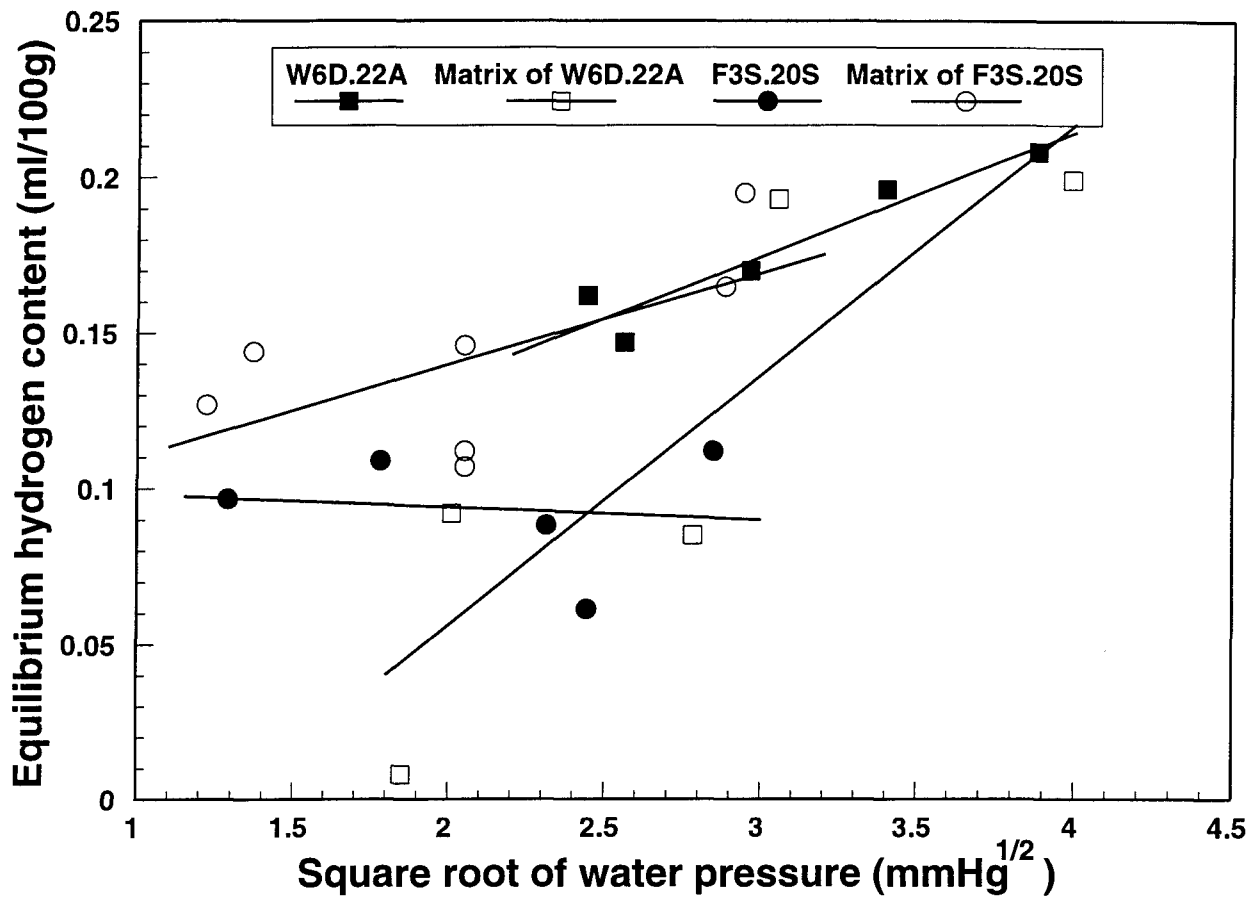


Figure 5-25. Relationship between the equilibrium values of hydrogen content and water partial pressure for degassing.

else, which could be explained below. As presented earlier in section 3.5.2 that Alscan works on the basis of Sieverts' law expressed in Eqns. (3.1) and (5.5), where K represents hydrogen solubility of the melt, which varies with melt temperature and chemical composition. Hydrogen solubility of molten DURALCANTM composites has been believed to be different from those of their matrices due to the presence of the ceramic particles. This is conceivable if only the volume factor of the reinforcing particles is considered, i.e., less hydrogen should be contained by a same amount of composite than its matrix alloy, because a considerable volume of the composite is occupied by the ceramic particles which contain no hydrogen. In the present investigation,

however, the same alloy correction factor was used for each pair of composite-matrix alloy due to the lack of correction factors for the reinforcing particles, and the melt temperatures were always the same for all the experiments. Alscan should give the same reading if the environmental conditions were the same, i.e., at the same value of p_{H_2O} . The reason that causes the relatively low Alscan readings of hydrogen content in the composites may be the blocking effect of the ceramic particles on Alscan probe. This effect has been shown in Fig. 3-9, from which we can see that a longer time is needed for hydrogen probe to get equilibrium with the melt in composites than in the matrices. In the experiments, however, the same Alscan cycle time (15 min) was employed for all the experiments, which means that at the end of a cycle the equilibrium of Alscan probe has already been established for the matrix alloy but for the composite this equilibrium has not been reached. This is the Alscan reading at the end of a cycle is lower for the composites than the actual hydrogen content that should be detected in a longer time. Another factor for the lower reading of hydrogen content in the composites may be the fact that hydrogen can be adsorbed to the surface of the reinforcing particles and not all dissolved in the alloy, and hence a lower reading is observed. Fortunately, even though the absolute values of hydrogen contents observed in this present investigation in the molten DURALCAN™ composites of W6D.22A and F3S.20S are under question, the kinetic parameters obtained should be reliable because they represent a relative measure.

The relationship between the equilibrium value of hydrogen content for degassing and the water partial pressure is not certain, which is shown in Fig. 5-25. It can still be seen from Fig.

5-25 that the equilibrium hydrogen content increases with water partial pressure but the linear relationship is not as good as that for hydrogen absorption. This is because during the process of degassing the melt surface was not exposed completely to air and the atmosphere could not act on the liquid metal as directly as in the process of hydrogen absorption. However, the atmosphere could still have its influence on degassing because the melt surface could not be isolated completely and some water vapour could penetrate through the N₂ layer and react with the metal, and this effect would be stronger in the days when the water partial pressure was higher.

5.2.4 The Half-Recover Period of Hydrogen Absorption

In the study of chemical kinetics, an important parameter which denotes the apparent reaction rate is the half-recover period, $t_{1/2}$. Under the present situation of hydrogen absorption, the half-recover period can be defined as the time required for the molten metal to attain a hydrogen level expressed below,

$$[H]_{t_{1/2}} = [H]_0 + \frac{1}{2}([H]_e - [H]_0) \quad (5.6)$$

Substituting Eqn. (5.6) into Eqn. (4.40) we have the expression of the half-recover period, $t_{1/2}$, as,

$$t_{1/2} = \frac{\ln 2}{k_a} \quad (5.7)$$

which is also illustrated in Fig. (5-26). This parameter is important in practice during composite

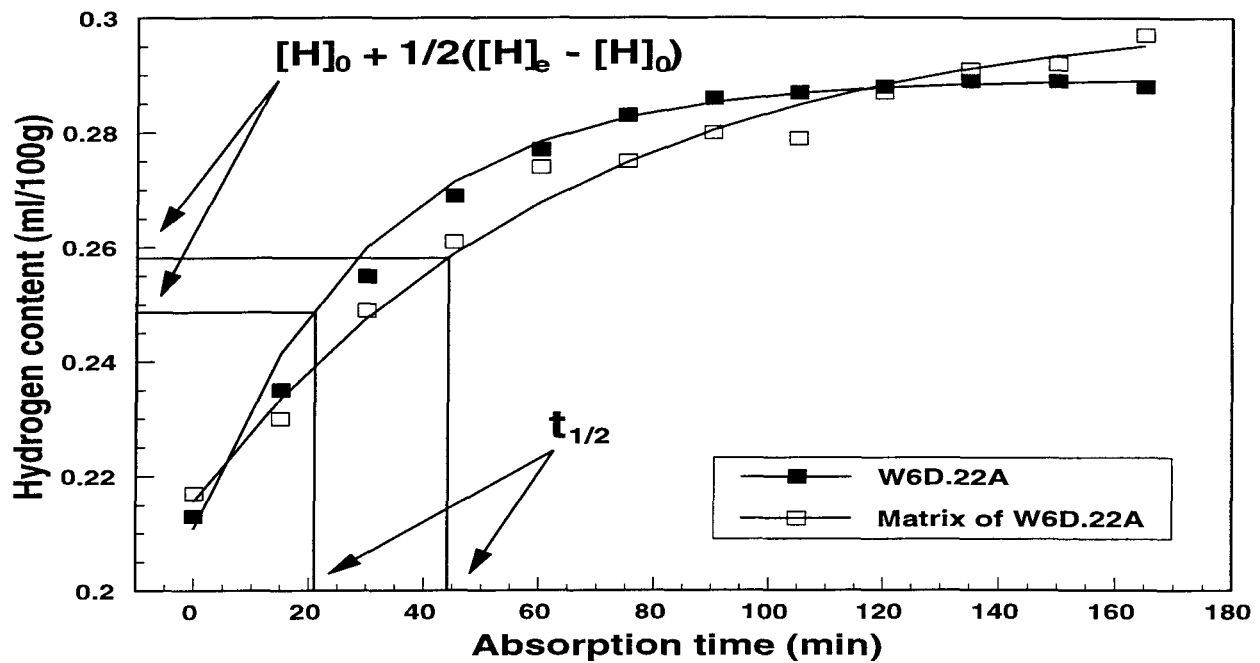


Figure 5-26. A graphical illustration of the half-recover period for hydrogen absorption of molten W6D.22A composite and its matrix alloy.

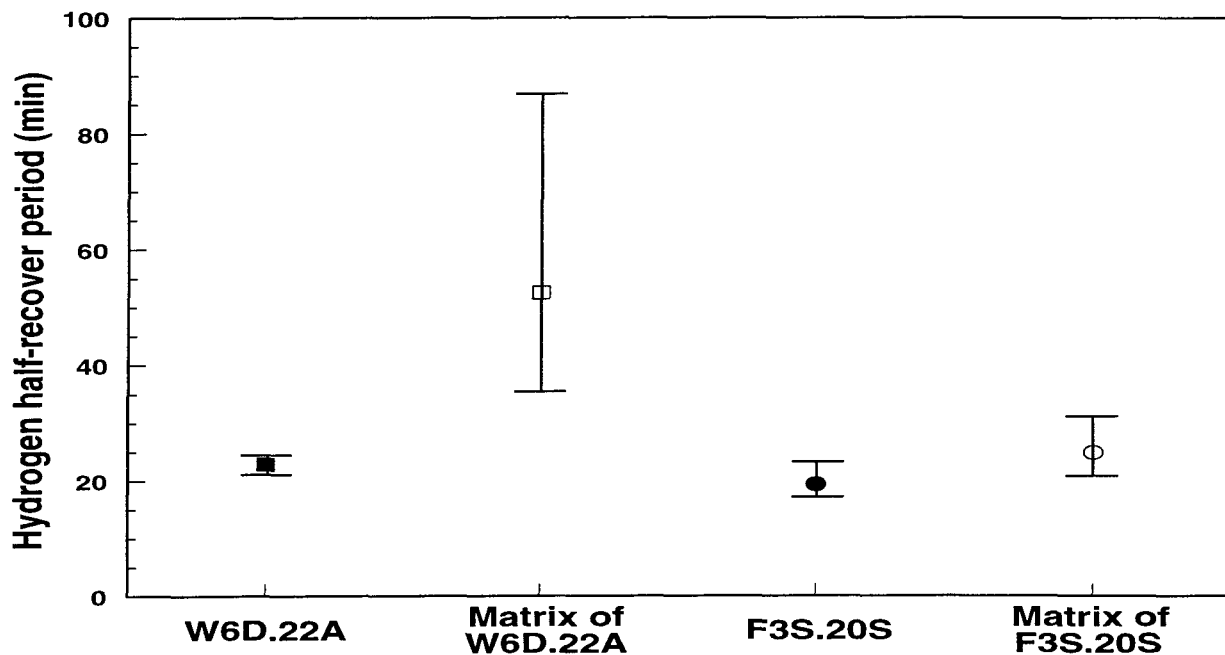


Figure 5-27. A graphical comparison of the half-recover period, $t_{1/2}$ for hydrogen absorption between the composites and their matrices.

melt treatments and during the production of the composite material, because it gives an idea of

the time needed for a particular molten composite to absorb hydrogen from the atmosphere to a certain level under given conditions, such as melt temperature, etc. Eqn. (5.7) indicates that the half-recover period is inversely proportional to the rate constant, k_a . It is a function of the material and melt temperature only and has nothing to do with the atmospheric conditions. The calculated values of the $t_{1/2}$ for each composite and the matrix alloy are given in Table 5-3, and they are graphically shown in Fig. 5-27.

Table 5-3 The Half-recover Period for the Composites and their Matrices

$t_{1/2}$ (min)	Materials	W6D.22A	Matrix of W6D.22A	F3S.20S	Matrix of F3S.20S
Maximum		24.493	86.861	23.338	31.223
Minimum		21.068	35.546	16.783	20.629
Average		22.864	52.499	19.345	24.855
Standard Deviation		1.327	18.758	2.283	3.862

It can be seen from Table 5-3 and Fig. 5-27 that the values of half-recover period, $t_{1/2}$, for hydrogen absorption, like k_a , are roughly constant for a particular alloy under the current experimental conditions. It is evident that the $t_{1/2}$ values for the composites are smaller than those of their matrix counterparts, this is an important information for the design of melt processing and quality control in the composite production because sometimes the $t_{1/2}$ value is more apparent and more direct in describing the rate of hydrogen absorption.

5.2.5 Effect of the Ratio of Melt Surface Area to its Volume

In the present investigation of the kinetic behaviour of hydrogen absorption in molten

DURALCAN™ composites, the only source of hydrogen has been assumed to be the reaction on the surface of liquid metal with water vapour in the atmosphere, and the controlling step of hydrogen absorption is the transport of hydrogen atoms across the melt-gas interface (melt surface) into the liquid metal from the bulk gas (atmosphere). In these circumstances, the ratio of interfacial area (melt surface area) to melt volume is usually of interest and becomes important to the kinetics of the reaction.

As indicated in section 4.2.4, a parameter of kA/V has been used, as a whole, as the rate constant of hydrogen absorption, k_a , i.e.,

$$k_a = k \frac{A}{V} \quad (5.8)$$

where A is the interfacial area, V is the melt volume, and k is actually the mass transfer coefficient for the process defined in Chapter 4. It should be noted that the mass transfer coefficient, k , has a unit of m/s, and the rate constants, k_a , and k_d , used in this presentation have a unit of 1/s. The accuracy of the kinetic parameters evaluated could not be influenced by this difference, because the same value of the ratio of melt surface area to the melt volume, A/V , has been used through out the experiments. However, in order to experimentally study the effect of the ratio of interfacial area to the melt volume on hydrogen absorption of the liquid metal, experiments with the matrix alloy of F3S.20S of hydrogen absorption have been conducted with various values of A/V as described in section 3.4. The results of the evaluated rate constant, k_a , are given together with the ones calculated according to Eqn. (5.8) in Table 5-4 below.

Table 5-4 Results of Evaluated k_a Values from Experiments with Various A/V Values

Experiment No.	A/V Value (1/cm)	Calculated k_a (1/min)	Evaluated k_a (1/min)
1	0.0502 [†]	0.0285*	0.0285*
2	0.0650	0.0304	0.0369
3	0.0752	0.0565	0.0427

† Initial A/V value. * The average k_a value given in Table 5-1.

In column 4 of Table 5-4 are given the k_a values calculated with Eqn. (5.8). The calculations were performed based on an initial k_a value as follows. From Eqn. (5.8) we have,

$$k = \frac{(k_a)_{initial}}{(A/V)_{initial}} \quad (5.9)$$

Substituting Eqn. (5.9) into Eqn. (5.8), we can calculate k_a with a given A/V as:

$$k_a = \left(\frac{(k_a)_{initial}}{(A/V)_{initial}} \right) \frac{A}{V} \quad (5.10)$$

The average k_a value of the matrix alloy of F3S.20S given in column 8 of Table 5-1 has been selected as the initial k_a value because it is an average of seven experiments with an identical A/V value (0.0502 1/cm), which has been called the initial A/V value given in Table 5-4. The effect of the ratio of A/V on the rate of hydrogen absorption could be seen better from Fig. 5-28, in which the evaluated k_a values are plotted, together with the calculated k_a values, against the measured A/V values. It is evident that the rate of hydrogen absorption should be higher with a larger ratio of interfacial area to melt volume. This is conceivable since the melt surface is the site for the reaction of liquid metal with water vapour in the atmosphere, and this reaction is the

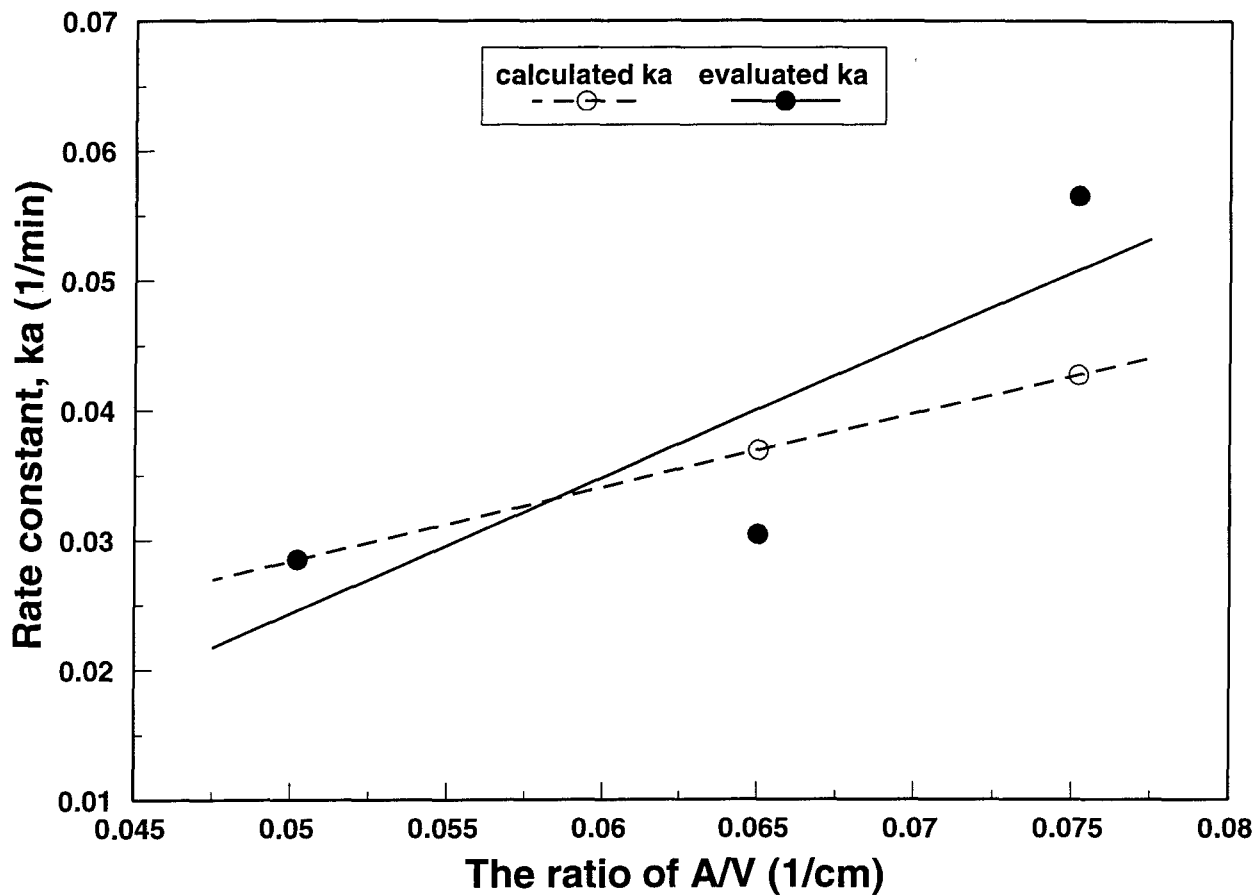


Figure 5-28. A diagram showing the effect of A/V on the rate of hydrogen absorption.

major source of hydrogen under the present experimental conditions for hydrogen absorption. To increase the area of the interface with regard to the melt volume means to enlarge the area of reaction site and is equivalent to increasing the hydrogen supply to the liquid metal and also to increasing the chance for hydrogen atoms to transport across the interface.

The effect of A/V ratio should be similar for the process of degassing because it is a reverse process to hydrogen absorption. Therefore, to enlarge the interfacial area will increase the chance for hydrogen atoms to transport from the melt to the free surface and, of course, will increase the rate of degassing of the melt. However, in the experiments, the ratio of A/V was

changed by reducing the amount of metal while the same crucible was used. When the amount of metal was reduced, the gap between the melt surface and the refractory cover would be enlarged correspondingly, as shown in Fig. 3-5a, and this will reduce the sealing effect of N_2 gas because the density of N_2 is almost the same with air. Consequently, the melt will have more chances to contact the air to increase the hydrogen supply on the melt surface, and degassing will be slowed. Therefore, under the particular experimental conditions in the present investigation, the effect of an increase in A/V value is two fold for degassing process, and the final result will depend upon which one is dominant.

5.3 SOURCES OF ERROR

Since the kinetic parameters for the processes of hydrogen absorption and degassing were evaluated from the measured values of hydrogen content, the measurement of hydrogen concentration in liquid metal during the processes became the critical part of this present investigation. In order to acquire a hydrogen concentration-time profile, a continuous measurement is required during the processes of hydrogen absorption and degassing, and Alscan is the only technique available to do this job. The accuracy of Alscan measurement of hydrogen content in common liquid aluminum alloys has been widely accepted. However, in the case of molten DURALCANTM composites, the Alscan probe may be blocked by the reinforcing ceramic particles present in a large percentage in liquid metal. This blocking effect has been found occasionally in the experiments and it is believed to be the major source of error in the present investigation. Fig. 5-29 shows the failure Alscan readings of hydrogen concentration seen in

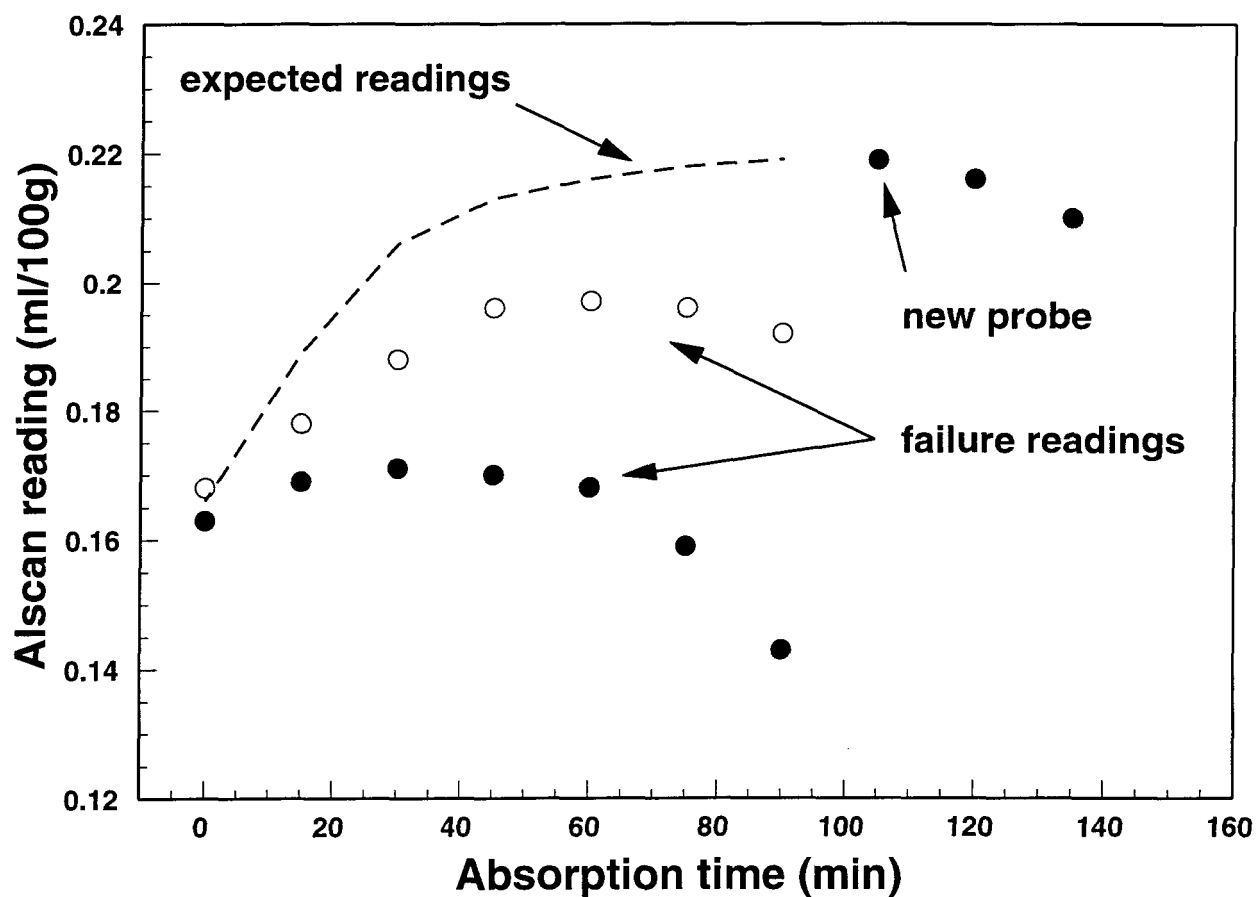


Figure 5-29. Failure Alscan readings during hydrogen absorption of molten W6D.22A composite.

experiments of hydrogen absorption carried on molten W6D.22A composite. Comparing the failed Alscan readings to the expected ones for hydrogen absorption, we can see that Alscan occasionally failed to detect the true hydrogen concentration of the melt. In practical investigation, the failed readings were simply discarded and reasonable ones were used in the evaluation of the kinetic parameters. Since this kind of failure has only happened in the composites, it is believed to be due to the blocking effect of ceramic particles on the Alscan probe. Another phenomena related to the blocking effect was shown in Fig. 3-9, from which we can see that a longer time is needed for Alscan probe to establish an equilibrium in molten

composite than in its matrix alloy. This also may be the reason for the difference between the composites and their matrices in the equilibrium values of hydrogen content in absorption as discussed earlier in section 5.2.3.

Another source of error which is associated with the measurement of hydrogen concentration is that Alscan occasionally gave unreasonably low readings at the beginning of the degassing process, as shown in Figs. 5-2, 5-6 and 5-3, 5-7. These erroneous readings were not considered in the curve fitting, and the fitted curves with the rest of observed values can perfectly

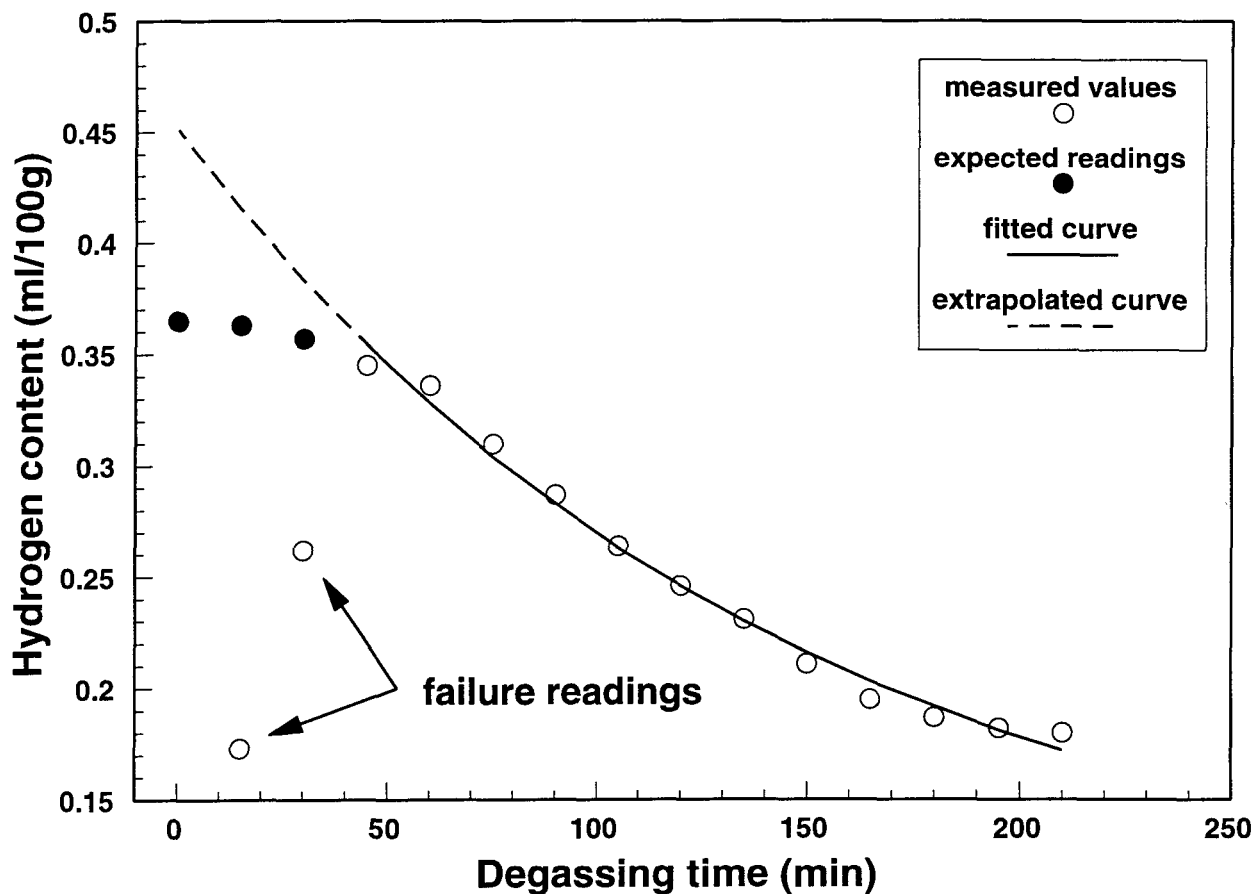


Figure 5-30. A comparison of the calculated values of hydrogen content to the expected ones at the beginning of degassing.

describe the later part of the process as seen from Figs. 5-13 through 5-16. However, these fitted curves did not take into account the true values of hydrogen concentration at the start of degassing which somehow have not been detected by Alscan. If the values of the hydrogen content at the beginning of degassing were calculated by extrapolating the fitted curve, the calculated values would not be equal to the true ones; in fact they are larger than the expected ones as shown in Fig. 5-30. One of the reasons causing this difference may come from the lag of the protection effect of N_2 , since it needs some time for N_2 gas to fill the gap between melt surface and the refractory plate to isolate the melt from the atmosphere at the beginning of degassing, and this will delay the protection effect of N_2 and slow down the rate of degassing at the beginning of the process. Actually the present mathematical model for degassing could not describe the very beginning of the process, even though the rest of the process could be described perfectly. This shortcoming of the mathematical model could bring errors by enlarging the scattering of the evaluated kinetic parameters for degassing, but it could not considerably influence the accuracy of the results.

In addition to the two sources of error discussed above, there is a factor which could also influence the accuracy of the experimental results. In the experiments with F3S.20S composite, a thick layer of sponge like foam could be formed on top of melt surface during the purging of Alscan probe. Since this has occurred only to F3S.20S composite, it is believed to be related to the silicon carbide particles which may be blown up above the melt surface by the bubbles of the purging gas from Alscan probe. Once the metal is blown up, it will solidify and gradually pile up to form sponge like layer of foam floating on top of the melt. The foam layer could be

as thick as 2 to 3 cm, and it may or may not affect the transport of hydrogen atoms across the interface into or out of the liquid metal. It should be noted that if there are no gas bubbles out of the melt, the foam won't be formed. In that case there is only oxide layer on top of the melt like the case of the other molten composite. The formation of the sponge like foam could limit the application of the kinetic parameters evaluated under the present experimental conditions for this material, since the surface condition of the melt could be a little different if no gas bubbles out during the processes of degassing and hydrogen absorption.

CONCLUSIONS

CONCLUSIONS

From the results of the present investigation, the following conclusions can be drawn:

1. The kinetic behaviour of degassing and hydrogen absorption in molten DURALCAN™ composites and their matrices could be studied by means of a continuous measurement of hydrogen concentration in the liquid metal during the processes, and Alscan apparatus can be used to acquire the hydrogen concentration-time profile for this purpose.
2. Degassing of the molten DURALCAN™ composites and their matrices can be carried out by isolating the melt surface from the atmosphere with an inert protection gas, N₂, and stirring the liquid metal to facilitate the diffusion of hydrogen atoms inside the melt. Hydrogen is eliminated from the liquid metal through the melt surface which is the interface of the liquid metal and the atmosphere.
3. In the present investigation, the only source of hydrogen in the process of hydrogen absorption was the reaction of the liquid metal with water vapour in the atmosphere. The equilibrium value of hydrogen concentration in the liquid metal was determined by the

value of water partial pressure in the atmosphere, and their relationship was found to obey Sieverts' law as follow,

$$[H]_e = K\sqrt{p_{H_2O}}$$

4. Under the present experimental conditions, the processes of hydrogen absorption and degassing could be expressed by the following equations,

$$\begin{aligned} [H] &= [H]_e - \Delta[H]e^{-k_a t} \\ [H] &= [H]_e - \Delta[H]e^{-k_d t} \end{aligned}$$

where k_a and k_d are rate constants for the processes of hydrogen absorption and degassing, respectively.

5. The rate of a process, degassing or hydrogen absorption, can be expressed as follow,

$$\begin{aligned} \left(\frac{d[H]}{dt}\right)_{\text{absorption}} &= \Delta[H]k_a e^{-k_a t} \\ \left(\frac{d[H]}{dt}\right)_{\text{degassing}} &= \Delta[H]k_d e^{-k_d t} \end{aligned}$$

and it is influenced by two different factors: the driving force, $\Delta[H]$, of the process; and the rate constant, k_a , or k_d . The rate constant, or the mass transfer coefficient, of a process of hydrogen absorption or of degassing is a function of material and melt temperature only. It does not vary with the change in atmospheric conditions above the melt surface. The rate constant of degassing process, k_d , is also independent of the flow rate of the protection gas, N_2 , on top of the melt surface. The atmospheric conditions could affect

the rate of hydrogen absorption by changing the value of the driving force of the process, $\Delta[\mathbf{H}]$, since $\Delta[\mathbf{H}] = [\mathbf{H}]_e - [\mathbf{H}]_0$, and $[\mathbf{H}]_e$ increases with increasing water partial pressure.

6. The values of rate constant of the process of hydrogen absorption for the DURALCAN™ composites have been found to be higher than those of their matrices. This could be attributed to the effect of ceramic particles. This effect of increasing the rate of hydrogen absorption of Al_2O_3 (for W6D.22A) was stronger than that of SiC (for F3S.20S). A possible reason for this effect was that the oxide on the top of the molten composites made it easier for hydrogen atoms to penetrate and diffuse through, due to the presence of a large volume percent of ceramic particles, and consequently the rate of hydrogen absorption for the composites was higher. The difference in the rate constant of degassing process between the composites and their matrices is not as evident as of hydrogen absorption because in the process of degassing there was less oxide formed on the top of the liquid metal and the effect of oxide is less significant.

7. Due to the difference in the values of the rate constant for hydrogen absorption between the composites and their matrices, the half-recover time of hydrogen absorption for the composites is shorter than that for their matrices. This indicates that it will take a shorter time for the composites to absorb the same level of hydrogen from the atmosphere than the matrices, and also the time needed to reach the equilibrium of hydrogen absorption is shorter for the composites than their matrices.

-
8. There was a difference in the equilibrium values of hydrogen content in the process of hydrogen absorption under the same environmental condition for each composite-matrix pair. In fact the equilibrium hydrogen concentration of a composite was always lower than that of the corresponding matrix alloy. This was not due to the difference in hydrogen solubility between the composites and their matrices, because the same alloy correction factor has been used for each composite-matrix pair, but it was caused by the blocking effect of the ceramic particles on the Alscan probe. As a result of this blocking effect, Alscan will give a lower reading of hydrogen content for the composites than their matrices under the same atmospheric condition if the cycle time for Alscan is the same.

 9. Under the present experimental conditions that the reaction on top of the melt surface of the liquid metal with water vapour is the only source of hydrogen. An increase in the value of the ratio of melt surface to its volume will increase the hydrogen absorption rate of the liquid metal because it increases the hydrogen supply with respect to the same volume of metal, and consequently, more hydrogen will transport into the melt during the same period of time. The value of the ratio of melt surface to its volume should have the same effect on the degassing process, since the chance to eliminate hydrogen out of the melt through the interface will be increased with a larger value of the A/V ratio.

REFERENCES

REFERENCES

1. John E. Hatch, Aluminum: Properties and Physical Metallurgy, ASM, Metals Park, Ohio, 1984.
2. P.D. Hess and G.K. Turnbull, "Effects of Hydrogen on Properties of Aluminum Alloys", Hydrogen in Metals, Proceedings of an International Conference on the Effects of Hydrogen on Materials Properties and Selection and Structural Design, Chmapion, PA, 23-27, Sep. 1973, I.M. Bernstein and A.W. Thompson eds., ASM 1974, pp. 277-87.
3. D.E.J. Talbot, "Effects of Hydrogen in Aluminum, Magnesium, Copper and their Alloys", Int. Met. Rev., 1975, vol. 20, pp. 166-83.
4. C.E. Ransley and H. Neufeld, "The Solubility of Hydrogen in Liquid and Solid Aluminum", J. Inst. Met., 1948, vol. 74, pp. 599-620.
5. D.E.J. Talbot and D.A. Granger, "Secondary hydrogen porosity in Aluminum", J. Ins. Met., 1963-64, vol. 92, pp. 290-97.
6. E.J. Whittenberger and F.N. Rhines, "Origin of Porosity in Castings of Magnesium-Aluminum and other Alloys", Trans. A.I.M.E., J. of Metals, April 1952, pp. 409-420.
7. P.M. Thomas and J.E. Gruzleski, "Threshold Hydrogen for Pore Formation during the Solidification of Aluminum Alloys", Met. Trans.B, 1978, vol. 9B, pp. 139-41.
8. B.R. Deoras and V. Kondic, "Testing the Gas Content of Molten Metals in a Foundry", Foundry Trade J., May 1956, pp. 361-66.
9. Robert D. Pehlke and Arden L. Bement, Jr, "Mass Transfer of Hydrogen between Liquid Aluminum and Bubbles of Argon Gas", Transactions of the Metallurgical Society of A.I.M.E., vol. 224, December 1962, pp. 1237-1242.
10. J.A. Dantzig, J.A. Clumpner and D.E. Tyler, "Degassing of Static Melts by Insoluble Purge Gases", Met. Trans.B, 1980, vol. 11B, pp. 433-438.

11. G.K. Sigworth and T.A. Engh, "Chemical and Kinetic Factors Related to Hydrogen Removal from Aluminum", Met. Trans.B, 1982, vol. 13B, pp. 447-460.
12. G.K. Sigworth, "A Scientific Basis for Degassing Aluminum", AFS Transactions, 87-81, pp. 73-78.
13. F.C. Dimayuga, N. Handiak and J.E. Gruzleski, "The Degassing and Regassing Behaviour of Strontium-Modified A356 Melts", AFS Transactions, 88-17, pp. 83-88.
14. J. Weigel and E. Fromm, "Determination of Hydrogen Absorption and Desorption Processes in Aluminum Melts by Continuous Hydrogen Activity Measurements", Met. Trans.B, vol. 21B, 1990, pp. 855-860.
15. P.D. Waite, "Use of a Hydrogen Diffusion Model for Prediction of Aluminum In-line Degasser Performance", RECENT DEVELOPMENTS IN LIGHT METALS, proceedings of 33rd annual conference of metallurgists of CIM , Toronto, Canada, 1994, pp. 431-440.
16. W.R. Opie and N.J. Grant, "Hydrogen Solubility in Aluminum and Some Aluminum Alloys", Trans. A.I.M.E., J. Met., 1950, vol. 188, pp. 1237-1241.
17. D.E.J. Talbot and P.N. Anyalebechi, "Solubility of Hydrogen in Liquid Aluminum", Mater. Sci. Tech., 1988, vol. 4, pp. 1-4.
18. P.N. Anyalebechi, D.E.J. Talbot and D.A. Granger, "The Solubility of Hydrogen in Liquid Binary Al-Li Alloys", Met. Trans.B, 1988, vol. 19B, pp. 227-32.
19. J.D. Fast, Interaction of Metals and Gases, Academic Press, New York, 1965.
20. C.H.P. Lupis, Chemical Thermodynamics of Materials, Elsevier Science Publishing Co., Inc., New York, 1983.
21. O. Kubaschewski and C.B. Alcock, Metallurgical Thermochemistry, Pergamon Press, 1979.
22. H. Liu, L. Zhang and M. Bouchard, "Determination of Hydrogen Solubility in Molten Aluminum and Aluminum-Copper Alloys", RECENT DEVELOPMENTS IN LIGHT METALS, proceedings of the 33rd annual conference of metallurgists of CIM , Toronto, Canada, 1994, pp. 257-268.
23. T. Abel Engh, Principles of Metal Refining, Oxford University Press, 1992.
24. J. Cambell, The Solidification of Metals, The Iron and Steel Institute, ISI Report No. 110, 1967.

-
25. M.C. Flemmings, Solidification Processing, McGraw-Hill Book Company, 1974.
 26. T.S. Piwonka and M.C. Flemmings, "Pore Formation in Solidification", Trans. A.I.M.E., 236(1966)1157-1165.
 27. M.F. Jordan, G.D. Denyer and A.N. Turner, "Porosity in High-Strength Semi-Continuously Cast Aluminum-Copper-Magnesium Alloy Ingots", J. Inst. Metals, 91(1962-63)48-53.
 28. C.E. Ransley and D.E.J. Talbot, "Wasserstoff-Porosität in Metallen unter besonderer Berücksichtigung des Aluminiums und seiner Legierungen", Z. Metallkde, 46(1955)328-337.
 29. K.E. Tynelius, "A Parametric Study of The Evolution of Microporosity in Al-Si Foundry Alloys", Ph.D. thesis, Drexel University, 1992.
 30. R. Jay and A. Cibula, "Influence of Magnesium Content on Layer Porosity and Tensile Properties of Sand-cast Aluminum/Magnesium Alloys, B.S. 1490-LM10 and B.S. (Aircraft) L.53", Foundry Trade Journal, 101(1956)131 and 407.
 31. W.R. Opie and N.J. Grant, "Effect of Hydrogen on Mechanical Properties of Some Aluminum Alloys", The Foundry, 78(1950)104.
 32. R.W. Ruddle and A. Cibula, "The Metallurgical Principles of the Control of Quality of Non-ferrous Castings", J. Inst. Metals, 85(1956-57)265.
 33. R.W. Ruddle, "Mould Reaction", Foundry Trade Journal, 94(1953)145.
 34. Marjorie Whitaker, "Mould-reaction in Aluminum-alloy Castings", Foundry Trade Journal, 95(1953)195.
 35. Marjorie Whitaker, "The Oxidation of Aluminum-Magnesium Alloys by Steam: A Contribution to Research on Mould Reaction", J. Inst. Metals, 82(1953-54)107.
 36. A.J. Swain, "Experiments on the Reaction of Aluminum-Magnesium Alloys with Steam", J. Inst. Metals, 80(1951-52)125.
 37. A.N. Turner and A.J. Bryant, "The Effect of Ingot Quality on the Short-Transverse Mechanical Properties of High-Strength Aluminum Alloy Thick Plate", J. Inst. Metals, 95(1967)353.
 38. L.W. Eastwood, Gas in Light Alloys, John Wiley & Sons, Inc., New York, 1946.

39. O. Kubaschewski, "Gas-Metal Equilibria", Gases and Metals, American Elsevier Publishing Company, Inc., New York, 1970.
40. A. Cibula, "Gases in Cast and Wrought Metals", *ibid.*
41. L.I. Sokol'skaya, Gases in Light Metals, Pergaman, London, 1961.
42. J.E. Gruzleski and B.M. Closset, The Treatment of Liquid Aluminum-Silicon Alloys, The American Foundrymen's Society, Inc., Des Plaines, Illinois, U.S.A., 1990.
43. Bruce Chalmers, Principles of Solidification, John Wiley & Sons, Inc., 1964.
44. Fred O. Traenkner, "Practical Techniques for Casting Aluminum", Modern Casting, December, 1981, pp. 44-48.
45. R.K. Owens, H.W. Antes and R.E. Edelman, "Effect of Nitrogen and Vacuum Degassing on Properties of a Cast Aluminum-Silicon-Magnesium Alloy (Type 356)", Trans. AFS, 65(1957)424-431.
46. G.K. Sigworth, "Practical Degassing of Aluminum", Modern Casting, March, 1988, pp. 42-44.
47. G.H. Geiger and D.R. Poirier, Transport Phenomena in Metallurgy, Addison-Wesley Publishing Company, Inc., 1973.
48. J.P. Martin, F. Trembley and G. Dube, "HyDRAL: A New and Simple Technique for In-line Analysis of Hydrogen in Aluminum Alloys", Light Metals, A.I.M.E., 1989, pp. 903-921.
49. AISCAN User's Manual, Version 2.2, BOMEM INC., January 1991.
50. Prince N. Anyalebechi, "Techniques for Determination of the Hydrogen Content in Aluminum and its Alloys", Light Metals, A.I.M.E., 1991, pp. 1025-1046.
51. Lawrence D. Ray, "A Comparative Assessment of Quantitative Hydrogen Analyzers Commonly Used in the Aluminum Industry", Light Metals, A.I.M.E., 1992, pp. 1031-1047
52. R. Gee and D.J. Fray, "Instantaneous Determination of Hydrogen Content in molten Aluminum and its Alloys", Met. Trans. B, 1978, vol. 9B, pp. 427-30.
53. G.K. Sigworth, "A Novel Method for Gas Measurement in Aluminum", Light Metals, A.I.M.E., 1993, pp. 981-89.

-
54. D.A. Anderson, D.A. Granger, and R.R. Avery, "the Alcoa Telegas II™ Instrument", Light Metals, A.I.M.E., 1990, pp. 769-73.
 55. Lawrence D. Ray, "Long-Term Assessment of the Alscan Hydrogen Analyzer", Light Metals, A.I.M.E., 1992, pp. 1069-1074
 56. Colin Bodsworth, The Extraction and Refining of Metals, CRC Press, Inc., Boca Raton, Florida, 1994.
 57. CRC Handbook of Chemistry and Physics, 59th edition, Robert C. Weast and Melvin J. Astle eds., CRC Press, Inc., Florida, 1978-1979.

APPENDIX

A LIST OF THE PROGRAM USED FOR DATA ANALYSIS

```

C
C   Reg_absorption.f
C
C=====
C           REGRESSION FOR EXPERIMENTAL DATA OF ABSORPTION
C           The required function is
C            $Y = A + B \cdot \exp(C \cdot X)$ 
C=====
C
C
C *****
C DEFINITION OF VARIABLES
C *****
C
C   X(n):           The vector of x.
C   Y(n):           The vector of y.
C   YT(n):          The transform of Y,  $YT = \ln(A - Y)$ .
C
C   Yhat(n):        Y hat,  $Yhat = C0 + C1 \cdot x$ .
C   Resi(n):        The vector of residual.
C   Rsqr:           The sum of square of the residual.
C                    $R2 = Y2 - Yhat2$ .
C   R0sqr:           $R0sqr = Y2 - n \cdot Ybar2$ .
C   regsqr:         The coefficient of regression.
C                    $r2 = 1 - R2/R02$ .
C
C   n:              The number of values.
C
C *****
C MAIN PROGRAM
C *****
C
C   program Reg
C
C   implicit real (a-h, o-z)
C
C   common / array / X(20), Y(20), YT(20), Yhat(20), Rate(20)
C   common / var / Ymax, trial, C0, C1, regsqr, Rsqr, R0sqr
C   common / var / step, dstnc
C   common / int / n
C
C   call data
C   trial=Ymax+step
C   call initia
C   call call
C   call cal2
C
C   bstc=trial
C   r2min=regsqr

```

```
c
do while (trial.LE.(Ymax+dstnc))
    trial=trial+step
    call initia
    call cal1
    call cal2
    if(abs(1.0-regsqr).LE.abs(1.0-r2min)) then
        bstc=trial
        r2min=regsqr
    endif
enddo

c
trial=bstc
call initia
call cal1
call cal2
call output

c
stop
end

c
c
c *****
c SUB PROGRAMS
c *****
c
c Data input
c -----
c subroutine data

c
implicit real (a-h, o-z)

c
common / array / X(20), Y(20), YT(20), Yhat(20), Rate(20)
common / var / Ymax, trial, C0, C1, regsqr, Rsqr, R0sqr
common / var / step, dstnc
common / int / n

c
open(unit=10, file='y.dat', status='unknown')
read(10, *)
read(10, *)
read(10, *)
read(10, 100)n
read(10, 110)Ymax
read(10, 120)step
read(10, 130)dstnc
read(10, *)
read(10, 110)(Y(i), i=1, n)
close(unit=10)

c
100 format(I4)
110 format(F6.3)
```

```
120 format(E10.1)
130 format(F6.2)
c
  return
  end
c
c
c Data initialisation
c -----
c subroutine initia
c
c implicit real (a-h, o-z)
c
c common / array / X(20), Y(20), YT(20), Yhat(20), Rate(20)
c common / var / Ymax, trial, C0, C1, regsqr, Rsqr, R0sqr
c common / var / step, dstnc
c common / int / n
c
c do 200 i=1, n
c   X(i)=0.0
c   YT(i)=log(trial-Y(i))
c   X(i)=float(i-1)*15.0
200 continue
c
c return
c end
c
c
c Calculations of Xbar, Ybar, sumx, sumy, sumx2, sumxy, and C0,
c C1.
c -----
c subroutine call
c
c implicit real (a-h, o-z)
c
c common / array / X(20), Y(20), YT(20), Yhat(20), Rate(20)
c common / var / Ymax, trial, C0, C1, regsqr, Rsqr, R0sqr
c common / var / step, dstnc
c common / int / n
c
c sumx=0.0
c sumy=0.0
c sumx2=0.0
c sumxy=0.0
c
c do 300 i=1, n
c   sumx=sumx+X(i)
c   sumy=sumy+YT(i)
c   sumx2=sumx2+X(i)*X(i)
c   sumxy=sumxy+X(i)*YT(i)
```

```

300  continue
c
      Xbar=sumx/float(n)
      Ybar=sumy/float(n)
c
      C1=(sumxy-Ybar*sumx)/(sumx2-Xbar*sumx)
      C0=Ybar-Xbar*C1
c
      return
      end
c
c
c  Calculations of Yhat, residual, and coefficient.
c  -----
c  subroutine cal2
c
c  common / array / X(20), Y(20), YT(20), Yhat(20), Rate(20)
c  common / var / Ymax, trial, C0, C1, regsqr, Rsqr, R0sqr
c  common / var / step, dstnc
c  common / int / n
c
c  avgy=0.0
c  Rsqr=0.0
c  R0sqr=0.0
c  do 400 i=1, n
c      avgy=avgy+Y(i)
c      Yhat(i)=0.0
c      Rate(i)=0.0
c      Yhat(i)=trial-exp(C0+C1*X(i))
c      Rate(i)=60.0*(-1.0)*C1*exp(C0+C1*X(i))
c      Rsqr=Rsqr+(Y(i)-Yhat(i))**2
c      R0sqr=R0sqr+Y(i)*Y(i)
400  continue
c
c  avgy=avgy/float(n)
c  R0sqr=R0sqr-float(n)*avgy*avgy
c  regsqr=1.0-Rsqr/R0sqr
c
c  return
c  end
c
c
c  Output the result
c  -----
c  subroutine output
c
c  implicit real (a-h, o-z)
c
c  common / array / X(20), Y(20), YT(20), Yhat(20), Rate(20)
c  common / var / Ymax, trial, C0, C1, regsqr, Rsqr, R0sqr
c  common / var / step, dstnc

```

```
common / int / n
c
  open(unit=20, file='result', status='unknown')
  write(20, *)
  write(20, *)
  write(20, 500)
  write(20, *)
  write(20, 510)
  write(20, 520) (X(i), Y(i), Yhat(i), Rate(i), i=1, n)
  write(20, *)
  write(20, 530)
  write(20, 540)
  write(20, 550)
  write(20, 560) trial, exp(C0), C1
  write(20, *)
  write(20, 570)
  write(20, 580) Rsqr
  write(20, 590) R0sqr
  write(20, 600) regsqr
  close(unit=20)
c
500 format(6x, 'REGRESSION OUTPUT FOR ABSORPTION')
510 format(6x, 'X', 6x, 'Y', 11x, 'Yhat', 9x, 'Rate')
520 format(2x, F6.1, 2x, F6.3, 5x, F10.6, 3x, F10.6)
530 format(4x, 'The function is')
540 format(6x, 'Y = A + B*EXP(C*X)')
550 format(4x, 'The coefficients are')
560 format(6x, 'A = ', E13.6, 2x, 'B = ', E13.6, 2x, 'C = ',
E13.6)
570 format(4x, 'Residual and precision')
580 format(6x, 'R2 = ', E13.6)
590 format(6x, 'R02 = ', E13.6)
600 format(6x, 'r2 = ', F13.6)
c
  return
  end
```

```

C
C   Reg_degass.f
C
C=====
C               REGRESSION FOR EXPERIMENTAL DATA OF DEGASSING
C               The required function is
C               Y = A + B*EXP(C*X)
C=====
C
C
C *****
C DEFINITION OF VARIABLES
C *****
C
C   X(n):           The vector of x.
C   Y(n):           The vector of y.
C   YT(n):          The transform of Y, YT = ln(Y - A).
C
C   Yhat(n):        Y hat, Yhat = C0 + C1*x.
C   Resi(n):        The vector of residual.
C   Rsqr:           The sum of square of the residual.
C                   R2 = Y2 - Yhat2.
C   R0sqr:          R0sqr = Y2 - n*Ybar2.
C   regsqr:         The coefficient of regression.
C                   r2 = 1 - R2/R02.
C
C   n:              The number of values.
C
C *****
C MAIN PROGRAM
C *****
C
C   program Reg_degass
C
C   implicit real (a-h, o-z)
C
C   common / array / X(50), Y(50), YT(50), Yhat(50), Rate(50)
C   common / var / Ymax, trial, C0, C1, regsqr, Rsqr, R0sqr
C   common / var / step, dstnc
C   common / int / n
C
C   call data
C   trial=Ymax+step
C   bstc=trial
C   r2min=0.0
C
C   do while (trial.GE.(Ymax-dstnc))
C       call initia
C       call call
C       call cal2

```

```
        if(abs(1.0-regsqr).LE.abs(1.0-r2min)) then
            bstc=trial
            r2min=regsqr
        endif
        trial=trial+step
    enddo
c
    trial=bstc
    call initia
    call call
    call cal2
    call output
c
    stop
    end
c
c
c *****
c SUB PROGRAMS
c *****
c
c Data input
c -----
c subroutine data
c
c implicit real (a-h, o-z)
c
c common / array / X(50), Y(50), YT(50), Yhat(50), Rate(50)
c common / var / Ymax, trial, C0, C1, regsqr, Rsqr, R0sqr
c common / var / step, dstnc
c common / int / n
c
c open(unit=10, file='yd.dat', status='unknown')
c read(10, *)
c read(10, *)
c read(10, *)
c read(10, 100)n
c read(10, 110)Ymax
c read(10, 120)step
c read(10, 130)dstnc
c read(10, *)
c read(10, 110)(Y(i), X(i), i=1, n)
c close(unit=10)
c
c 100 format(I4)
c 110 format(F6.3, 2x, F6.3)
c 120 format(E15.1)
c 130 format(F6.2)
c
c return
c end
```

```
c
c
c   Data initialisation
c   -----
c   subroutine initia
c
c   implicit real (a-h, o-z)
c
c   common / array / X(50), Y(50), YT(50), Yhat(50), Rate(50)
c   common / var / Ymax, trial, C0, C1, regsqr, Rsqr, R0sqr
c   common / var / step, dstnc
c   common / int / n
c
c   do 200 i=1, n
c       YT(i)=log(Y(i)-trial)
200 continue
c
c   return
c   end
c
c   Calculations of sumx, sumy, and C0.
c   -----
c   subroutine call
c
c   implicit real (a-h, o-z)
c
c   common / array / X(50), Y(50), YT(50), Yhat(50), Rate(50)
c   common / var / Ymax, trial, C0, C1, regsqr, Rsqr, R0sqr
c   common / var / step, dstnc
c   common / int / n
c
c   sumx=0.0
c   sumy=0.0
c   sumx2=0.0
c   sumxy=0.0
c
c   do 300 i=1, n
c       sumx=sumx+X(i)
c       sumy=sumy+YT(i)
c       sumx2=sumx2+X(i)*X(i)
c       sumxy=sumxy+X(i)*YT(i)
300 continue
c
c   Xbar=sumx/float(n)
c   Ybar=sumy/float(n)
c   C1=(sumxy-Ybar*sumx)/(sumx2-Xbar*sumx)
c   C0=Ybar-Xbar*C1
c
c   return
c   end
```

```

c
c
c   Calculations of Yhat, Rate, residual, and coefficient.
c   -----
c   subroutine cal2
c
c   common / array / X(50), Y(50), YT(50), Yhat(50), Rate(50)
c   common / var / Ymax, trial, C0, C1, regsqr, Rsqr, R0sqr
c   common / var / step, dstnc
c   common / int / n
c
c   avgy=0.0
c   Rsqr=0.0
c   R0sqr=0.0
c   do 400 i=1, n
c       avgy=avgy+Y(i)
c       Yhat(i)=0.0
c       Rate(i)=0.0
c       Yhat(i)=trial+exp(C0+C1*X(i))
c       Rate(i)=60.0*C1*exp(C0+C1*X(i))
c       Rsqr=Rsqr+(Y(i)-Yhat(i))**2
c       R0sqr=R0sqr+Y(i)*Y(i)
400 continue
c
c   avgy=avgy/float(n)
c   R0sqr=R0sqr-float(n)*avgy*avgy
c   regsqr=1.0-Rsqr/R0sqr
c
c   return
c   end
c
c
c   Output the result
c   -----
c   subroutine output
c
c   implicit real (a-h, o-z)
c
c   common / array / X(50), Y(50), YT(50), Yhat(50), Rate(50)
c   common / var / Ymax, trial, C0, C1, regsqr, Rsqr, R0sqr
c   common / var / step, dstnc
c   common / int / n
c
c   open(unit=20, file='result_degas', status='unknown')
c   write(20, *)
c   write(20, *)
c   write(20, 500)
c   write(20, *)
c   write(20, 510)
c   write(20, 520)(X(i), Y(i), Yhat(i), Rate(i), i=1, n)
c   write(20, *)

```

```
write(20, 530)
write(20, 540)
write(20, 550)
write(20, 560)trial, exp(C0), C1
write(20, *)
write(20, 570)
write(20, 580)Rsqr
write(20, 590)R0sqr
write(20, 600)regsqr
close(unit=20)

c
500 format(6x, 'REGRESSION OUTPUT FOR DEGASSING')
510 format(6x, 'X', 6x, 'Y', 11x, 'Yhat', 9x, 'Rate')
520 format(2x, F6.1, 2x, F6.3, 5x, F10.6, 3x, F10.6)
530 format(4x, 'The function is')
540 format(6x, 'Y = A + B*EXP(k*X)')
550 format(4x, 'The coefficients are')
560 format(6x, 'A = ', E13.6, 2x, 'B = ', E13.6, 2x, 'k = ',
E13.6)
570 format(4x, 'Residual and precision')
580 format(6x, 'R2 = ', E13.6)
590 format(6x, 'R02 = ', E13.6)
600 format(6x, 'r2 = ', F13.6)

c
return
end
```